SYNTHESIS AND CHARACTERIZATIONS OF AMORPHOUS CARBON NANOTUBES/ CADMIUM SELENIDE QUANTUM DOTS HYBRID MATERIALS

TAN KIM HAN

FACULTY OF ENGINEERING
UNIVERSITY OF MALAYA
KUALA LUMPUR

2012

SYNTHESIS AND CHARACTERIZATIONS OF AMORPHOUS CARBON NANOTUBES/ CADMIUM SELENIDE QUANTUM DOTS HYBRID MATERIALS

TAN KIM HAN

DISSERTATION SUBMITTED IN FULFILMENT OF THE REQUIREMENTS FOR THE DEGREE OF MASTER OF ENGINEERING SCIENCE

FACULTY OF ENGINEERING
UNIVERSITY OF MALAYA
KUALA LUMPUR

2012

UNIVERSITY OF MALAYA

ORIGINAL LITERARY WORK DECLARATION

Name of Candidate: TAN KIM HAN   **I.C No:**

Registration/Matric No: KGA 090067

Name of Degree: Master of Engineering Science

Title of Dissertation ("this Work"):

Synthesis and Characterizations of Amorphous Carbon Nanotubes/Cadmium Selenide

Quantum Dots Hybrid Materials

Field of Study: Nanotechnology

I do solemnly and sincerely declare that:
  (1) I am the sole author/writer of this Work;
  (2) This Work is original;
  (3) Any use of any work in which copyright exists was done by way of fair dealing and for permitted purposes and any excerpt or extract from, or reference to or reproduction of any copyright work has been disclosed expressly and sufficiently and the title of the Work and its authorship have been acknowledged in this Work;
  (4) I do not have any actual knowledge nor do I ought reasonably to know that the making of this work constitutes an infringement of any copyright work;
  (5) I hereby assign all and every rights in the copyright to this Work to the University of Malaya ("UM"), who henceforth shall be owner of the copyright in this Work and that any reproduction or use in any form or by any means whatsoever is prohibited without the written consent of UM having been first had and obtained;
  (6) I am fully aware that if in the course of making this Work I have infringed any copyright whether intentionally or otherwise, I may be subject to legal action or any other action as may be determined by UM.

Candidate's Signature: **Date:**

Subscribed and solemnly declared before,

Witness's Signature: **Date:**

Name:

Designation:

ABSTRACT

Carbon nanotubes (CNTs) have attracted great attention. Most of the works being conducted in the past mainly focus on the crystalline CNTs. In this work, amorphous CNTs (α-CNTs) were synthesized successfully via a simple chemical technique at 230 °C in a short period of time. Surface morphological studies revealed that the as-prepared nanotubes present in straight tubular structures with open ends, having certain dimensions (80 - 110 nm for outer diameter; 45 - 65 nm for inner diameter; 8 - 10 μm for length). Both structural and elemental studies confirmed that the nanotubes were made of amorphous carbon. Acidic purification and oxidation treatment caused the surface of nanotubes rougher and introduced defects in their structures. Oxidation also increased dispersion stability of nanotubes in deionised water and ensured the successful hybridization between the α-CNTs and cadmium selenide (CdSe) quantum dots (QDs). The α-CNTs displayed π plasmon absorbance phenomenon in ultraviolet-visible absorption spectra and had high band gap of 4.65 eV. The hybrid material exhibited size quantization effect due to the attachment of CdSe QDs on the nanotubes surfaces, giving the least band gap of 3 eV among the other samples. The presence of two identical bands (D and G bands) in Raman spectra deduced that both the oxidation and hybridization reduced crystallinity of the nanotubes substantially and confirmed the existence of defective walls of the nanotubes that were composed of disordered carbon. The α-CNTs exhibited lower permittivity in frequency range of 500MHz - 4.5 GHz due to quantum size effects. However, the oxidation increased the permittivity of the α-CNTs via chemical functionalization. Highest permittivity was found in the hybrid material and it was the most thermally stable sample compared to others.

ABSTRAK

Karbon nano tiub (CNTs) semakin menarik perhatian besar. Kebanyakan kerja penyelidikan dijalankan pada masa dahulu bertumpu pada CNTs berhablur. Dalam kerja penyelidikan ini, CNTs amorfus (α-CNTs) berjaya disintesiskan melalui teknik kimia ringkas pada suhu 230 °C dalam tempoh yang singkat. Kajian permukaan morfologi mendedahkan bahawa tiub nano yang dihasilkan hadir dalam struktur berbentuk tiub dengan hujungnya terbuka, mempunyai dimensi tertentu (garis pusat luar: 80 - 110 nm; garis pusat dalam: 45 - 65 nm untuk; panjang: 8 - 10 μm). Kedua-dua kajian unsur dan struktur mengesahkan bahawa tiub nano ini adalah karbon yang berstruktur amorfus. Penulinan berasid dan rawatan pengoksidaan menyebabkan permukaan tiub nano lebih kasar dan memiliki kecacatan-kecacatan dalam strukturnya. Pengoksidaan juga meningkatkan kestabilan penyerakan tiub nano dalam air ternyah ion dan menjanjikan penghibridan yang berjaya antara α-CNTs dan kadmium selenida (CdSe) kuantum dot. α-CNTs mempamerkan fenomena serapan π plasmon dalam spektrum penyerapan UV-Vis dan mempunyai tenaga "band gap" tinggi, 4.65 eV. Bahan hibrid menunjukkan kesan pengkuantuman saiz disebabkan pendudukan CdSe kuantum dot pada permukaan tiub nano, memberi tenaga "band gap" yang paling kurang, 3 eV antara semua sampel. Kehadiran kedua-dua jalur D dan G dalam spektrum Raman menyimpulkan bahawa kedua-dua proses pengoksidaan dan penghibridan banyak mengurangkan kehabluran tiub nano dan mengesahkan kewujudan kerosakan dinding tiub nano yang diperbuat daripada karbon yang tersusun rawak. α-CNTs menunjukkan ketelusan yang lebih rendah dalam julat frekuensi 500MHz - 4.5 GHz disebabkan oleh kesan saiz kuantum. Bagaimanapun, pengoksidaan menambahkan ketelusan α-CNTs melalui pemfungsian kimia. Ketelusan lebih tinggi ditemui dalam bahan hibrid dan ia mempunyai kestabilan haba tertinggi berbanding dengan sampel yang lain.

ACKNOWLEDGEMENT

TABLE OF CONTENTS

LIST OF FIGURES

LIST OF TABLES

LIST OF SYMBOLS AND ABBREVIATIONS

CNTs	Carbon nanotubes
α-CNTs	Amorphous carbon nanotubes
SWCNTs	Single-walled carbon nanotubes
DWCNTs	Double-walled carbon nanotubes
MWCNTs	Multi-walled carbon nanotubes
CdSe QDs	Cadmium selenide quantum dots
UV-Vis	Ultraviolet-visible
TEM	Transmission electron microscopy
HRTEM	High resolution transmission electron microscopy
FE-SEM	Field emission scanning electron microscopy
XRD	X-ray diffraction
EDX	Energy-dispersive X-ray
FTIR	Fourier transform infrared
VNA	Vector network analyzer
TGA	Thermogravimetric analyzer
E_g	Band gap
CVD	Chemical vapour deposition
DC	Direct current
PTFE	Polytetrafluoroethylene
AAO	Aluminium oxide templates
$Fe(C_5H_5)_2$	Ferrocene
PEG	Polyethylene glycol
MW	Molecular weight
ε'	Dielectric constant
ε''	Dielectric loss factor
ε_r	Relative complex permittivity

RBM	Radial breathing mode
EMC	Electromagnetic compatibility
EMI	Electromagnetic interference
E	External electric field
MEMS	Microelectromechanical
NEMS	Nanoelectromechanical
AFM	Atomic force microscopy
M	Molarity
Cu-K α	Copper K-alpha
Å	Ångström
d_{hkl}	Interplanar spacing
α	Absorption coefficient
$h\nu$	Photon energy of the incident light
n	Type of optical transition
B	Constant in Tauc/Davis-Mott model
I_D/I_G	Intensity ration between G and D bands

LIST OF PUBLICATIONS

Leo, B. F., **Tan, K. H.**, Ng, M. N., Ang, B. C., & Johan, M. R. (2011). Physico-Chemical Properties of Titania Nanotubes Synthesized via Hydrothermal and Annealing Treatment. *Applied Surface Science, 258*, 431-435.

Tan, K. H., Leo, B. F., Ng, M. N., Ahmad, R., & Johan, M. R. (2011). Optical Studies on Multiwalled Carbon Nanotubes via Modified Wolff-Kishner Reduction Process. *Advanced Materials Research, 194-196*, 618-624.

Leo, B. F., **Tan, K. H.**, Ng, M. N., & Johan, M. R. (2011). Synthesis, Characterization and Gas Adsorption of Titania Nanotubes, *Advanced Materials Research*, *194-196*, 446-449.

Tan, K. H., Leo, B. F., Ahmad, R., Yew, M. C., Ang, B. C., & Johan, M. R. (2012). Physico-Chemical Studies of Amorphous Carbon Nanotubes Synthesized at Low Temperature. *Materials Research Bulletin, 47*, 1849-1854.

Tan, K. H., Leo, B. F., Ng, M. N., Ahmad, R. and Johan, M. R., 'Optical Studies on Multiwalled Carbon Nanotubes Via Modified Wolff-Kishner Reduction Process', International Conference on Manufacturing Science & Engineering (ICMSE 2011), 9-11 April 2011, Guilin, China, Paper ID: D6566.

CHAPTER ONE: INTRODUCTION

This chapter contains a brief introduction of different types of carbon nanotubes (CNTs) with their relevant characteristics and features that suit them in various applications. The issues, objectives and the outline concerned with this research are also highlighted.

1.1   Background

In general, CNTs are a form of carbon made by rolling up graphite sheets to narrow but long tubes into cylindrical patterns. CNTs can be categorized into two major divisions, which are crystalline CNTs and amorphous CNTs (α-CNTs). Crystalline CNTs are then further divided into three types, which based on the different arrangement and number of their graphite sheets, which are single-walled CNTs (SWCNTs), double-walled CNTs (DWCNTs) and multi-walled CNTs (MWCNTs) (Peter, 2009; O'Connell, 2006). All crystalline CNTs can be represented by a pair of indices (n, m) called the chiral vector or chirality. In contrast, α-CNTs possess a high degree of disorder structures due to their amorphous wall with defects in the carbon network. Any possible problem due to chirality is the absence for α-CNTs (Rakitin *et al.*, 2000). It is troublesome to characterize the chirality of the crystalline CNTs accurately.

Undeniably, CNTs have attracted great attention since their early discoveries (Iijima, 1991; Bethune *et al.*, 1993). CNTs seem like the most important materials because of their unique structure that exhibits extraordinary strength, excellent electrical properties and efficient thermal conductivity which suit them to a tremendously diverse range of applications such as sensors, probes, lithium batteries, gas adsorption and hydrogen storage and others (Meyyappan, 2005; O'Connell, 2006; Peter, 2009). However, their significant optical properties could not be neglected, which also lead to various optical and electronic applications. Interestingly, the CNTs have been applied in

field emission display devices as cathode-ray tube-type lighting elements, vacuum-fluorescence display panels (Saito *et al.*, 2000), cold electron emitter and other applications in electro optics. It is because the α-CNTs are capable of showing impressive field emission properties in some previous works (Ahmed *et al.*, 2007a; Ahmed *et al.*, 2007b).

In spite of many developed techniques for the production of crystalline CNTs, some drawbacks could arise from their synthesizing processes. The possible drawbacks could be the requirement of high operating temperature, complicated processing steps, catalyst support, long synthesis period and expensive production cost (Wang *et al.*, 2005a; Wang *et al.*, 2005b). The difficulties in synthesizing crystalline CNTs make the α-CNTs as the substituent material. These amorphous nanotubes are relatively simple to be synthesized in a large quantity (Banerjee *et al.*, 2009; Jha *et al.*, 2011).

The α-CNTs are easily self-agglomerated and bound together due to their high Van der Waals force, surface area and high aspect ratio. According to previous works (Gojny *wt al.*, 2003; Jha *et al.*, 2011), chemical modifications of the nanotubes' surface via oxidation and functionalization processes were necessary as they reduced agglomeration. The purpose of oxidation was to enable nanotubes became chemically reactive and to prevent agglomeration in nanotubes. Subsequently, the nanotubes could be attached with other relevant functional groups and promoted a good dispersion in a solution. Besides, some properties of nanotubes can be enhanced. The field emission property of the stearic acid functionalized α-CNTs was found to be improved and could be utilized in the optical applications (Jha *et al.*, 2011).

There is strong interest to develop hybrid materials between semiconductor nanoparticles and CNTs with the hope of discovering new properties and applications due to their unique and structurally defined optical and electronic properties. For instance, the attachment of cadmium selenide quantum dots (CdSe QDs) on both oxidized and functionalized SWCNTs and MWCNTs to become hybrid materials exhibited photoelectrical response (Robel *et al.*, 2005; Juárez *et al.*, 2007; Lu *et al.*, 2009). The luminescence characteristics of these hybrid materials could be applied in optoelectronic application such as solar cells and optical sensors. Cadmium selenide is an important II-VI semiconductor and it is an n-type semiconductor. The quantum confinement effect in this material makes their properties tunable according to their size. Thus, they have been developed for application in opto-electronic devices, laser diodes, liquid-crystal display (LCD) devices, nanosensors and biomedical imaging devices (Hamizi *et al.*, 2010; Paul *et al.*, 2010).

In this work, α-CNTs were synthesized via a simple chemical route by heating a mixture of feroccene ($Fe(C_5H_5)_2$) and ammonium chloride (NH_4Cl). Purification, oxidation and hybridization treatments were performed to obtain different samples: untreated, treated, oxidized α-CNTs and hybridized α-CNTs/CdSe QDs respectively. The used CdSe QDs were synthesized separately prior to the hybridization process. The morphological, microstructural, elemental and thermal studies of the α-CNTs were conducted. Both optical and dielectric characteristics were also investigated by ultraviolet-visible (UV-Vis), Raman spectroscopy and vector network analyzer (VNA).

1.2   Importance of Study

One-dimensional CNTs and other carbon nanomaterials have been especially investigated for many purposes due to their peculiar structures and properties (Peter,

2009). They have attracted much attention because of their many potential applications. CNTs possess large aspect ratio and low electron affinity that enable them to be the excellent field emitter. However, the synthesis of CNTs is relatively difficult as it requires very high temperature, complicated processing steps, catalyst support, longer synthesis period and expensive cost (Wang *et al.*, 2005a; Wang *et al.*, 2005b). Thus, amorphous CNTs (α-CNTs) come into play since the preparation of α-CNTs via a chemical route is relatively simple (Banerjee *et al.*, 2009). This work used an uncomplicated chemical approach to synthesize α-CNTs in a large quantity. The ease of production for α-CNTs may provide an alternative to the industries for applying this material into relevant gaseous adsorbent products, nano-devices and electro optics especially for the field emission display devices in the future. These applications are possible due to their amorphous wall with defects within their nanostructures (Jha *et al.*, 2011). It was the reason why the morphological, microstructural, elemental and thermal features of the as-prepared α-CNTs had to be examined by various characterization methods in order to provide better understanding about them and the feasibility of this synthesis technique. Additionally, the more established of these results the more controllable of this technique. Perhaps, the as-prepared α-CNTs could be easily modified and tailored accordingly to obtain nanotubes with desired nanostructures in order to suit them to a specific application.

Furthermore, α-CNTs are believed to be the potential material for the field emission display. Previously, the carbon-based films such as diamond, diamond-like carbon and amorphous carbon have been proven to show better field emission properties due to the alteration of the electronic structure by the incorporation of substitutional defect states and the donor activity of silicon or fluorine. They might become good candidates for the low-threshold field emitter (Ahmed *et al.*, 2007a; Ahmed *el al.*,

2007b). In addition, there are relatively few optical absorption studies that have been carried out that almost exclusively involved SWCNTs (Peter, 2009). The exploitation of the desirable optical properties of these carbons with defective walls is necessary as the fundamental understanding of how these functional properties are affected by the morphological characteristics of the inherent α-CNTs remain elusive. According to literature survey, there is also no report about the dielectric studies on α-CNTs that have been synthesized via a simple chemical route in this work. Therefore, the UV-Vis absorption and complex permittivity (dielectric) measurement on amorphous nanotubes were essential in this research in order to explore both the optical and dielectric properties of the amorphous nanotubes.

Hybridization between α-CNTs and CdSe QDs was conducted and investigated for the first time. There was only crystalline CNTs (SWCNTs and MWCNTs)/CdSe QDs hybrid that had been worked previously according to literature (Hungria *et al*., 2008; Lu *et al*., 2009). The CdSe QDs are very useful semiconductor materials, especially their properties vary with their particle sizes due to quantum confinement effect. The more established features of CdSe QDs due to their unique and structurally defined optical and electronic properties may enhance the optical property of the as-prepared α-CNTs/CdSe QDs hybrid. The various morphological, structural, elemental and optical characterization studies conducted on this hybrid material were able to generate new insight into its advantages and disadvantages.

1.3   Research Objectives

The objectives of this study are as follows:

- To produce α-CNTs using a simple chemical route at low temperature

- To produce α-CNTs/CdSe QDs hybrid materials through purification, oxidation and hybridization steps

- To determine the morphological, microstructural, elemental, optical, dielectric and thermal characteristics for the untreated, treated, oxidized α-CNTs and hybridized samples (α-CNTs/CdSe QDs)

1.4   Scope of Research Work

In this work, α-CNTs were synthesized using a relatively simple technique that only required a low temperature and pressure conditions in a short processing period. Precursor materials were put into a pressure vessel known as Parr reactor and were heated inside a furnace. Four different samples were prepared. Firstly, the as-prepared α-CNTs (untreated sample) were synthesized at 230 °C in one hour. The untreated sample was soaked and washed with concentrated hydrochloric acid (HCl) to obtain purified α-CNTs (treated sample). Oxidation was then conducted towards the treated sample by using a combination of concentrated acids to prepare the oxidized α-CNTs (oxidized sample). Finally, the α-CNTs/CdSe QDs (hybridized sample) was prepared via a series of steps which involved ultrasonication, heating and stirring processes.

The morphological, microstructural, elemental and thermal studies were conducted to all samples. Instruments such as transmission electron microscope (TEM), higher resolution transmission electron microscope (HRTEM), field emission scanning electron microscopy (FE-SEM), X-ray diffraction (XRD) spectrometer and energy-dispersive X-ray (EDX) spectrometer and thermogravimetric analyzer (TGA) were utilized. The optical and dielectric properties, especially for the hybridized α-CNTs/ CeSe QDs are investigated and reported for the first time. Fourier transform infrared (FTIR) and ultraviolet-visible (UV-Vis) and Raman spectroscopy studies were

conducted to examine optical features such as FTIR characteristics, transmittance and absorption of UV-Vis, optical band gap (E_g) and Raman characteristics. The interaction between the samples and electromagnetic field for exploring their complex permittivity over a broad frequency range had also been examined using a vector network analyzer (VNA). The complex permittivity measurement in dielectric study involved dielectric constant ($\varepsilon^{'}$) and dielectric loss factor ($\varepsilon^{''}$). The obtained morphological, microstructural, elemental and thermal studies were then related to each other and correlated with both the optical and dielectric results. The pathway of the research work is summarized in Figure 1.1.
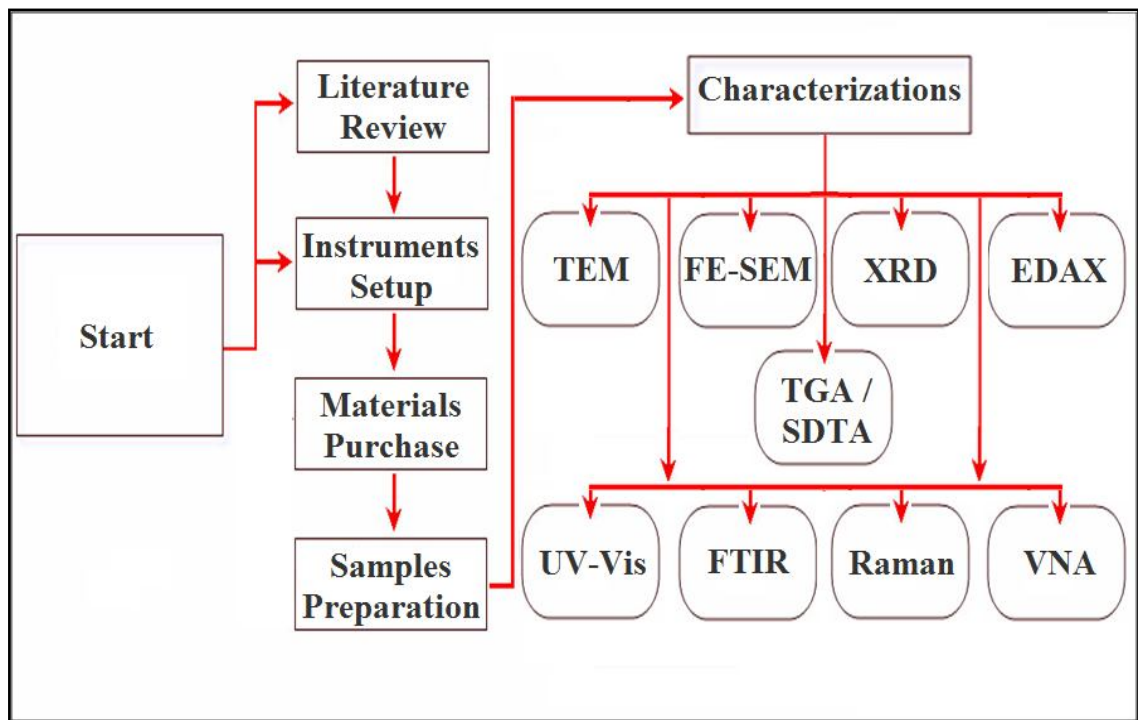
Figure 1.1 : The pathway of the research work.

CHAPTER TWO: LITERATURE REVIEW

In this chapter, a detailed introduction to the types, structures, natures of CNTs with their historical developments are explained. The previous synthesis techniques for both crystalline and amorphous nanotubes are also outlined. Various properties of α-CNTs and their applications are included.

2.1   Carbon Nanotubes (CNTs)

CNTs are a new form of carbon made by rolling up a single graphite sheet to a narrow but long tube closed at both sides by two hemispheres (half of section of fullerene carbon) like end caps. In 1991, Sumio Iijima invented two types of nanotubes namely SWCNTs and MWCNTs (Iijima, 1991). SWCNT consists only of a single graphite sheet with one atomic layer in thickness while MWCNT is formed from two to several tens of graphite sheets arranged concentrically into tube structures, respectively. The construction of another type of nanotubes, DWCNTs is similar to that of SWCNTs as they consist of double graphite sheets with the atomic layers in thickness. All the crystalline nanotubes, like SWCNTs, DWCNTs and MWCNTs are promising one-dimensional periodic structure along the axis of the tube with an extraordinary length-to-diameter ratio of up to 132,000,000:1 (Wang *et al.*, 2009). On the other hand, the chemical bonding of CNTs is constructed entirely of sp^2 bonds, similar to graphite. It is this bonding structure that provides unique strength to CNTs. In comparison to the crystalline CNTs, another common type known as α-CNTs have highly disordered structures in the presence of defects (Rakitin *et al.*, 2000; Jha *et al.*, 2011). Their amorphous walls with defects within their nanostructures lead to the potential development in field emission displays devices, gaseous adsorbent and catalyst support or other nanodevices (Xiong *et al.*, 2004; Banerjee *et al.*, 2009; Jha *et al.*, 2011). Figure 2.1, shows different types of CNTs.
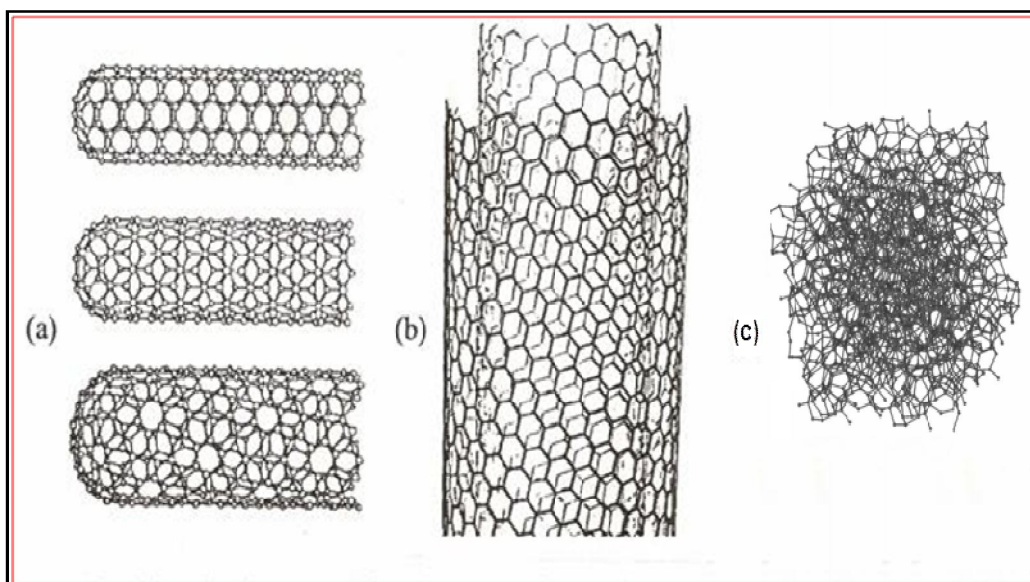
Figure 2.1 : Types of carbon nanotubes: (a) SWCNTs; (b) MWCNTs; (c) α-CNTs (Peter, 2009).

Since the discovery of the CNTs (Iijima, 1991; Bethune *et al.*, 1993), several techniques of preparing CNTs have been worked out and explored with the aim of developing an uncomplicated synthesis process with low cost and no catalyst support required for a large-scale production of CNTs. Various methods include chemical vapour deposition (CVD), electric arc discharge, laser ablation, hydrothermal and solvothermal techniques, pyrolysis of precursor organic molecules and electrochemical route were developed to obtain MWCNTs and SWCNTs (Scott *et al.*, 2001). However, these methods have disadvantages such as requiring high temperature, complicated processing steps, catalyst support, longer synthesis period and expensive cost (Wang *et al.*, 2005a; Wang *et al.*, 2005b). As a result, α-CNTs are then gradually receiving attentions due to their simple synthesis condition and potential development in the field emission displays devices and electro optics (Banerjee *et al.*, 2009; Jha *et al.*, 2011). Similarly, α-CNTs also could be successfully synthesized by using CVD and direct current (DC) arc discharge (Yacaman *et al.*, 1993; Ci *et al.*, 2001; Zhao *et al.*, 2006). Literature survey indicates the structure of CNTs has been extensively investigated,

especially by the high resolution TEM and Raman studies (Cheng, *et al.*, 2004; Wang *et al.*, 2005b). In order to have a further comprehension about CNTs, especially for amorphous nanotubes, their types, structures and nature will be explained in the following sections. Historical developments of CNTs are also discussed.

2.1.1   General Properties of CNTs

Diamond and graphite are the two well-known forms of crystalline carbon. Diamond has four-coordinate sp^3 carbon atoms that form an extended three-dimensional network. Graphite has three-coordinate sp^2 carbon atoms that form planar sheets. Meanwhile, amorphous graphite has random stacking of graphitic layer segments. Due to the weak interplanar interaction between two graphitic planes, these planes can move easily relative to each other, thereby forming a solid lubricant. In this sense, amorphous graphite can behave like a two-dimensional material (Saito *et al.*, 1998).

The new emerging carbon allotropes that are fullerenes and are closed-cage carbon molecules with three-coordinate carbon atoms form the spherical or nearly-spherical surfaces. However, CNTs, which are derived from fullerenes are the only form of carbon with extended bonding and yet without dangling bonds (Meyyappan, 2005). CNTs are allotropes of carbon with a cylindrical nanostructure which are also known as tubular fullerenes or bucky tubes. CNTs naturally align themselves into "ropes" held together by Van der Waals forces.

CNTs can be multi-walled with a central tubule in nanometric diameter surrounded by a certain amount of graphitic layers separated by about few angstroms, which are called multi-walled nanotubes (MWCNTs). However, single-walled nanotubes (SWCNTs) are composed of one tubule with no other surrounding graphitic

layers. Meanwhile, DWCNTs are similar as SWCNTs. The structure of DWCNTs is made of a tubule encircled by one graphitic layer. Interestingly, MWCNTs, DWCNTs and SWCNTs possess a similar feature. They are crystalline nanotubes that have long-range periodicity in their structures and results in a definite helicity or chirality as defined by their primitive lattice vector (O'Connell, 2006). As stated before, all crystalline CNTs can be represented by a pair of indices (n, m) called the chiral vector, which relates the amount of rotation that a tube has closely related to the tube's physical properties, like diameter and electronic character.

Another type of CNT known as amorphous CNTs (α-CNTs) do not have a certain long-range periodicity in their structures. Thus, they have no definite helicity because α-CNTs have high disordered structures in the presence of defects (Rakitin *et al.*, 2000; Jha *et al.*, 2011). In detail, α-CNT consists of amorphous carbon that is disordered, three-dimensional material in which sp^2 and sp^3 hybridizations are both present in the random manner (Saito *et al.*, 1998). Nevertheless, the walls of α-CNTs are composed of many carbon clusters with a short- and long-distance order. Therefore, their properties are different from crystalline CNTs (Zhao *et al.*, 2006).

Nanomaterials such as boron nitride, molybdenum, carbon and others are currently fabricated into nanotubes from various materials. However, CNTs seem to be superior (at least at this moment) and most important due to their unique structure with interesting properties. CNTs have the length-to-diameter ratio of up to 132,000,000:1, which is significantly larger than any other material. They exhibit extraordinary strength, unique electrical and efficient thermal conductivity which suit them to a tremendously diverse range of applications. The applications for CNTs is indeed wide ranging such as micro or nanoscale electronics, quantum wire interconnects, field emission devices,

composites, chemical sensors, biomedical devices, nanocomposites, gas storage media, scanning probe tips and others (Meyyappan, 2005; Peter, 2009). However, toxicity factor may hinder the usage of CNTs (Kolosnjaj *et al.*, 2007).

Currently, α-CNTs become another focus of research due to the defects in their carbon networks can lead to interesting properties and new potential nanodevices. Chik *et al.* (2004) indicate that α-CNTs have good electronic conductivity. Moreover, there is no need of chirality separation for metallic or semiconductive nanotube compared to the crystalline CNTs with different band structures. Thus, α-CNTs are favourable for certain applications such as nanoelectronics and sensor devices (Chik *et al.*, 2004). Furthermore, these amorphous nanotubes are capable of showing impressive field emission properties (Ahmed *et al.*, 2007a; Ahmed *et al.*, 2007b). Therefore, any possible problem due to chirality is absent for α-CNTs (Rakitin *et al.*, 2000). In addition, α-CNTs are relatively simple to be synthesized in a large quantity.

However, α-CNTs were easily self-agglomerated and bound together due to their high Van der Waals force, surface area and high aspect ratio. Additional processes such as oxidation and functionalization are necessary to modify chemically the surface of nanotubes and thus reduce agglomeration (Gojny *et al.*, 2003). Besides, some properties of nanotubes could be enhanced. The field emission property of the stearic acid functionalized α-CNTs had been improved (Jha *et al.*, 2011).

2.1.2   Historical Developments of CNTs

Interest in carbon nanotubes (CNTs) was a direct consequence of the synthesis of buckminsterfullerene, C_{60} and other fullerenes in 1985. New impetus was generated to this search as C_{60} was synthesized in a simple arc-evaporation apparatus by the Japanese scientist Sumio Iijima in 1991 (Iijima, 1991). The tubes were discovered to contain at least two layers, often more and ranged in outer diameter from about 3 to 30 nanometers. They were known as MWCNTs. In 1993, a new class of CNT, SWCNTs were discovered, with just a single graphite layer (Bethune *et al.,* 1993). These SWCNTs were generally narrower than the MWCNTs, with diameters typically in the range of 1 - 2 nm. The discovery of carbon which could form stable and ordered structures other than graphite and diamond stimulated researchers worldwide. DWCNTs were then developed by the arc discharge technique with a mixture of different catalysts in 2001 (Hutchison *et al*., 2001). DWCNTs bundles had an outer diameter in the range of 1.9 - 5 nm and inner tube diameters in the range of 1.1 - 4.2 nm.

Another type of nanotubes with highly disordered structure called as α-CNTs were produced successfully for the first time in 2001 via the CVD process based on floating catalyst method (Ci *et al*., 2001). This work was to study the crystallization behaviour of α-CNTs. In fact, in earlier work showed that the carbon with nanometric pores showed non-graphitizing behaviour (Speck *et al*., 1989). Subsequently, α-CNTs were also obtained from the organic fragment, polytetrafluoroethylene (PTFE) with a catalyst by another method similar to CVD (Nishino *et al*., 2003). The as-prepared α-CNTs had a straight tubular shape with amorphous carbon wall consisting of very small sheets of randomly aligned hexagons. By a floating catalyst method (CVD), the mass production of α-CNTs was possible (Ci *et al*., 2003). The pyrolysis of ethylene confined in porous aluminium oxide templates (AAO) could yield α-CNTs (Yang *et al*., 2003).

Furthermore, a self-catalysis-decomposition of ferrocene (Fe(C$_5$H$_5$)$_2$) in benzene solution at temperatures below 210 °C had been performed for the synthesis of α-CNTs (Xiong *et al*., 2004).

2.2 Synthesis For Crystalline CNTs

Owing to the facts that these kinds of CNTs have a wide range of exceptional properties (Meyyappan, 2005), an explosion of research especially into methods of synthesis for CNTs has been sparked. Methods developed so far include chemical vapour deposition (CVD), electric arc discharge, laser vaporization, laser ablation, pyrolysis, high temperature hydrothermal and low- and high-temperature solvothermal. The growth of crystalline CNTs during synthesis is believed to commence from the recombination of carbon atoms split by heat from their precursor. Although a number of newer production techniques have been invented, three main methods in producing CNTs are the CVD, electric arc discharge and laser ablation.

2.2.1 Chemical Vapour Deposition (CVD)

CVD technique is most widely used to synthesize crystalline CNTs due to its benefit of significantly lower synthesis temperatures than arc-discharge and laser ablation techniques. In addition, CVD is becoming very popular because of its potential for scale up production. In this technique, CNTs grow from the decomposition of hydrocarbons in temperature range 500 - 1200 °C. They can grow on substrates such as carbon, quartz, silicon or others, which use the catalysts seeded on a substrate within a reactor (seeded catalyst method). Besides, they can even grow on floating fine catalyst particles like ion, nickel, or cobalt from numerous hydrocarbons, which uses the catalysts floating in the reactor space (floating catalyst method) (Yacaman *et al*., 1993;

Ci *et al.*, 2001). The hydrocarbons can be benzene, xylene, natural gas or acetylene. On the whole, CVD technique is a two-step process that consisting of a catalyst preparation step followed by synthesis of the nanotube. Normally, CVD requires a growth temperature of 500 - 1200 °C to produce MWCNTs. For producing SWCNTs, a higher growth temperature than those used for MWCNTs, typically 900 - 1200 °C is needed.

A typical catalytic CVD system is shown in Figure 2.2. It was equipped with a horizontal tubular furnace as the reactor. It was normally operated between 500 - 1200 °C for about 30 min and 200ml/min of hydrogen was used to cool the reactor. The tube was made of quartz. Precursor chemicals were carbon atoms while ferrocene and benzene vapor acted as the catalyst (Fe) (Oberlin, 1976). They were transported respectively either by argon, hydrogen or mixture of both into the reaction chamber. Ions of Fe and carbon atoms were subsequently decomposed and producing crystalline CNTs. The growth of the nanostructures occurred in either the heating zone, before or after the heating zone (O'Connell, 2006).
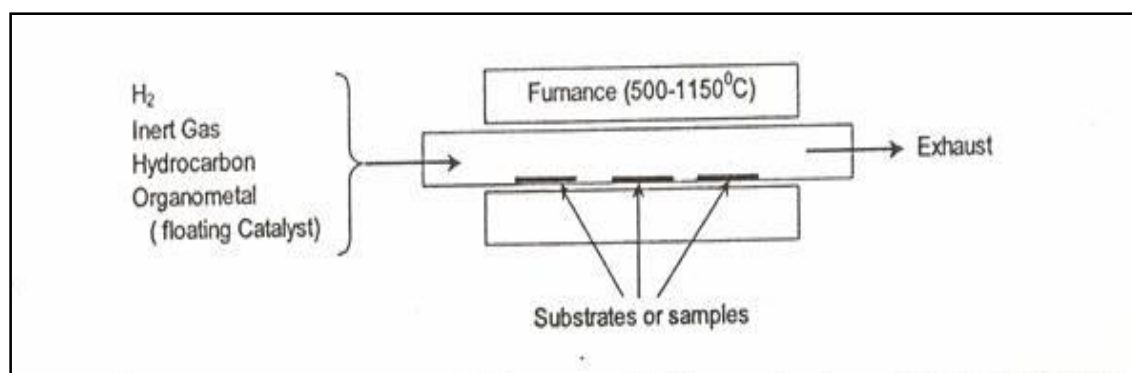
Figure 2.2 : Schematic diagram of catalytic CVD (O'Connell, 2006).

The use of metal complexes to produce MWCNTs has become popular. The same approach was conducted in the late 1980s (Endo, 1988). In 1994, the gas-phase synthesis in the flowing mixtures of methane or hexane with organometallics including

ferrocene and iron pentacarbonyl has been reported (Tibbetts *et al.* 1993). In 2004, CVD was capable of producing significant improvement in the quality of MWCNTs. Another approach to grow crystalline CNTs on substrates involves the use of plasma. This technique known as plasma enhanced chemical vapour deposition (PECVD) was first used to produce CNTs on nickel particles deposited onto glass (Ren *et al.* 1998). The as-prepared CNTs had excellent aligned arrays of tubes. PECVD had been widely used for coating glass plates and substrates for applications in flat panel displays, solar cells or other devices.

2.2.2   Arc Discharge

The arc discharge method produces a number of carbon nanostructures such as fullerenes, whiskers, soot and highly graphitized CNTs from high temperature plasma that approaches 3700 °C. At present, arc discharge remains the easiest and cheapest way to obtain significant quantities of SWCNTs. This method has also conveniently been used to produce both SWCNTs and MWCNTs with a higher degree of perfection than those prepared by CVD. However, the as-produced nanotubes are less pure than those produced by laser ablation (Meyyappan, 2005). The first ever produced CNTs was fabricated with the DC arc discharge method between two carbon electrodes, anode and the cathode in the environment that was filled with a noble gas such as helium or argon (Figure 2.3).

Relatively large scale yield of CNTs ($\approx$75 %) was produced at 100 - 500 Torr He and about 18 V DC (Ebbesen *et al.*, 1992). Typical nanotubes deposition rate was around 1 mm/min. The incorporation of transition metals such as cobalt, nickel or iron into the electrodes as the catalyst favours crystalline CNTs formation against other nanoparticles and reduced operating temperature. However, the arc discharge unit must

require a cooling system, whether the catalyst is used or not. This is to prevent overheating that will result in safety hazards and coalescence of the nanotube structure. CNTs with the smaller diameter between 2 - 30 nm and length 1 μm can be deposited on the cathode via this method as revealed by TEM analysis (Peter, 2009).
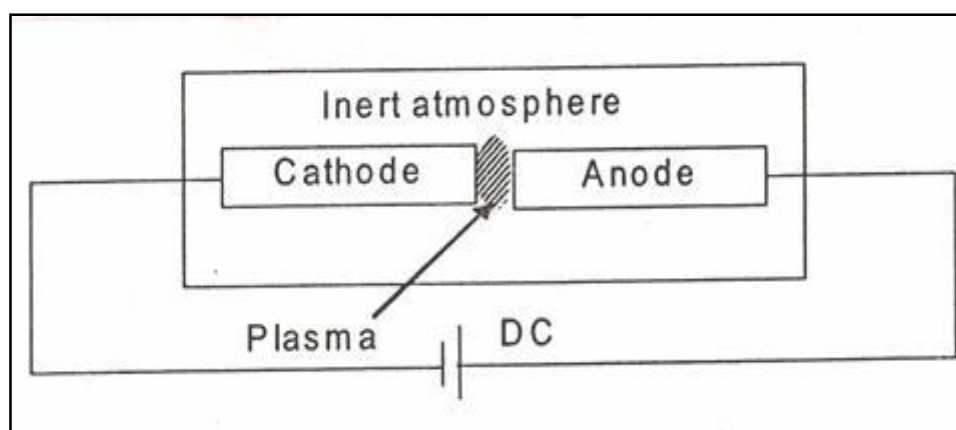
Figure 2.3 : Schematic diagram of a simplified arc discharge system (Meyyappan, 2005).

MWCNTs were first discovered on the cathode surface by Ijima (Iijima, 1991). Sooner, a larger amount of MWCNTs in gram with the diameter of about 14 nm was found successfully (Ebbesen *et al.*, 1992). The choice of metal catalyst for this process determines primarily the yields of SWCNTs. The combination of two different types of metal had produced much higher yields of SWCNTs than did individual metals. The synthesis of DWCNTs was a challenge for a long time. The breakthrough of DWCNTs was made with the arc discharge technique (Hutchision *et al.*, 2001). Most DWCNTs had an outer diameter in range 3 - 5 nm with wall separation distance of 0.39 ± 0.02 nm. Larger diameter generally corresponds to higher process temperature.

2.2.3   Laser Ablation

The use of a laser beam to vaporize a target of a mixture of graphite and metal catalyst, such as cobalt or nickel at temperature approximately 1200 °C under a flow of controlled inert gas (argon) and pressure is known as laser ablation technique (Figure 2.4). The nanotube deposits can be recovered at water cooled collector at a much lower and convenient temperature. This method was used in early days to produce high yield of CNTs (more than 70 - 90 %). Changing the reaction temperature could control the tube's diameters. Two laser pulses were employed to maintain the growth conditions of CNTs over a higher volume and time. The "ropes" of SWNTs with remarkably uniform narrow diameters ranging from 5 - 20 nm could be synthesized. Since the high electronegativity of a metal atom (catalyst) was applied, it deprived the growth of fullerenes and thus a selective growth of CNTs with open ends was obtained (Scott *et al.*, 2001). Nevertheless, due to the relative operational complexity, the laser ablation method appears to be economically disadvantageous, which, in effect hampers its scale up potentials as compared to the CVD method. Furthermore, a high operating temperature is a must.
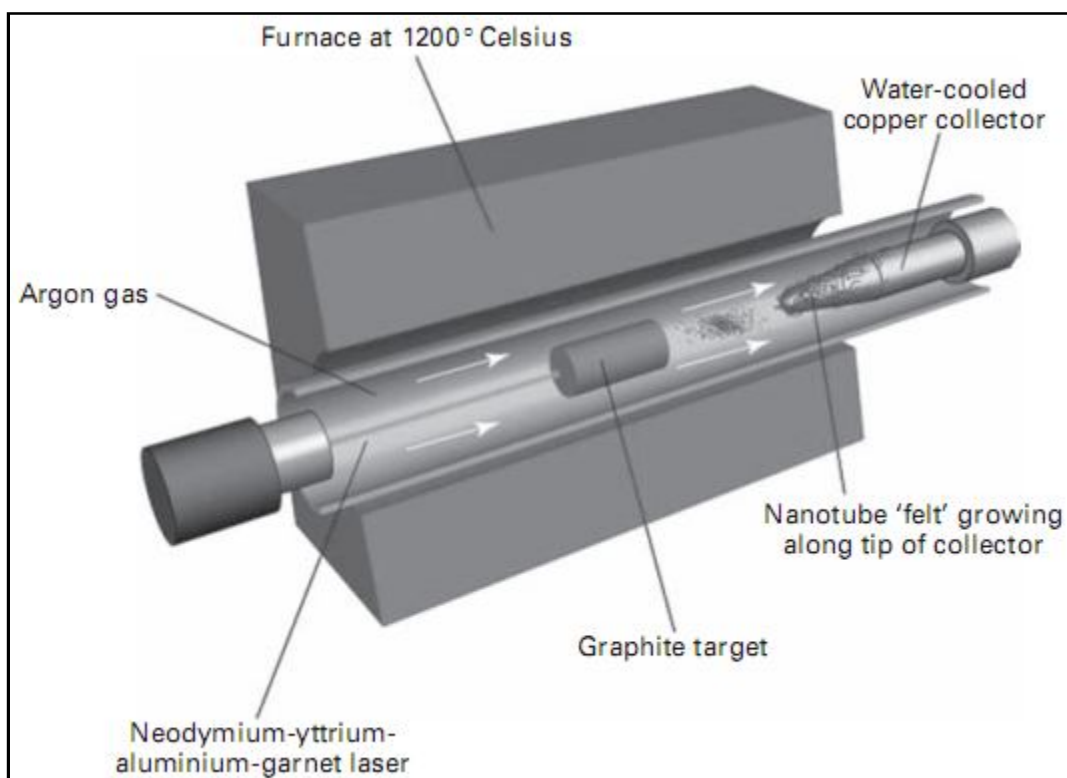
Figure 2.4 : Schematic diagram of a laser ablation apparatus (Peter, 2009).

Through this complicated method, the closed-ended MWCNTs were produced in the gas phase through homogeneous carbon-vapour condensation in a hot argon atmosphere (Guo *et al.*, 1995). These laser-produced MWCNTs are relatively short, with length of 300 nm and the inner diameter is in the range 1.5 - 3.5 nm, which are similar to those of arc-produced MWCNTs. The yield and quality of MWCNTs decline at the involved operating temperature below 1200 °C whereby no nanotubes could be obtained at 200 °C. On the other hand, the yield and properties SWCNTs are rather sensitive to factors such as light intensity, process temperature, types of carrier gas, pressure and flow conditions (Meyyappan, 2005). With the accuracy of the cooling-time determination, a conservative estimate of 3 - 30 ms is responsible for the growth of SWCNTs. The yield of SWCNTs reduces sharply with decreasing length and diameter when the ambient temperature set by a furnace falls from 1200 to 900 °C.

2.2.4 Hydrothermal Synthesis

Hydrothermal processing can be defined as any heterogeneous chemical reaction in the presence of a solvent (whether aqueous or non-aqueous) under high pressure and temperature conditions at pressure greater than 1 atm in a closed system (Byrappa *et al.*, 2008). Thus, this method is also termed as solvothemal. It is to dissolve and recrystallize materials that are relatively insoluble under ordinary conditions. It is capable of preparing materials with different nanoarchitectures such as nanowires, nanorods, nanobelts, nanotubes and so forth. It has advantages over conventional technologies as the final products are in high purity and homogeneity, metastable compounds with unique properties, dense sintered powders, micrometric and nanometric particles with a narrow size distribution and thus providing a host of other applications.

Since the growth mechanism is similar as in the gas phase in a high temperature condition under vacuum or in an inert atmosphere, hydrothermal routes may lead to a reproducible fabrication method of crystalline CNTs. The involved reaction temperature is also low and thus making this method as an alternative route for the synthesis of crystalline CNTs. Nanotubes were synthesized by using polyethylene, ethylene glycol and other sources with and without catalysts Fe/Co/Ni under hydrothermal conditions at 700 - 800 °C and 60 - 100 MPa. A much lower temperature of 175 °C used for the synthesis of MWCNTs was developed from catalytic decomposition of carbon tetrachloride (Jason *et al.*, 2004).

Although lower synthesis temperature was developed, the purity of MWCNTs decreased due to the usage of catalyst. To date, the lowest-reported temperature for the synthesis of MWCNTs under hydrothermal conditions was at 160°C, by the

decomposition of polyethylene glycol (PEG; MW 20,000) in a basic aqueous solution with high concentration of sodium hydroxide solution without using catalysts Fe/Co/Ni. PEG was used as the carbon source in this work (Wang *et al.*, 2005b). The diameters of the as-prepared MWCNTs were much smaller than those prepared by high temperature hydrothermal methods. The yield of the as-prepared MWCNTs in this work was just about 35% relative to the samples on copper grids which was estimated by TEM observations.

2.3   Synthesis For Amorphous CNTs

α-CNTs have attracted much attention because of their high potential usage in different applications such as field emitter, gaseous adsorbent, nanoelectronics and other electro optics. These potential applications are mainly attributed to the amorphous walls with defects in their nanostructures (Chik *et al.*, 2004; Ahmed *et al.*, 2007a; Ahmed *et al.*, 2007b; Jha *et al.*, 2011). Herein, this section will discuss the synthesis techniques for α-CNTs which have also been utilized for the production of crystalline CNTs.

2.3.1   Chemical Vapour Deposition (CVD)

Generally, the crystalline CNTs are normally synthesized by the CVD process in both industry and laboratory scales. This method has been developed well for a certain period of time. Therefore, CVD method requires lower cost and is capable of providing a large-scale synthesis for commercial application in comparison to the methods such as arc discharge, laser-ablation, hydrothermal, solvothermal or other related approaches (O'Connell, 2006).   Herein, the synthesis of amorphous CNTs (α-CNTs) in large qualities by a low-temperature CVD is possible. Further research has then discovered

that crystallization degree of the as-grown CNTs via CVD is very poor (α-CNTs) due to incomplete graphitization (Ci *et al.*, 2003).

In a previous work, by using a suitable catalyst, like nickel-aluminium alloy or nickel particles supported on alumina catalyst, carbon source such as methane (60ml/min) and hydrogen (420ml/min) as the carrier gas, the CVD process was carried out at 480 °C for 30 min followed by a cooling process to room temperature under a nitrogen atmosphere (Yacaman *et al.*, 1993; Zhao *et al.*, 2006). The successfully produced α-CNTs from this seeded catalyst method was mostly governed by the cooperative function of a low temperature and hydrogen carrier gas.

In another work, amorphous nanotubes were prepared by the floating catalyst method (Ci *et al.*, 2001). It was found that crystallization degree of the as-prepared CNTs synthesized via the floating catalyts method is very poor and thus known as the α-CNTs. Benzene solution with a given content of ferrocene and a small amount of thiophene was introduced into a vertical quartz reactor. The reactor was heated to the temperature of 1100-1200 °C. Hydrogen flowed as the buffer gas at a rate of 100 cm^3/min. Thus the growth parameters are such as the carrier gas composition or flow rate, temperature in the furnace and the used catalyst during a CVD process.

2.3.2 Arc Discharge

α-CNTs can also be produced by using DC arc discharge. Typically, an arc discharge was carried out in an atmosphere of hydrogen gas at a pressure of 50 kPa. The arc current was maintained at 80-100 A. An inner stainless steel chamber containing raw materials and cobalt-nickel alloy powders as the catalyst was mounted on a DC arc discharge furnace with a temperature controlling system. The temperature was

controlled by a thermocouple during heating and arc discharge. After a certain time of evaporation, the soot (α-CNTs) with small crystalline component was observed on the wall of the inner chamber and also around the anode and cathode rods (Liu *et al.*, 2004; Zhao *et al.*, 2005). Typically, α-CNTs with the diameter in range 10 - 15 nm had been synthesized in the presence of ferrous sulfide (FeS) served as the catalyst. There was a modified arc discharge being conducted and had successfully produced α-CNTs with the diameter about 7 - 20 nm.

It was found that the cooling rates and types of the gas, the temperature in the furnace and the catalyst all play an important role in this process. The furnace temperature has a large effect on the α-CNT diameter because the diameter increases with increasing temperature. The growth mechanism was explained that the random deposition of small carbon clusters from the gas phase on to a straight template of iron halide. Due to fast cooling rate of hydrogen gas, the carbon clusters are easily formed before atoms deposit onto the catalyst to form a crystal structure. Instead of forming long distance ordered crystalline tubes due to the lack of enough energy and time, the clusters formed the disordered structures which called as amorphous nanotubes (Nishino *et al.*, 2003; Liu *et al.*, 2004).

2.3.3 Template-Confined Growth

Template-confined growth is one of the techniques to synthesize different kinds of one-dimensional nanomaterials. It has advantages by obtaining aligned nanomaterials with adjustable diameter, length and morphology. Actually, mesoporous silica template was the first template to form aligned CNTs (Li *et al.*, 1996). The porous anodic aluminium oxide (AAO) templates are the widely used template. Due to the different channel structures of AAO, the morphology of the CNTs inside the channels could be

conveniently regulated by altering anodization parameters (Wang *et al.*, 2002). Normally, the wall structures for CNTs grown within AAO template are highly disordered and are different from those synthesized by arc discharge or laser ablation (Sui *et al.*, 2001). The highly disordered α-CNTs formed within AAO templates could probably possess uniform properties due to the homogeneity, by analogy with the case for amorphous alloys (Yang *et al.*, 2003).

In the year of 2003, α-CNTs with amorphous structure and irregular end were successfully prepared by AAO template-confined through the pyrolysis of acetylene in the presence of Ni catalyst (Yang *et al.*, 2003). The formation of disordered structure of nanotubes was as the result of the lattice mismatch between alumina and carbon species. The aligned arrays, Y-branched as well as novel dendriform nanotubes was revealed. In the recent year, another work that used similar approach to produce α-CNTs by a relatively simple template at the low temperature of 450 °C. The absence of catalyst resulted in the final product free of any contaminations and purification steps (Zhao *et al.*, 2009). AAO was used as template and citric acid was acted as the precursor. AAO template was prepared by a conventional two-step anodic process (Wang *et al.*, 2002). This work was claimed that the diameter, length and even the wall thickness of the walls of α-CNTs could be tuned by changing the pore diameter and the thickness of AAO templates, respectively. Besides, the orientation of graphene layers and the graphitization degree could be controlled by the pH of the citric acid solution.

2.3.4   Other Methods

Preparation conditions and any involved synthesis parameters are essential for the production of α-CNTs based on the fact that they affect the nanotube shapes, diameters, and lengths significantly. Numerous synthesis works other than CVD and arc discharge methods have been conducted to obtain α-CNTs by realizing some disadvantages arising from the aforementioned techniques. For instance, a relatively simple technique was used by heating a mixture of PTFE and ferrous chloride tetrahydrate inside a horizontal quartz tube furnace (Nishino *et al.*, 2003). The atmosphere within the tube furnace was filled with nitrogen at room temperature before the start of the heating process. α-CNTs were obtained after heating to 900 °C and most of them had open ends while their lengths and widths were several micrometers and 50 - 100 nm, respectively. As confirmed by TEM and XRD studies, nanotubes were composed of carbon of very poor crystallinity with amorphous walls that were totally different from the CNTs prepared by CVD. Normally crystalline CNTs have well-aligned sheets along the tube axis even though the graphitization extent is not high. In this work, the as-prepared amorphous nanotubes had a straight tabular shape with very small sheets of randomly aligned hexagons to form their amorphous carbon wall. Besides, their large interlayer spacing was suggested for the accommodation of small gaseous molecules such as hydrogen, thus providing a good adsorption capability.

Synthesis of α-CNTs had also been prepared via a solution-based approach at much lower temperatures, which could be named as solvothermal process. It was reported that long α-CNTs bundles and nanoribbons being produced via the self-catalysis-decomposition of ferrocene in benzene solution inside a Teflon-lined autoclave at low temperatures (< 210°C) (Xiong *et al.*, 2004). High reaction temperatures or a strong alkaline reducing agent did not facilitate this route. Similarly,

nanotubes with poor crystallinity were obtained whereby ferrocene was used as the catalyst for the pyrolysis of benzene (Ci *et al.*, 2003).

Poorly crystalline CNT bundles were also successfully prepared via a simple one-step solvothermal reaction between sodium (Na) and hexachlorobenzene (HCB) as the carbon source using nickel chloride ($NiCl_2$) as the catalyst precursor at 230 °C (Hu *et al.*, 2003). The as-prepared tubes had a uniform outer diameter of about 20 nm, an inner diameter of 4 nm. They were highly ordered and assembled as bundles, which have a two-dimensional hexagonal arrangement. Another solvothermal treatment of ferrocene ($Fe(C_5H_5)_2$) and sulphur produced long α-CNTs and Fe/C coaxial nanocables after being heated at 200 °C and maintained for 70 h (Luo *et al.*, 2006). The formation of the final products was largely depended on the amount of sulphur.

Recent works on synthesis of α-CNTs have been improved significantly whereby low temperature and simple steps are required. Liu et al. demonstrated that α-CNTs were prepared successfully by heating a mixture of $Fe(C_5H_5)_2$ and ammonium chloride (NH_4Cl) at 200 °C for a short period in an air furnace. The formation of nanotubes could be a CVD process. All nanotubes existed as bundles with uniform diameters and open ends after purification treatment (Liu *et al.*, 2007). Similarly, Banerjee et al. applied the same technique to obtain amorphous carbon needles at 250 °C. This method was claimed to have the simplicity both in terms of process control and the equipment setup which was favourable for large-scale production. Additionally, the as-prepared α-CNTs were reported to have a good field emission property (Banerjee *et al.*, 2009; Jha *et al.*, 2011). The chemical approach used for synthesizing α-CNTs in this work is same as the aforementioned techniques. Besides, α-CNTs had even been coated with lead (II)

sulfide (PbS) successfully and showed enhanced field emission property (Jana *et al.*, 2011).

2.4 Properties of Amorphous CNTs

α-CNTs have unique nanostructures that render them outstanding mechanical and electronic properties. Properties of nanotubes can also be expanded to optical and thermal properties as well. These characteristics have sparked great interest in their possible applications such as nanoelectronic device, electro optic, sensor and probe, composite, batteries, hydrogen storage, catalyst support and others. The comprehension on properties of nanotubes is important in the field of research in order to develop novel applications by selecting nanotubes based on their suitable characteristics accordingly. Some brief information about the general properties of CNTs is shown in Table 2.1. Herein, four major properties of nanotube which are mechanical, thermal, electronic and optical aspects will be explained in brief.

Table 2.1 : Selected electrical and mechanical properties of CNTs (Peter, 3009).

	Characteristics	Measure
#	Electrical conductivity	Metallic or semi conducting
❖	Electrical transport	Ballistic, no scattering
	Maximum current density	10^{10} A/cm^2
	Thermal conductivity	About 6 kWm^{-1}K^{-1}
	Diameter	1-100 nm
	Length	Up to millimeters
	Gravimetric surface	>1500 m^2/g
➤	E-modulus	1000 GPa, harder than steel

❖ These one-dimensional nanotubes exhibit electrical conductivity as high as copper, thermal conductivity as high as diamond.

❖ Nanotubes can be either electrically conductive (metal) or semi conductive (semiconductor), depending on their chirality (helicity).

➢ Strength 10 - 100 times greater than steel at faction of the weight; High strain to failure.

2.4.1   Mechanical and Thermal Properties

The mechanical characteristic of a solid depends largely on the strength of its interatomic bonds. Based on the known knowledge on the property of graphite, the mechanical property of CNTs is excellent whereby their elastic modulus is greater than 1 TPa and have high strengths (10 - 100 times higher than the strongest steel at a faction of weight), according to their experimental and theoretical results. Nanotube reinforced composites such as boron nitrides (BN), boron carbides (BC_3), and carbon nitrides (CN) are predicted to have the highest Young's modulus. The nanotubes have also been discovered to be flexible as they can be elongated, twisted, flattened or bent into circles before fracturing. These characteristics are due to their 'twist-like' nanostructures, allowing the structure to relax elastically while under compression. Instead, carbon fibers will be fractured easily (Saito *et al.*, 1998; Melissa *et al.*, 2007; Peter, 2009).

A phonon is the quantum acoustic energy similar to the photon. The existence of phonons is due to the lattice vibrations observed in the Raman spectra. These phonons are responsible for determining the thermal property of CNTs that includes specific heat, heat capacity and thermal conductivity. It was predicted that CNTs had unusual thermal conductivity of 6600 $Wm^{-1}K^{-1}$ for an isolated (10, 10) nanotube at room temperature (Berber *et al.*, 2000). However, thermal conductivity is one-dimensional for nanotubes

like electrical conductivity and therefore, the measurements of this characteristic give a broad range in 200 - 6000 $Wm^{-1}K^{-1}$, depending on the nanotube quality and alignment. Nanotubes may have similar thermal properties at room and elevated temperatures but unusual behaviour at a low temperature because of the effect of phonon quantization (Meyyappan, 2005). On the other hand, the measurement of thermoelectric power of nanotube is capable of providing direct information for the type of carriers and conductivity mechanisms (Melissa *et al.*, 2007).

2.4.2   Electronic Properties

The relatively low growth temperatures for the α-CNTs provide a more practical prospect for a large-scale production for many applications. However, the electronic properties of α-CNTs are not well studied and developed from the past to the present. In fact, the effect of defects and disorder play important influence towards the electronic properties of α-CNTs. Understanding the role of defects is essential for the exploration into nanotubes electronic structure as well as transport properties to enable a better comprehension on the α-CNTs.

In fact, the electronic properties of crystalline CNTs are sensitive to their geometric structure with different sized of energy gaps, depending strongly on the diameter and helicity or chirality of the tubes, characterized by the chiral vector (n, m). In contrast, for α-CNTs, a definite helicity could not be defined due to the lack of long-range periodicity in these tubes. The periodic boundary conditions along the circumference of the tube used to determine the electronic properties of crystalline CNTs are absent in α-CNTs. Nevertheless, this amorphous nanotube structure is assumed to have a locally "soft" lattice, whereby the elastic energy per carbon atom is less than that for the crystalline CNTs. Consequently, the electronic-lattice interactions

in α-CNTs are enhanced (Matthews *et al.*, 1999). The electronic states at the Fermi energy could become unstable and would cause an energy gap that lowering electronic energies below the Fermi level (total system energy). Therefore, α-CNTs are predicted to display a semiconductor band gap (E_g) that scales inversely with the nanotube diameter. This E_g shows a similar trend as for crystalline CNTs but with a more rapid increase with the inverse diameter (Rakitin *et al.*, 2000).

2.4.3 Optical Properties

The optical properties of CNTs refer specifically to the UV-Vis optical absorption, Raman, FTIR and photoluminescence spectroscopy studies. These methods offer quick, non-destructive and reliable characterization of the "nanotube quality" on CNTs. This so-called "nanotube quality" is strongly related to non-tubular carbon content, structure (chirality) and structural defects (impurities) of the as-produced nanotubes. These features play important roles on governing CNTs properties such as optical, mechanical and electrical properties. Despite the fact that mechanical, electrical and electrochemical (supercapacitor) properties of the CNTs are well-established and have immediate applications, the practical use of optical properties is yet unclear. Some applications can be seen in optics are such as emitting diodes (light) and photonics or photo-detectors based on SWCNTs (Freitag *et al.*, 2003; Chen *et al.*, 2005). The fundamental optical properties of CNTs have been investigated for relatively long time. In this section, the use of different optical spectroscopy for characterizing CNTs will be considered.

Optical absorption spectroscopy has not been widely used to study CNTs as this method is not informative enough to determine nanotube structure. According to a previous study on as-prepared and purified SWCNTs (Kataura *et al.*, 1999), three absorption peaks were observed to superimpose on the absorption spectra with their

positions varied slightly between spectra from SWCNTs with different diameter distributions. Such resulted absorption bands are due to transitions between spikes in the densities of states in the electronic structure of the nanotubes. Based on the fact that the positions of these singularities in the densities of states depend on the structure and diameter of the nanotube, the Kataura plot is then produced (Figure 2.5). Kataura plot shows peaks (theoretical gap energies between mirror-image spikes) should be observed in an absorption spectrum for tubes with a given range of diameters. Based on this plot, the absorption features from nanotubes with different structures often overlap, giving an obscure comprehension about nanotube structure. Thus, this plot indicates that simple optical absorption spectroscopy is limited in indentifying nanotube structure.
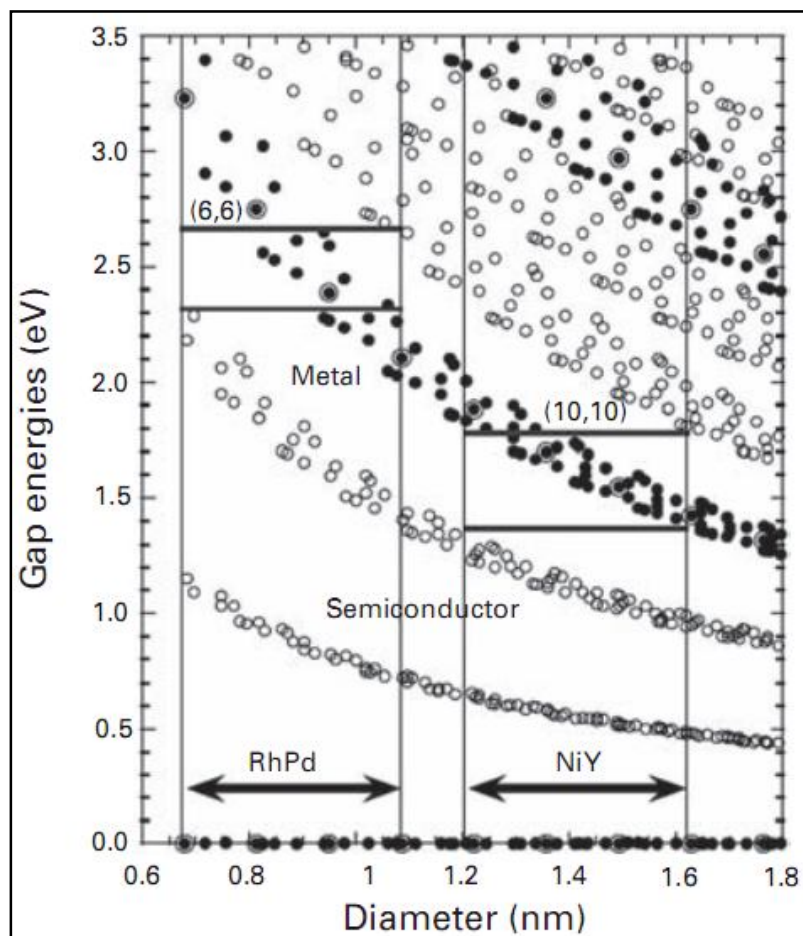
Figure 2.5 : The Kataura plot that shows calculated gap energies with different diameters for different types of materials (Peter, 2009).

CNTs have been proven to have capabilities of acting as either a metallic or semiconductor, which depends on tubule diameter and chiral angle. For metallic nanotube, metallic conduction can be achieved without introduction of doping effects. Meanwhile, for semiconducting nanotube, the E_g have been discovered to be proportional to a fraction of the diameter and there is no relationship between E_g and the tubule chirality (Saito *et al.*, 1998).

CNTs show the phenomena of Raman scattering when an electromagnetic wave is irradiated to them. The incident beam can be transmitted, absorbed or scattered by the molecules of CNTs. Raman scattering is the inelastic scattering of a photon. This occurs when an electron is excited by an incident photon (an electromagnetic wave irradiates onto a sample) and transfers from the electronic ground state to the first electronic excited state. The excited electron loses or gains energy by emitting or absorbing a phonon. Then it emits a photon and relaxes back to the ground state. There are two types of Raman scattering: Stokes and anti-Stokes process. The energy level diagram of these two scattering processes is shown in Figure 2.6. In Stokes scattering, the molecule obtains energy by absorbing a phonon, while in anti-Stokes process, the molecule loses energy since it emits a phonon (Jorio *et al.,* 2008).

Figure 2.6 : Energy level diagram of stokes and anti-stokes Raman scattering.

In general, Raman spectroscopy is a non-destructive and sensitive testing. In comparison to optical absorption spectroscopy, Raman measures phonon frequencies. Information about the electronic structure of nanotubes could be provided via this technique under resonance condit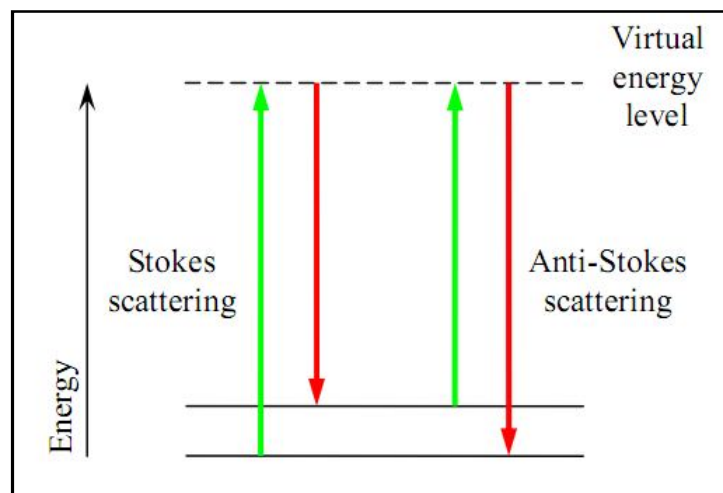ions. Since the electronic structure of a nanotube is distinctively determined by its (n, m) indices or chiral vector, the determination for the geometrical structure of a SWCNT from the resonance Raman spectrum is then possible. Thus, by conducting resonance Raman spectroscopy, chiral vector of isolated nanotubes can be inferred (Dresselhaus *et al.*, 2002). This technique is functioned based on: when the incident or scattered photons are in resonance with the energy of strong optical absorption electronic transitions (electronic transition between the singularities in the valance and conduction bands), the Raman intensity becomes large due to the strong coupling between the electrons and phonons. Both the nanotube diameter and chiral vector are thus depended on the various features (G-, D-lines or -bands and radial breathing mode (RBM)) in a Raman spectrum (Figure 2.7). Consequently, these features can also be used to determine nanotube diameter (Peter, 2009).

In this work, Raman spectroscopy acts as a method for detection of nanotubes in bulk samples and provides deep and comprehensive understanding on the structure of the nanotubes. The quality or structural ordering of nanotubes can be estimated efficiently. Thus, Raman is an essential characterization tool to provide information about the extent of the amorphous and structural disorders of α-CNTs after some treatments being conducted. The involved treatments in this work are such as purification, oxidation and hybridization processes. According to literature, CNT shows two independent peaks between 1000 cm^{-1} and 2000 cm^{-1} along its Raman spectrum. The band at about 1360 cm^{-1}, called D-band, corresponds to the Raman-inactive A_{1g} in-plane breathing vibration mode. In other words, the D-band is associated with the

vibrations of carbon atoms with dangling bonds in plane terminations of disordered graphite or glassy carbons. It represents the presence of dispersive defects within the hexagonal graphitic layers. Another band appeared at a higher frequency range of 1500 ~ 1600 cm^{-1} is called G-band. The G band is attributed to the Raman-active E_{2g} in-plane vibration mode of graphite, which are related to the vibration of sp^2 bonded carbon atoms in a two dimensional hexagonal lattice, such as in a graphite layer (Cheng *et al.*, 2006; Passacantando *et al.*, 2008).
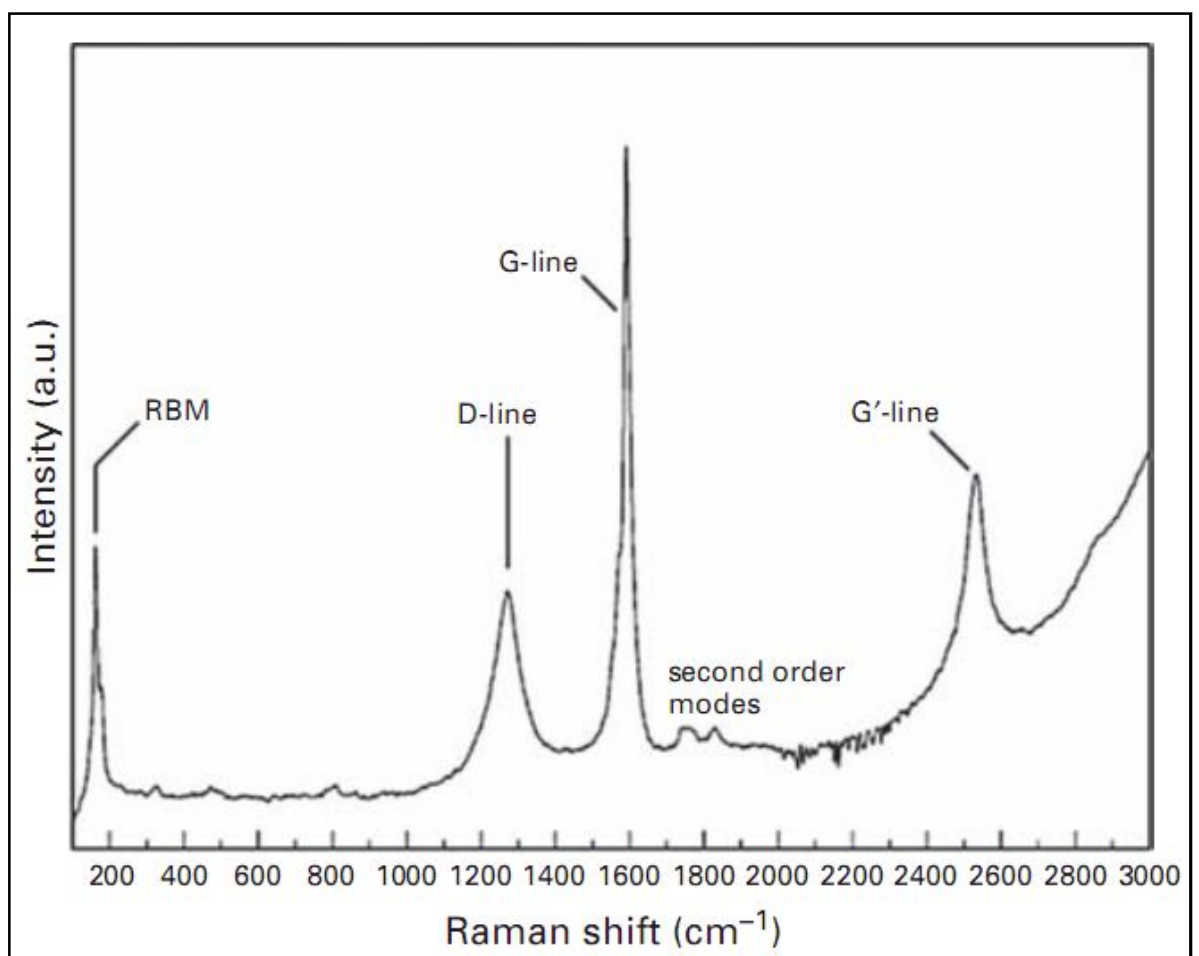

Figure 2.7 : A typical Raman spectrum from a SWCNT sample (Peter, 2009).

2.4.4 Dielectric Properties

Every material has a unique set of electrical characteristics that are dependent on its dielectric properties. Accurate measurements of these properties can provide

scientists and engineers with valuable information to properly incorporate the material into its intended application for more solid designs or to monitor a manufacturing process for improved quality control. A dielectric material's measurement can provide critical design parameter information for many electronic applications. The recent industrial applications such as microwave heating (microwave processing of food, rubber and plastic), energy storage, electro optics, non-destructive sensing for quality of fresh produce have also been found to benefit from knowledge of dielectric properties (Nelson *et al.*, 2007; Yang *et al.*, 2009). To solve the electromagnetic compatibility (EMC) and electromagnetic interference (EMI) problems, microwave absorbers (wireless communications devices, EMC in building, etc.) can be used to minimize the electromagnetic reflection. A low reflecting absorber in a desired frequency range can be prepared by fulfilling two fundamental conditions; an incident wave able to enter an absorber by the greatest extent (impedance matching characteristics) and good attenuation and absorption effects on the wave entering into a material is attained (Hussain *et al.*, 2007; Li, *et al.*, 2010).

In general, a material is classified as "dielectric" if it has the ability to store energy when an external electric field (E) is applied. Dielectric property can be defined in term of complex dielectric constant or relative complex permittivity (ε_r). This permittivity describes the interaction of a material with the E and is a complex quantity (Neelakanta, 1995). Thus, ε_r consists of a real part of relative complex permittivity / dielectric constant (ε') and an imaginary part of relative complex permittivity / dielectric loss factor (ε''), as shown in Equation (2.1):

$$\varepsilon_r = \varepsilon' - i \cdot \varepsilon'' \qquad\qquad (2.1)$$

The notation ε' is associated with energy storage and ε'' is associated with loss or energy dissipation within a material. In detail, ε' is a measure of how much energy from an external electric field is stored in a material while ε'' is a measure of how dissipative or lossy a material is to an external electric field (Hussain *et al.*, 2007). The ε'' includes the effects of both dielectric loss and electrical conductivity. Dielectric loss can occur due to the electrical conduction processes and effects of both dielectric resonance (associated with electronic or atomic polarization) and dielectric relaxation (associated with orientation polarization) (Neelakanta, 1995).

The relative complex permittivity is not constant. It can vary with frequency, temperature, orientation, mixture, pressure and molecular structure of the material. It is used to characterize materials such as dielectrics, metals and semiconductor. From a measurement point of view, the only differences between these materials at microwave frequencies are related to the values of ε' and ε''. The metals have the imaginary part that is much higher than the real part while for dielectrics always the real part is larger than the imaginary one.

The selected measurement technique for the ε_r at microwave frequencies is a non-resonant technique, which is based on reflection-transmission approach. From the measured complex reflection and transmission coefficients, a computer-controlled vector network analyzer (VNA) with the aid of coaxial probes is used to determine the ε' and ε'' a sample. The coaxial probes are one of the techniques well-suited for measurement of non-magnetic materials that offer quick, convenient, relatively cheap and non-destructive testing over broadband frequency coverage (Krupka, 2006). Sample preparation is easy in which only small quantities of samples are required.

To date, data concern the dielectric constants of CNTs at microwave frequencies is hardly found in the literature. This related research has rarely reported because the CNTs have high absorption to electromagnetic waves and so small to be measured by traditional method. It is said that the dielectric constant study of various kinds of CNTs is still premature. Their relative complex permittivity is hard to be confirmed since the dielectric properties strongly depend on the accurate determination of the numbers of wrapped sheets, radius, length, surface oxidation and molecular defects, which are difficult to be determined accurately. In a recent work on both SWCNTs and MWCNTs, the increase and decrease of the ε' and ε'' with the frequency were observed. The quantum size effect associated with sizes, length and structures of the nanosized CNTs intimately controlled their dielectric constant (Li *et al.*, 2007; Wang *et al.*, 2009).

Common polymers with very low dielectric constant ($\varepsilon_r < 3$) are not the suitable materials for making modern electronic and electric power systems. However, combinations between CNTs and polymers to form CNTs-based composites are essential for their ε_r enhancement (Li *et al.*, 2008). Additionally, surface modification on CNTs also improves compatibility between CNTs and polymer matrix. Flexible dielectric polystyrene-based composites containing MWCNTs coated with polypyrrole had been synthesized and exhibited a stable ε_r while retained their low dielectric loss characteristics, which suited such composites as high-energy-density capacitors and energy storage applications (Yang *et al.*, 2009).

2.5   Potential Applications of Amorphous CNTs

CNTs of various structures have been reported as novel functional materials for many unique applications in nanotechnology, semiconductors, electronics, optics, medical delivery systems and other fields of materials science. Among various types of

CNTs, the α-CNTs with their novel properties have enabled them becoming potentially useful in many applications such as gas storages, gas separations, catalyst supports and electron emissions. α-CNTs can be used as catalysts or catalyst supports because they have nanometric structure and high surface area. Carbon aerogels consisted of amorphous carbon have been made into supercapacitor materials and thermal insulators due to their low electrical resistivity, high surface area and good polarizability properties at an ambient pressure (Wu *et al.*, 2002). To date, α-CNTs have been proven to possess a unique structure mainly because of their amorphous walls and nanometric tubular shapes. Indeed, the construction of novel nanostructures of α-CNTs results in excellent properties (as mentioned before in previous sections).

The tubules of α-CNTs made of the amorphous wall with a lot of defects render a great contribution for α-CNTs to be applied into gaseous adsorbent products, nano-devices and electro optics especially for the field emission display devices. It was reported that α-CNTs had impressive field emission properties because of their high aspect ratio and low electron affinity making them as the excellent emitter. For the prospect of technology applications, good electron emissive materials should possess low threshold emission fields and superb stability at high current density (Melissa *et al.*, 2007). α-CNTs have the right combination of properties whereby they have nanometric diameter, structural integrity, electrical conductivity and chemical stability. Moreover, the relatively simple in preparing the α-CNTs may enhance their applications in the various fields of industry (Ahmed *et al.*, 2007a; Ahmed *et al.*, 2007b; Banerjee *et al.*, 2009; Jha *et al.*, 2011).

Graphite, carbonaceous materials and carbon fiber electrodes have been applied in fuel cells, batteries and several other electrochemical applications. CNTs are now being

considered for the mentioned applications. Herein, α-CNTs can be potentially applied as a coating substance for lithium ion batteries. The cycling performances of lithium batteries are greatly improved due to the role of amorphous nanotubes with high electrochemically accessible surface area of porous nanotube arrays combined with good electric conductivity. For instance, nanowire arrays of single-crystal tin dioxide (SnO_2) coated with α-CNTs has been easily fabricated and used as anodes in lithium ion batteries. The highly ordered tetragonal single-crystal SnO_2 nanowire arrays are formed by filling them towards anodic AAO template, followed by drying and annealing via a sol-gel route that employs a citric acid chelating agent. The as-prepared nanowires are then coated with in situ formed α-CNTs (Zhao *et al.*, 2009). The final microstructure of this combination has the advantage of regular electron screening length in the lateral direction and its outer carbon layer provides the electronic transportation. Thus, nanowire arrays of α-CNTs coated oxides can be applied as an ideal host for lithium storage (Zhao *et al.*, 2008; Zhao *et al.*, 2010).

CNTs become also the very promising candidate for hydrogen storage application due to their small dimensions, smooth surface topology and perfect surface specificity. Nanotubes with very poor crystallinity (α-CNTs) could be produced in mass via the floating catalyst method (CVD). These as-grown amorphous nanotubes showed to be a different structure from the nanotubes prepared by other methods, resulting in unique structure of the as-grown amorphous nanotubes. Subsequently, annealing treatment was subjected to the amorphous nanotubes, making them to have improved hydrogen storage capability due to the changes in their surface feature and microstructure (Ci *et al.*, 2001; Ci *et al.*, 2003). Meanwhile, by heating a mixture of PTFE and ferrous chloride tetrahydrate inside a horizontal quartz tube furnace, the as-prepared α-CNTs had large

interlayer spacing and thus providing a good adsorption capability to accommodate small gaseous molecules, especially for hydrogen gas (Nishino *et al.*, 2003).

On the other hand, microbatteries are very essential to serve microelectromechanical (MEMS) and nanoelectromechanical (NEMS) system (Zhang *et al.*, 2005). In order to obtain superior performance for microbatteries, the stabilities and efficiencies of cathodes of microbatteries must be enhanced. Individual nanotubes become attractive candidates for electrode materials of microbattery systems due to their excellent chemical stability, low resistivity, low mass density and large surface area (Melissa *et al.*, 2007). By using some sort of CVD process, the as-prepared nanotubes grown on Ni deposited porous alumina substrates in a medium of a flowing gas mixture of methane and hydrogen are mixed with the vanadium oxide (V_2O_5) sol-gel to form a composite and being applied to the cathode.

The excellent mechanical property of nanotubes enables the formation for a new class of composite materials. The first commercially used for MWCNTs was electrically conducting components in polymer composites (Melissa *et al.*, 2007). The great advantage offered by amorphous nanotubes is that they can achieve high stiffness along with high strength. Consequently, they could perform as reinforcing phases with polymer, ceramic and metallic matrices. For example, they acted as reinforcing component in ceramics because of their graphitization behaviour during the sintering process at a high temperature (Ci *et al.*, 2001). For industrial applications, large quantity of nanotube reinforced composites will be required; CVD technique offers the best method for high quantities and low cost production. Recent work showed that rubber compounds reinforced by nanotubes are potential applications in tire industry. By substituting the carbon black with CNTs, skid resistance was improved and abrasion of

tire was reduced. Nanotubes may provide a safer, faster, and eventually cheaper transportation (Kueseng *et al.*, 2006).

The development of novel methods for imaging, sensing and measurement is very vital in modern research. CNTs have been proven to offer some advantages for sensing applications. Their superb mechanical property and unique geometry enable them to be potentially used in atomic force microscopy (AFM). The high strength of nanotubes and low buckling force extend the probe's life by reducing damages during repeated hard hits into a specimen. To date, AFM tips often unable to probe narrow crevices on a specimen surface. Nanotubes with their cylindrical and elongated tubules of extremely small diameter are able to probe narrower fissures and even produce higher resolution imaging in comparison to conventional probes (Melissa *et al.*, 2007; Peter, 2009).

Besides, the small size of nanotubes with larger surface, good reversibility and fast response at room temperature make them suitable to be applied as a gas sensor. It was discovered that electronic properties like electrical resistivity of nanotubes are very sensitive to the presence of oxygen, nitrogen and ammonia (Collins *et al.*, 2000). The detection of different gases is quite faster than the conventional gas sensors. The nanotubed-made sensors could be operated at room temperature or at higher temperatures. Studies have also shown that surface modification conducted on CNTs enhanced the sensitivity of the nanotube sensors. Furthermore, the potential biosensors made of nanotubes also provide better retention capability of activity for their relevant purpose (Gao *et al.*, 2003).

There is a great research interest to work on the hybridization between CNTs and other compounds (both organic and inorganic compounds). The compounds are attached

on the surface of CNTs for optimizing their performance in various potential applications. Nanocrystalline semiconductors are always selected to decorate CNTs due to their size dependent optical, structural and electronic properties (Dinesh *et al.*, 2007). They have attracted a great attention since an as-prepared final hybrid material may have combined properties of two functional materials to provide a wide range of applications. Various semiconductor nanoparticles such as PbS, PbSe, CdS, ZnS, ZnO, TiO_2, SnO_2 and CdSe/ZnS have been attached on the surface of CNTs (Jana *et al.*, 2011). CdSe is another promising semiconductor material with its well-established optical properties. In this work, CdSe is referred as CdSe QDs. CdSe QDs are only useful and beneficial when they are in size below 100 nm. At this size, CdSe QDs only exhibit a property known as quantum confinement. Basically, quantum confinement occurs when the electrons in a material are confined to a very small volume. Since CdSe QDs have a size dependent fluorescence spectrum due to the effect of quantum confinement and this phenomenon is size dependent, which means the properties of CdSe QDs are tunable based on their size (Hamizi *et al.*, 2010; Paul *et al.*, 2010). Therefore, these CdSe QDs are applied in optical devices such as laser diodes. CdSe QDs are also suitable for making thin-film transistors (TFTs) which have been used in the liquid-crystal display (LCD) devices widely. These materials are also developed for use in biomedical imaging applications by injecting them appropriately into an injured human tissue. The human tissue is permeable to far infra-red light (Chan *et al.*, 1998).

CHAPTER THREE: MATERIALS AND METHODS

This chapter describes the precursor materials and the synthesis steps used in the study. The raw materials have been selected properly to suit the production of the α-CNTs and the hybrid material (α-CNTs/CdSe QDs) via a series of the involved research design and the research procedures. All relevant characterization methods with required conditions are also explained.

3.1   Raw Materials

The main precursor materials used in this work are ferrocene ($Fe(C_5H_5)_2$) and ammonium chloride (NH_4Cl) powders. $Fe(C_5H_5)_2$ powder with purity of 98 % was produced by ACROS Organics. It is an organometallic chemical compound which consisting of two cyclopentadienyl rings bound on opposite sides of a central metal atom. It acted as the carbon source for the formation of α-CNTs. On the other hand, NH_4Cl compound with analytical grade was used as the catalyst during the reaction.

Concentrated hydrochloric acid (HCl) in molarity of 5 M, methanol (CH_3OH) with purity up to 99.8% and deionised water with had been purified ((>15.0 MΩ cm) were used for purification treatment. A mixture of diluted sulphuric acid (H_2SO_4) and nitric acid (HNO_3), with molarities of 5 M, respectively in ratio 3:1 were also prepared to serve the purpose of performing oxidation. The oxidized α-CNTs were then hybridized by the as-prepared cadmium selenide (CdSe) QDs. On the other hand, the CdSe QDs was synthesized via inverse micelle technique by employing four other chemical reagents: cadmium oxide (CdO), selenium (Se), paraffin oil and oleic acid. The usage of $Fe(C_5H_5)_2$, the preparation of acid solutions into suitable concentration and the synthesis of CdSe QDs were all conducted under a fume hood due to the strong

characteristic odour and safety purpose. All mentioned analytical chemicals were used as received without any further purification.

3.2 Preparation of Amorphous Carbon Nanotubes

As-prepared samples were synthesized via a modified reduction process (Figure 3.1). Briefly, 4 g of NH_4Cl (analytical grade) and 2 g of $Fe(C_5H_5)_2$ (ACROS Organics, 98 %) were mixed homogenously. The mixture was then transferred to a Parr reactor with capacity of 125 mL. The Parr reactor was sealed and heated to 230 °C inside a convection oven and was hold at this temperature for 30 minutes. After the Parr reactor was cooled down to room temperature, the mixture was taken out and again being mixed homogeneously. The whole heating process was repeated again for 30 minutes. The obtained black powder was named as untreated sample (as-prepared α-CNTs).
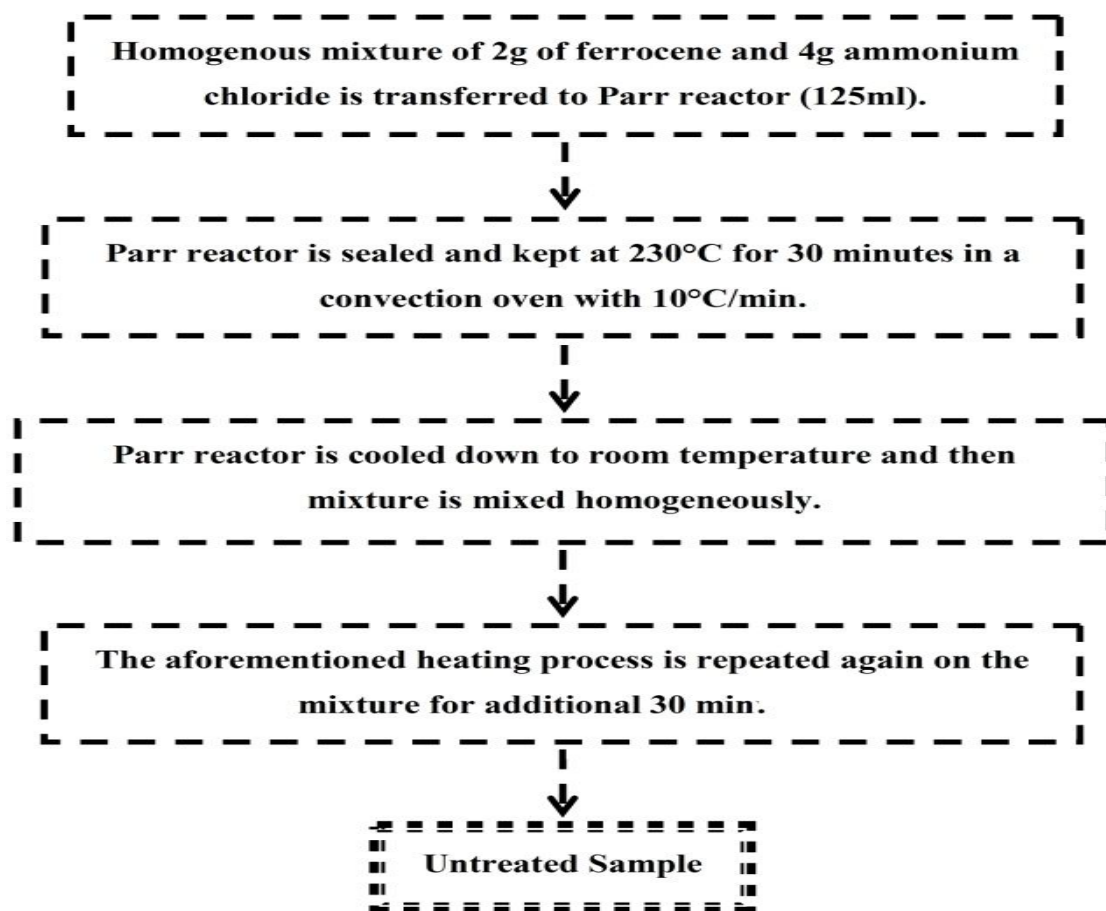

Figure 3.1 : Preparation flow chart for the untreated sample.

In the purification process as shown in Figure 3.2, the untreated sample was soaked and washed with concentrated HCl solution in 5 M, followed by CH_3OH (99.8%) and then by deionised water which had been purified (>15.0 MΩ cm). These processes were carried out for several times for better purification efficiency. Powder was collected on nylon filter membrane (0.2 μm) with aid of a vacuum pump. Dehydration was performed using a vacuum oven at 80 °C for 10 h to obtain the sample which was named as treated sample (treated α-CNTs).
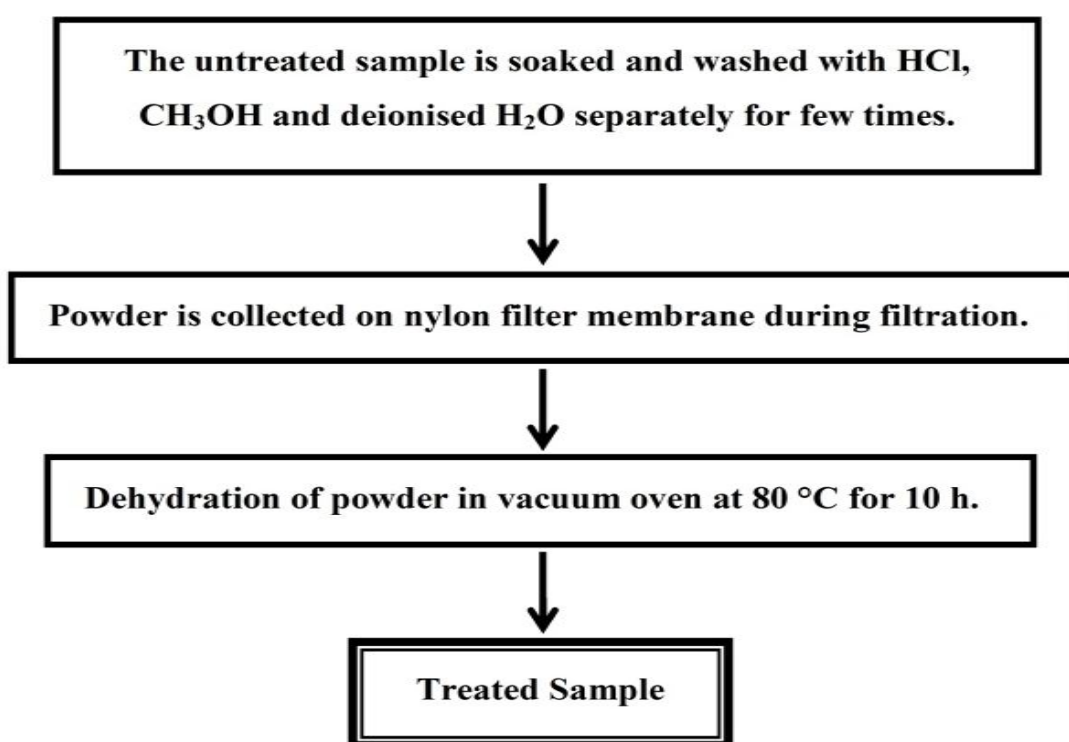
Figure 3.2 : Preparation flow chart for the treated sample.

A mixture of H_2SO_4 and HNO_3 with concentrations of 5 M each in ratio 3: 1 was prepared by mixing them while stirring for obtaining homogenous combination. For the purpose of oxidation (Figure 3.3), the treated sample was immersed into this solution, then ultrasonicated in an ultrasonic bath for 2 h followed by constant stirring for overnight (12 h). Subsequently, this solution was neutralized by ammonium hydroxide

(NH$_4$OH) solution. The oxidized sample (oxidized α-CNTs) was collected using the same way as done for the treated sample.
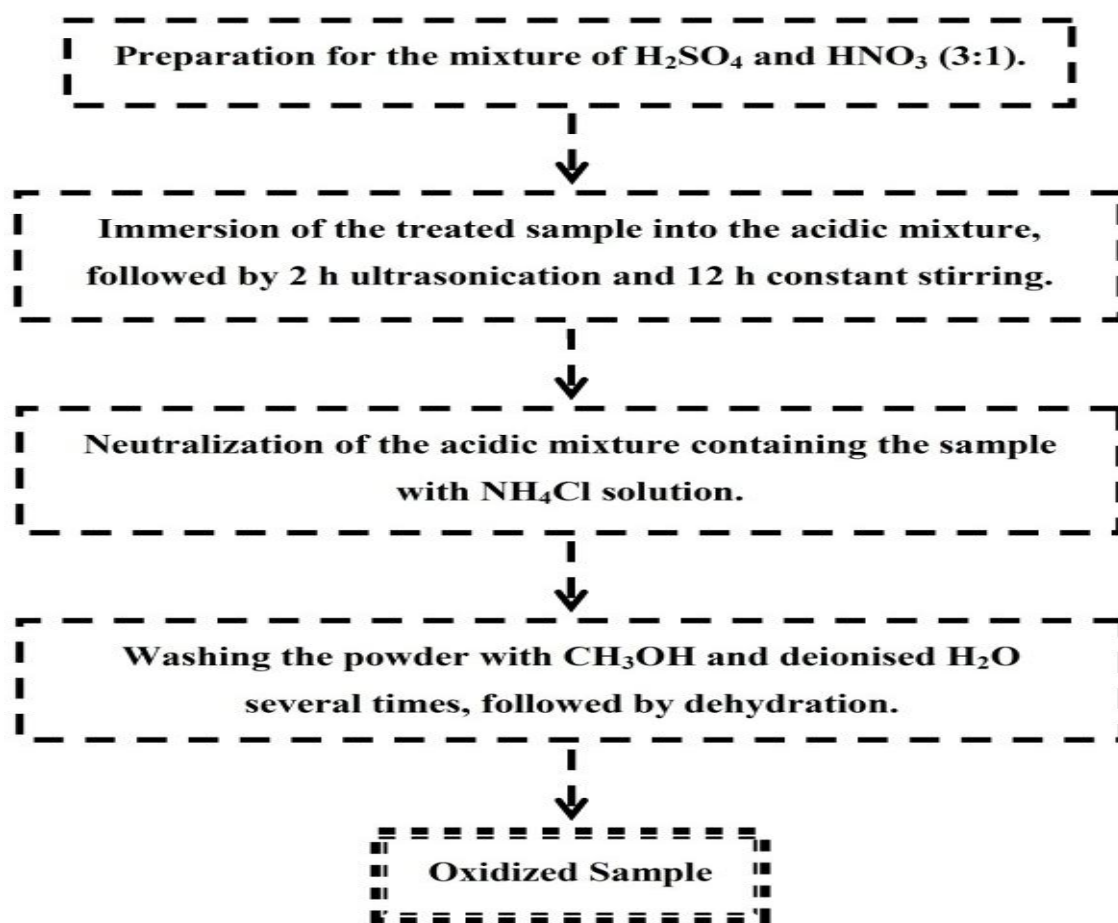
Figure 3.3 : Preparation flow chart for the oxidized sample.

The oxidized sample was then hybridized by the as-prepared CdSe QDs via a simple route as shown in Figure 3.4. The as-prepared CdSe QDs were dissolved in pyridine solution of 10 ml and ultrasonicated for 2 h. On the other hand, the oxidized sample was dissolved in CH$_3$OH solution of 40 ml and ultrasonicated for 20 min. Both dissolved solutions were then mixed together and ultrasonicated for 10 min and the combination was finally stirred for 20 h to facilitate hybridization between the oxidized α-CNTs and CdSe QDs.
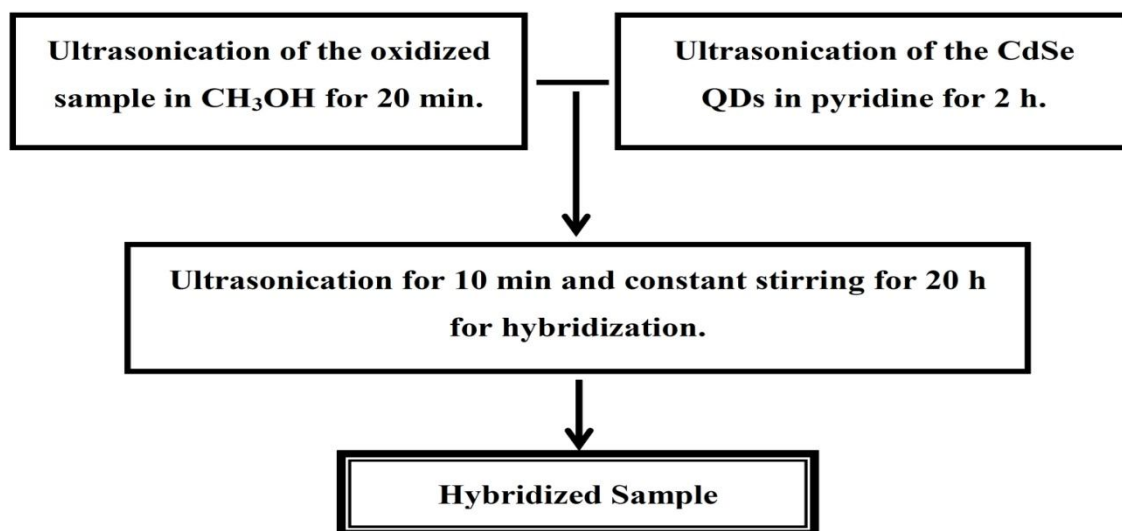
Figure 3.4 : Preparation flow chart for the hybridized sample.

The as-prepared CdSe QDs were synthesized via an inverse micelle technique whereby the preparation steps were in accordance with the methodology being explained in a recent work (Hamizi *et al.*, 2010). The CdSe QDs were synthesized by employing four other chemical reagents: CdO, Se, paraffin oil and oleic acid. The details of the preparation steps for CdSe QDs are shown in Figure 3.5.

Figure 3.5 : Schematic of preparation steps for CdSe QDs.

3.3   Characterization Methods

All samples (untreated sample, treated sample, oxidized sample, hybridized sample and CdSe QDs) were studies by few characterization methods, which could be divided into a few aspects: morphological, microstructural, elemental, optical, thermal and complex permittivity (dielectric) studies.
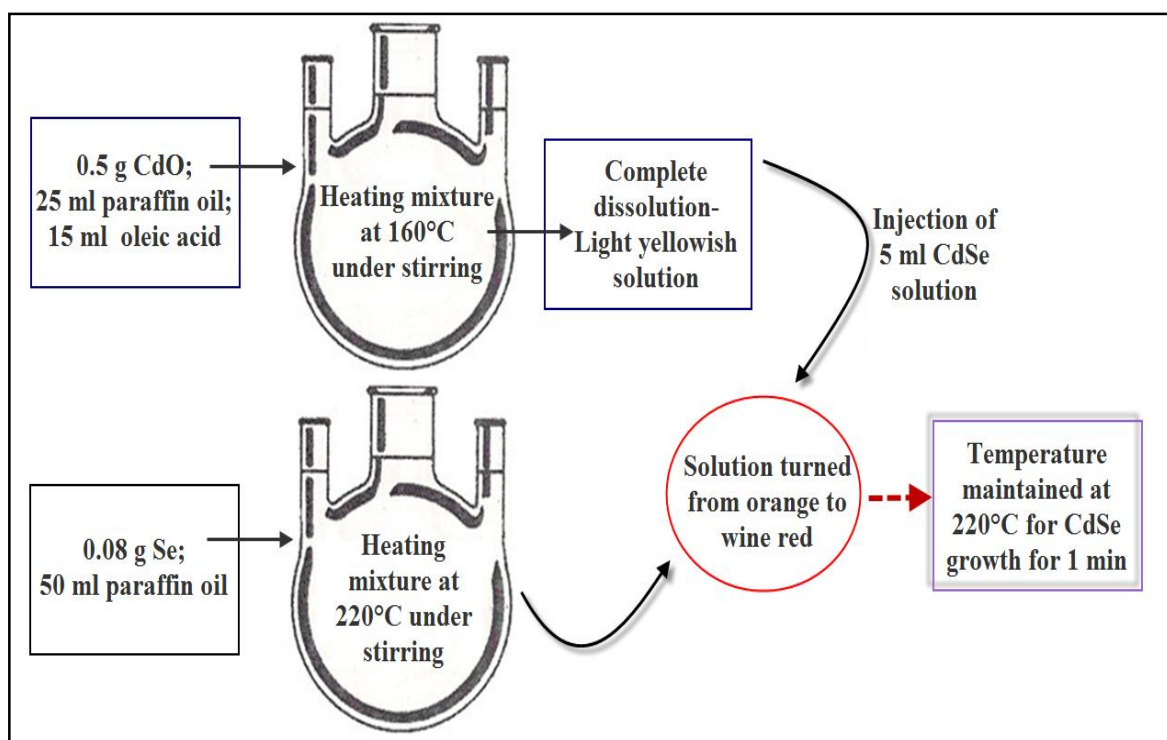
3.3.1.   Morphological Studies

All samples were observed under TEM (LIBRA® 120, Germany), HRTEM (Philips TECNAI 20, Netherlands) and FE-SEM (AURIGA, ZEISS, Germany) to study a qualitative analysis on the nanotubes surface morphology and microstructure. The used of TEM was operated using an accelerating voltage of 120 kV. For the HRTEM, images in high resolution were obtained using an accelerating voltage of 200kV that could produce magnification up to 1,000,000 x. Accessories of scanning transmission electron microscopy (STEM) and energy dispersive X-ray (EDX) spectrometer were embedded within this equipment as well. The FE-SEM was equipped with detectors of secondary electrons and an EDX spectrometer. The micrographs were generated by backscattered electron detector in FE-SEM. All of these characterization methods could estimate the morphology and geometry (diameter and length) of nanotubes.

3.3.2.   Microstructural Studies

Microstructural analysis was studied by using XRD (SIEMENS D5000, German) with Cu-K α X-radiation of wavelength 1.54056 Å at 60 kV and 60 mA. The diffraction was conducted in the Bragg angles between 5 ° to 100 ° in order to examine the crystallinity of nanotubes and CdSe. The presence of elements could also be performed and identified.

3.3.3. Elemental Analysis

EDX spectrometer embedded in both HRTEM and FE-SEM equipments was employed to conduct elemental analysis on the nanotubes at room temperature. During an observation, EDX test was performed under the STEM mode using the mentioned HRTEM above. The EDX test was also carried out by the FE-SEM. The EDX was conducted after HRTEM and FE-SEM images being captured. The voltage used for this test should be more than 10 kV and located at 8 mm working distance in order to obtain better quantitative elemental analysis.

3.3.4. Optical Studies

The UV-Vis optical absorption was recorded using a spectrophotometry (Cary Win UV 50, Australia). By using a 1 cm quartz cuvette, the optical absorption and transmittance measurement were then scanned at a slow rate over the range 190 - 800 nm (ultraviolet, infrared, visible and adjacent regions). Prior to UV-Vis measurement, ultrasonication process was performed towards a sample containing nanotubes in methanol as solvent for 1 hour in order to provide better dispersion of the sample. Unlike solution containing nanotubes, pyridine was used as solvent for CdSe QDs and the whole solution was ultrasonicated for 20 h.

Raman characteristics of the α-CNTs were conducted by inVia Raman microscope (RENISHAW, United Kingdom). The He-Ne laser with wavelength at 633 nm was excited to a solution containing well-dissolved nanotubes. On the other hand, FTIR spectroscopy was carried out in the range of 400-4000 cm^{-1} via a FTIR spectrometer (PerkinElmer, Spectrum 400, USA) to study the attachment of bonding groups in the nanotubes. The FTIR measurements were taken on all samples which were made into

pellets (average diameter of 10 mm and average thickness of 2.8 mm) at room temperature.

3.3.5. Thermal Studies

Thermal stability of the α-CNTs was investigated using a TGA instrument (TGA/SDTA 851^e - Mettler Toledo) at heating rate of 10 °C per minute in temperature range of 40 - 1000 °C. The measurement was conducted in argon atmosphere. All samples with weight of about 5 mg were used for this thermal analysis. Results presented in TGA spectra were then analyzed with the V8.10 STAR e software package. The weight losses experienced by the samples would be studied to determine their thermal strengths.

3.3.6. Dielectric Studies

Dielectric study involving complex dielectric constant or called as relative complex permittivity ($ε_r$) on nanotubes was also performed by using a vector network analyzer (Agilent E5071C ENA Network Analyzer). The vector network analyzer (VNA) system consists of consists of a signal source, a receiver and a display to make swept high frequency stimulus-response measurements. The working principle of the VNA is based on coaxial reflection/transmission technique, whereby the measurement of the reflection from or transmission through a material provides the information to characterize the permittivity of the material.

All permittivity measurements were conducted in the frequency range of 500 MHz - 4.5 GHz (microwave region) at room temperature by applying a coaxial probe in such a way that a contact between the probe and a sample is obtained. Accurate

measurements require intimate contact between the coaxial probe and the sample. The coaxial probe designed in a slim form is capable of determine complex permittivity of liquids or semi-solids under non-destructive mode in real time. The measured values of reflected and transmitted scattering parameters were used to determine both real part of relative complex permittivity/dielectric constant (ε') and imaginary part of relative complex permittivity/dielectric loss factor (ε'') as the function of frequency, respectively. The test samples were made into pellets with the average diameter of 10 mm and average thickness of 2.8 mm, respectively.

CHAPTER FOUR: RESULTS AND DISCUSSION

In this chapter, four different samples are prepared, i.e.: untreated, treated, oxidized and hybridized samples are examined via several analytical techniques. The morphological, microstructural, elemental, optical, thermal and dielectric properties of the samples are thoroughly discussed.

4.1 Morphological Studies

Figure 4.1 presents both low and high magnifications of FE-SEM images of the untreated sample. The sample is visually sighted in black (Figure 4.19(a)). The nanotubes are observed in a random arrangement which are hardly recognized as a tube structure (Figure 4.1(a)). The observation of dark regions indicates the existence of porosity within the nanotubes. The rough surfaces of the nanotubes and closely bound together in bundles are obviously shown at the high magnification of FE-SEM image (Figure 4.1(b)). The nanotubes may have agglomerated to each other heterogeneously. These morphological features are similar with the amorphous nanotubes in the earlier works (Lou *et al.*, 2003; Jana *et al.*, 2011; Jha *et* al., 2011).
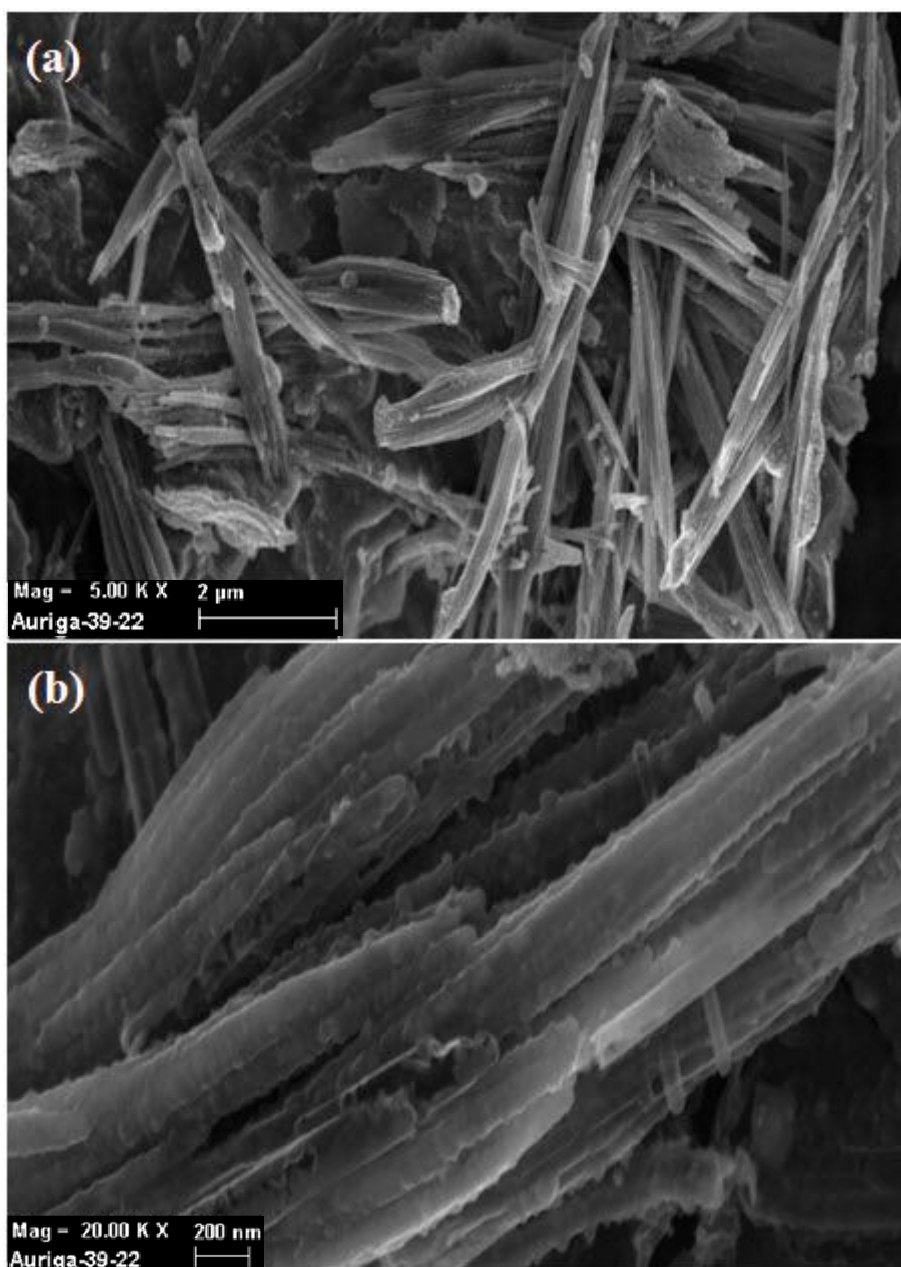
Figure 4.1 : FE-SEM images of the untreated α-CNTs at room temperature: (a) Low magnification; (b) High magnification.

Figure 4.2 shows the FE-SEM images at low and high magnifications for the treated α-CNTs with diluted acid. It shows the nanotubes having uniform diameters and open ends (within the white circle in Figure 4.2 (b)) after being treated with diluted acid, giving direct indication of tubular structures. The tubular structures of nanotubes become more visible in a higher magnification image due to the removal of residual

reactants and by-products. It is clear that the treated α-CNTs are also present in bundles due to the nature of nanotubes (Van der Waals).
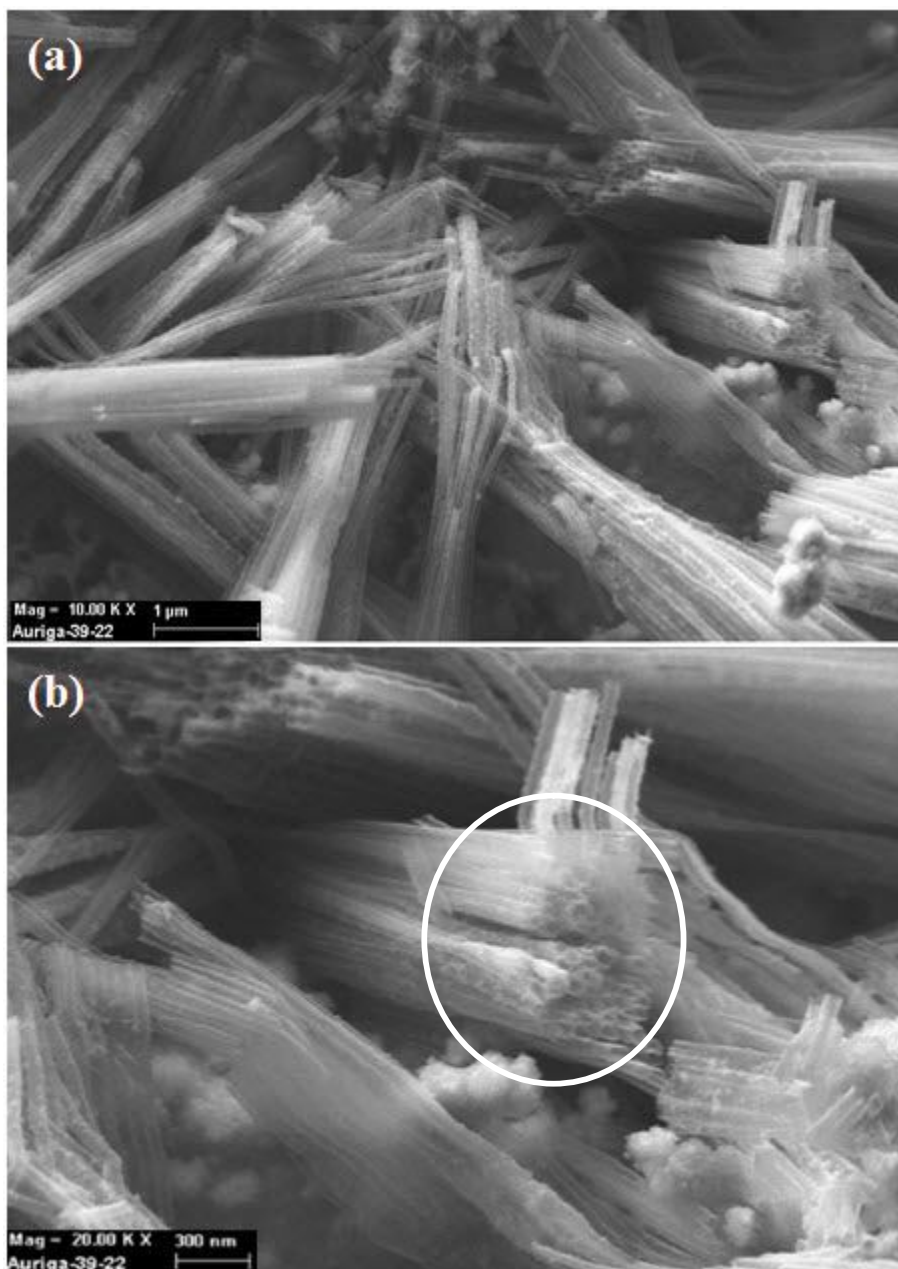

Figure 4.2 : FE-SEM images of the treated α-CNTs at room temperature: (a) Low magnification; (b) High magnification.

Figure 4.3 shows the FE-SEM image for sample after undergoing oxidation treatment. It is clearly shown that the nanotubes are not tightly bound but separated to

each other. The separation of nanotubes indicates that their agglomeration is reduced as a result of oxidation (Jha *et al.*, 2011).
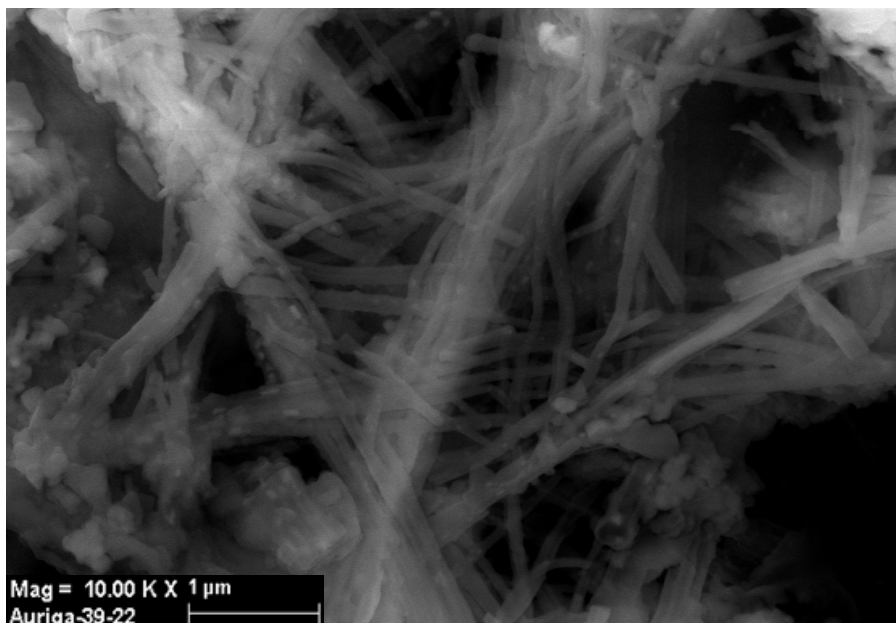

Figure 4.3 : FE-SEM image of the oxidized sample at room temperature.

Figure 4.4 shows the FE-SEM image of the hybridized sample with CdSe QDs. It is clear that most of the surfaces of the oxidized nanotubes have been attached by the CdSe QDs heterogeneously. The CdSe QDs are observed in darker tone.
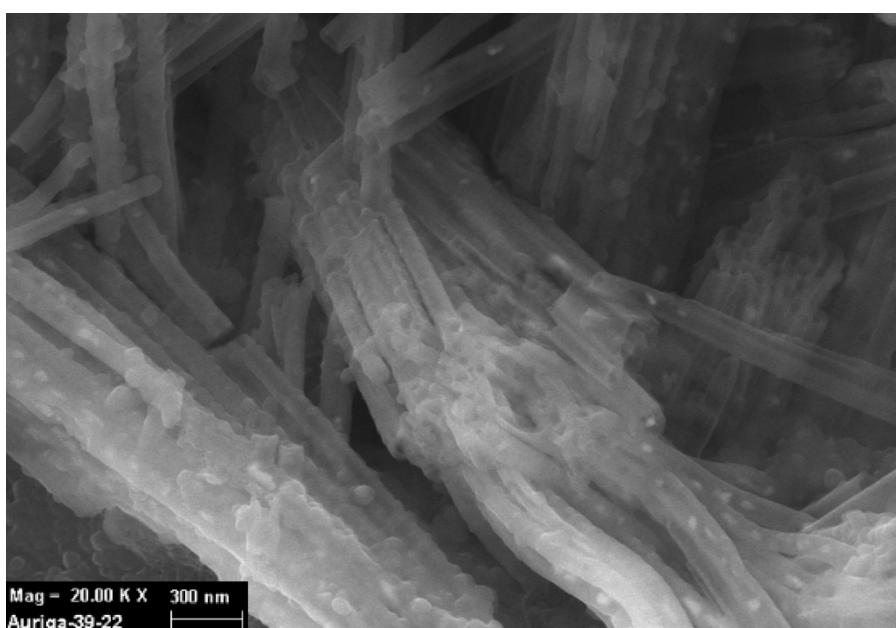

Figure 4.4 : FE-SEM image of the hybridized sample at room temperature.

Figure 4.5 shows the TEM image of the untreated nanotubes which aligned in bundle and closely bound to each other. The agglomeration of nanotubes is inevitable due to the nature of α-CNTs; high van de Waals force, large surface area and high aspect ratio (Jha *et al.*, 2011). The nanotubes are also surrounded by the unreacted NH_4Cl, as confirmed by the XRD analysis in Figure 4.14. Meanwhile, Figure 4.6 shows the HRTEM image of the nanotube wall of untreated sample. It is clear that no certain orientation is noticed and the image revealing the compact wall of the nanotube composed of amorphous carbon. This is in a good agreement with the XRD pattern shown in Figure 4.14. The carbon composition is also confirmed in the EDX analysis (Figure 4.16). It is also observed that a large amount of residual reactants is attached to the body of the untreated nanotubes, rendering the rough surfaces of nanotubes. These impurities are confirmed as the NH_4Cl compound by both of XRD and EDX analyses (see Figures 4.14 and 4.16). Their presence makes the structures of nanotubes hard to be noticed.
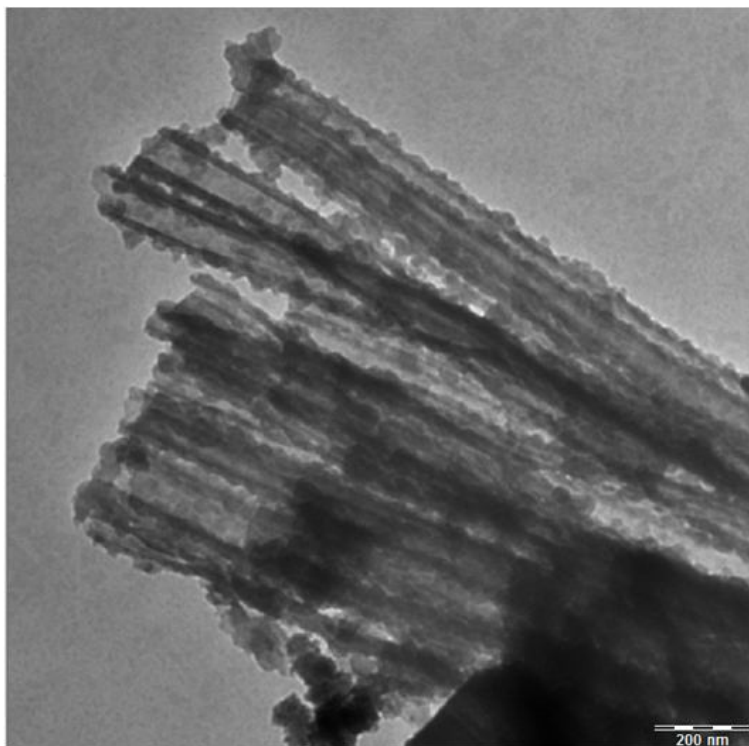

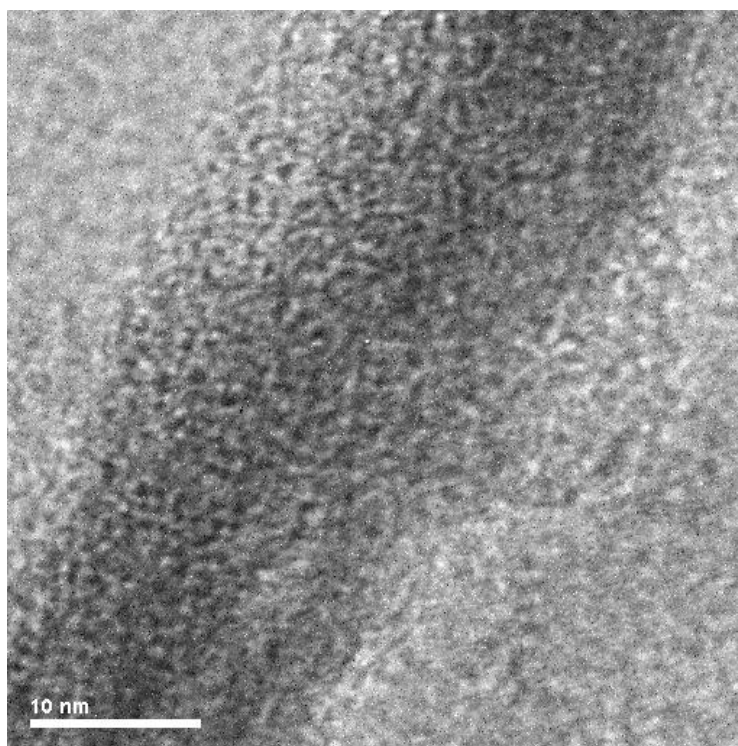**Figure 4.5 :** TEM image of the untreated sample at room temperature.

Figure 4.6 : HRTEM image of α-CNT wall in the untreated sample.

Figure 4.7 shows the TEM images of treated α-CNTs at different magnifications. The structure of nanotubes becomes more obvious after subjecting to the acid treatment (Figure 4.7(a)) due to most of the residual reagents are completely removed from the treated sample. This is supported by the XRD pattern (Figure 4.14) which shows no peak that is attributable to NH$_4$Cl phase (JCPDS 73-0365). The nanotubes are in straight dimension with the outer and inner diameter falls in the range of 80 - 110 nm and 45 - 65 nm, respectively. The length of nanotubes is in few micrometers; 8 - 10 μm. The average length and diameter of α-CNTs are in good agreement with the FE-SEM images (Figures 4.1 - 4.3). Figure 4.7(b) shows the image for higher magnification of the treated α-CNTs. The walls of nanotubes are irregular in shape and rough suggesting that a formation of defects due to the low synthesis temperature used in this work (Liu *et al.*, 2007). For further confirmation on the structure of this treated sample, the HRTEM image of the treated sample is captured and represented by Figure 4.8. The dark area in the image corresponds to the wall of the nanotube, which is amorphous as no certain

pattern being observed to reveal a crystalline structure. This feature is also in accordance with the XRD pattern (Figure 4.14).

Figure 4.7 : TEM images of the treated sample at room temperature at different magnifications: (a) 12.5 kx; (b) 31.5 kx.
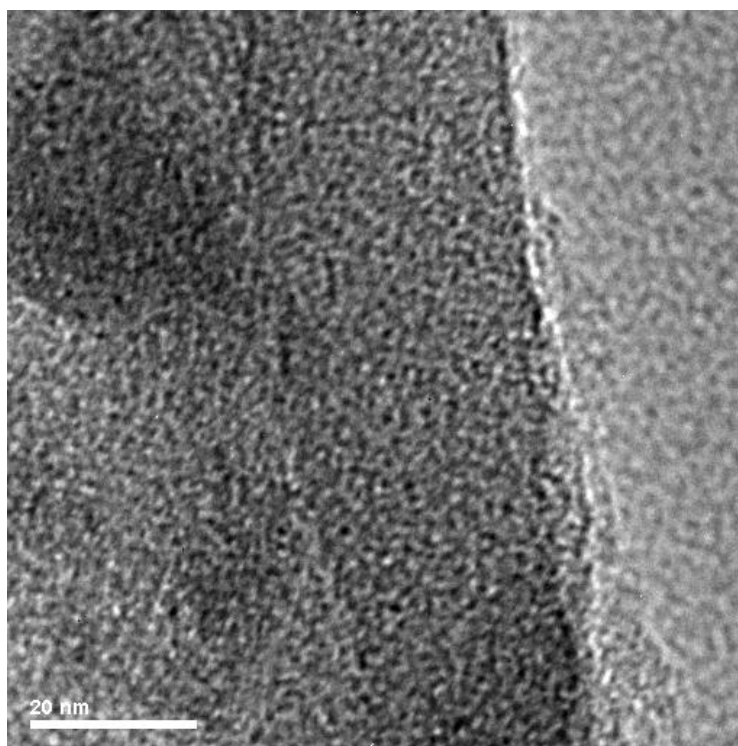
Figure 4.8 : HRTEM image of α-CNT wall in the treated sample.

Figure 4.9 shows the TEM images of oxidized α-CNTs at different magnifications. The image exhibit the reduction of agglomeration as the nanotubes are hardly attached to each other. It is observed that the wall of nanotubes shows no appreciable change compared to both the untreated and treated samples. They are just more irregular in shape and rougher. These observations are confirmed by the HRTEM image in Figure 4.10. Furthermore, the nanotube still retains its amorphous structure. Oxidation treatment conducted on the treated sample by using a mixture of H_2SO_4 and HNO_3 acids has introduced a large amount of defects for the nanotubes (Wiltshire *et al*., 2004; Rakov, 2006). This phenomenon results in greater extent of nanotube shape irregularity and roughness.
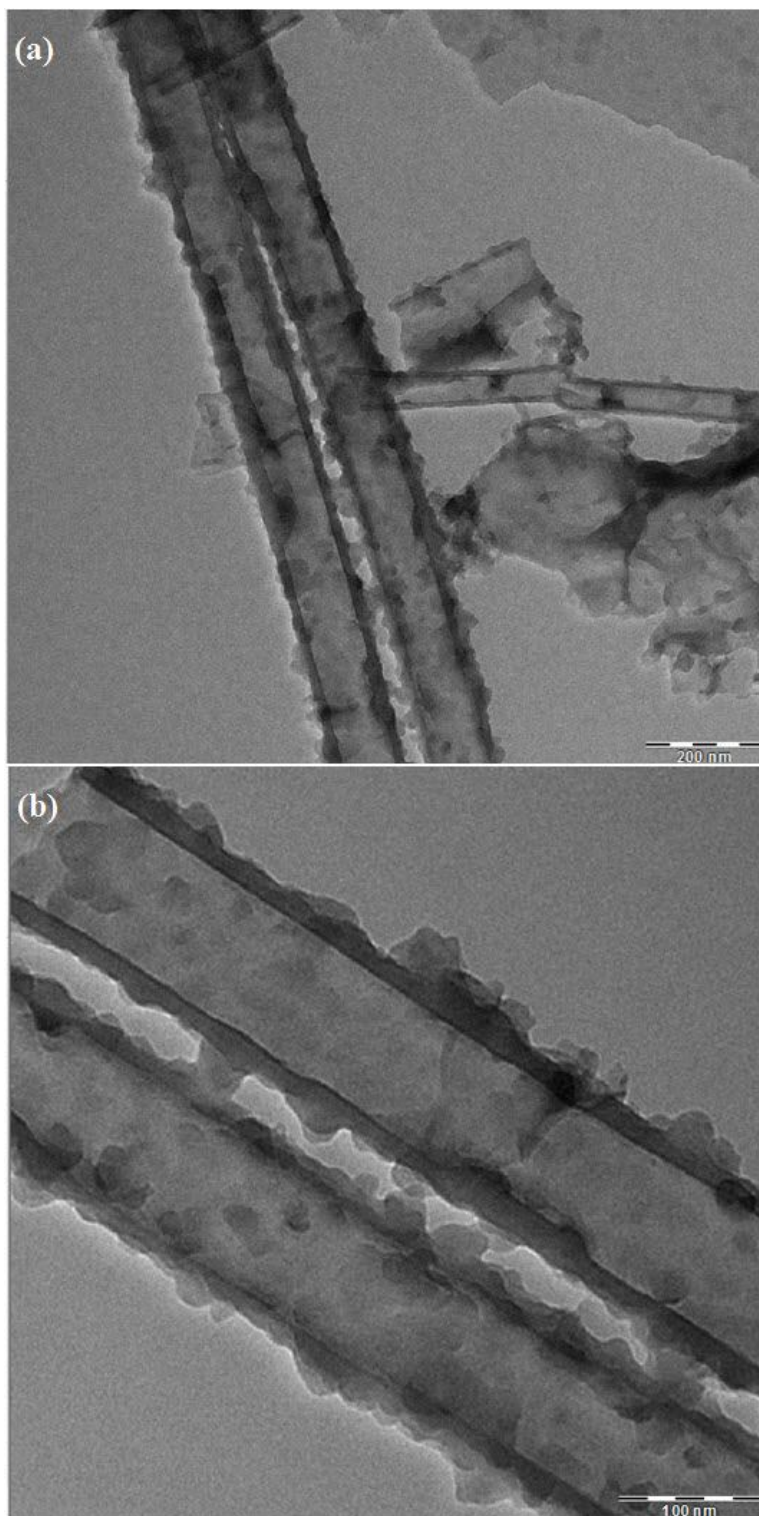
Figure 4.9 : TEM images of the oxidized sample at room temperature at different magnifications: (a) 20 kx; (b) 31.5 kx.
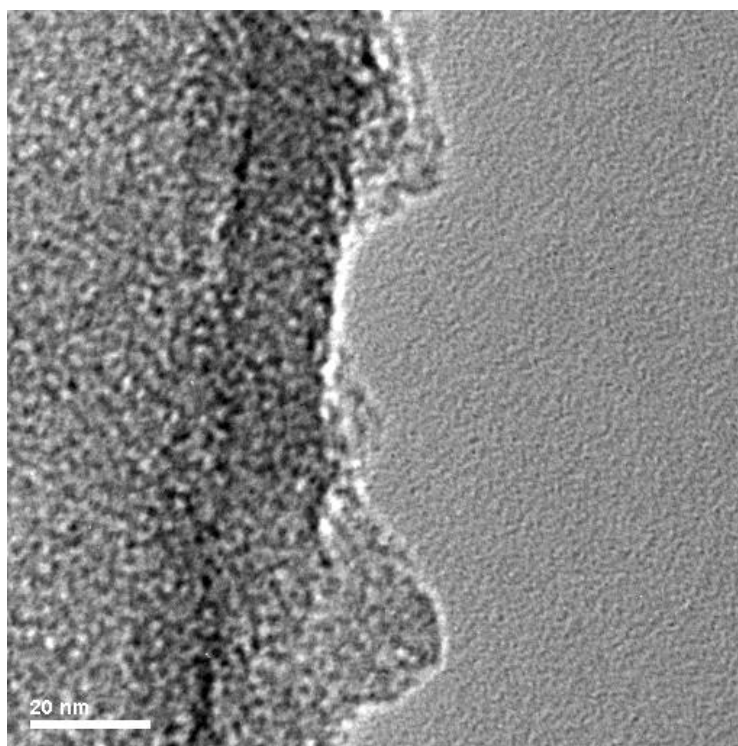
Figure 4.10 : HRTEM image of α-CNT wall in the oxidized sample.

Figure 4.11 shows the TEM images of hybridized α-CNTs with CdSe QDs at different magnifications. The CdSe QDs are attached heterogeneously on the whole body of nanotubes. This will increase the thickness and roughness of nanotubes walls as shown in Figure 4.11(b). The outer diameters of the hybridized nanotubes are the highest which lie in the range of 120-150 nm, compared to other samples. This result is comparable with the FE-SEM image (Figure 4.4). The surfaces of the nanotubes are highly rough due to the coating of CdSe QDs.

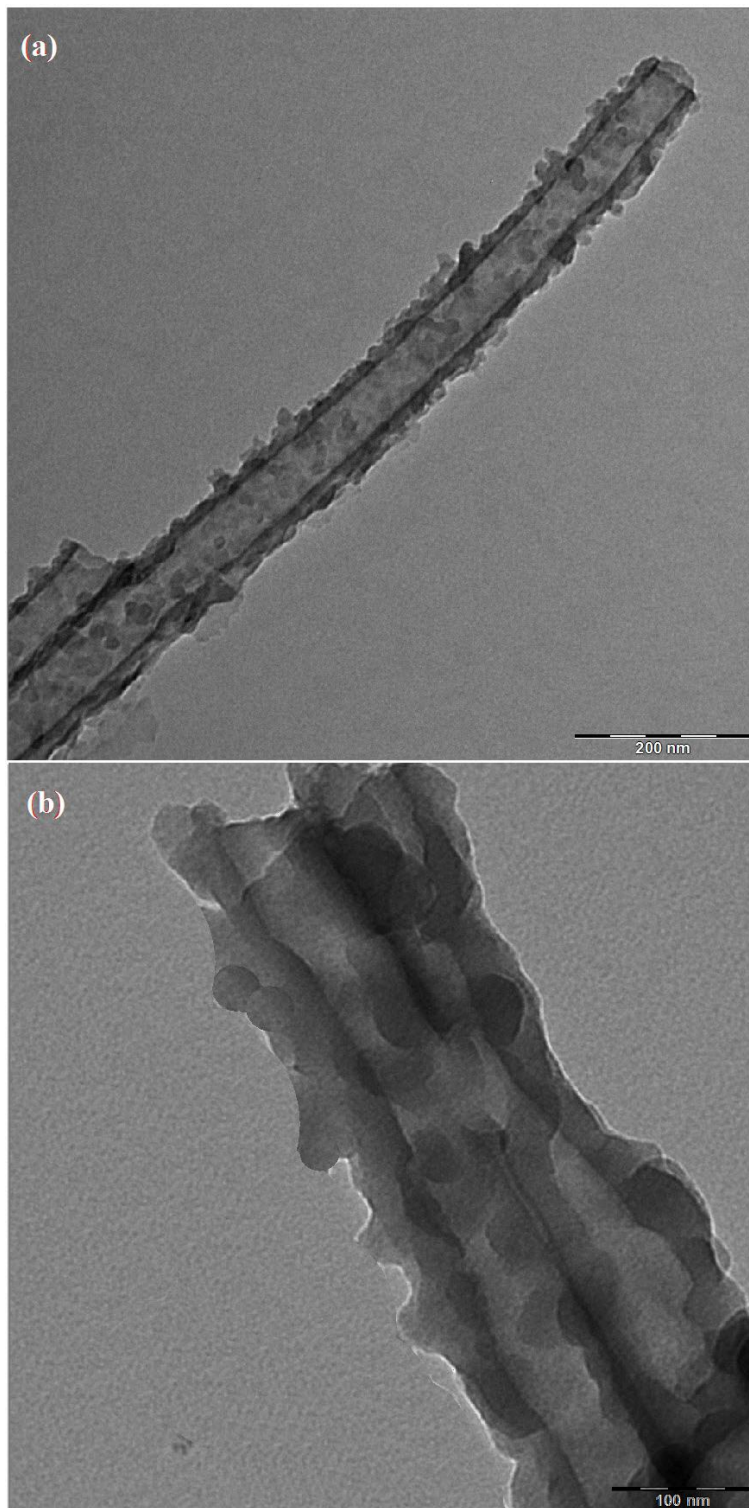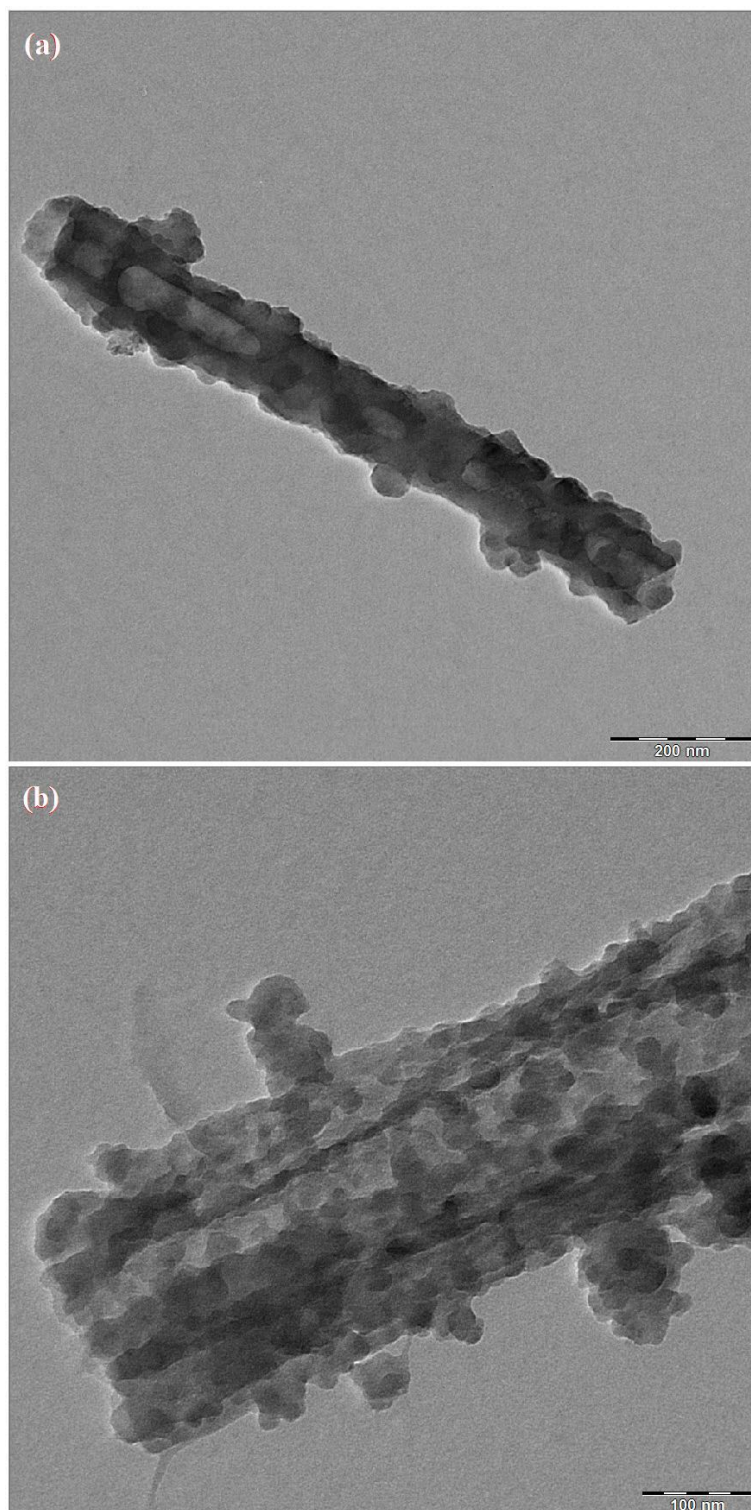**Figure 4.11 :** TEM images of the hybridized sample at room temperature at different magnifications: (a) 16.3 kx; (b) 25 kx.

Figure 4.12 presents the high magnification of HRTEM image for the wall of a hybridized nanotube. Few crystalline regions (white circles) are clearly spotted. This suggests that the CdSe QDs have been successfully attached to the surfaces of the nanotubes. The inset of Figure 4.12 shows the corresponding SAED image for the crystalline region. The uniform concentric rings suggest that the CdSe QDs have certain orientation and can be assigned as (111), (220) and (311) planes of cubic CdSe QDs. This result is confirmed by the XRD and EDX results in Figures 4.14 and 4.16, respectively.
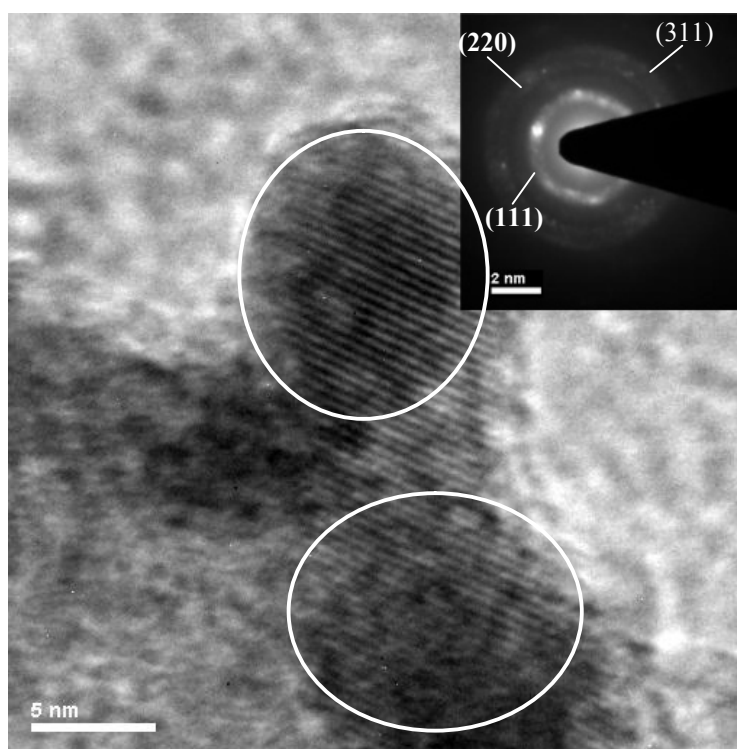
Figure 4.12 : HRTEM image of α-CNT wall in the hybridized sample with the corresponding SAED image.

Figure 4.13 shows the TEM image of CdSe QDs. Their sizes fall in the range of 15 - 40 nm with a narrow particle size distribution. The CdSe QDs have been synthesized separately prior to the hybridization process.
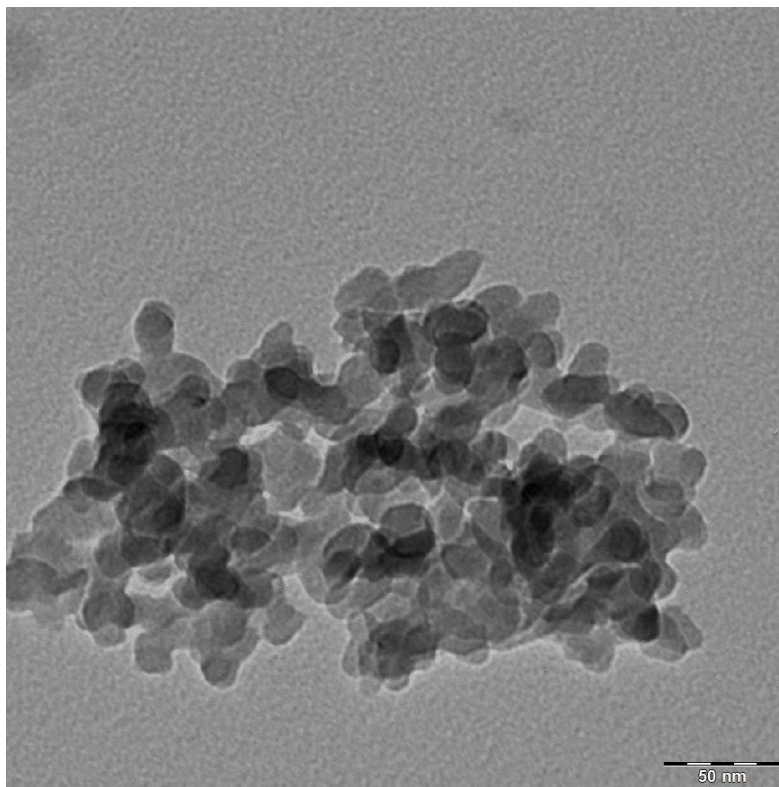
Figure 4.13 : TEM image of the as-prepared CdSe QDs.

4.2 Microstructural Studies

Figure 4.14 displays the XRD patterns for all samples at room temperature. It is clearly observed that no crystalline phase was present in the patterns. It proved that all the as-synthesized CNTs are amorphous in nature. However, the peaks which appeared in the XRD patterns are only detected for the unreacted reagents and compounds formed in minor quantities from the precursor materials.

The diffraction peaks for the untreated sample are only attributable to NH_4Cl phase (JCPDS 73-0365). This precursor material could not be consumed completely

during the heating process. This is in a good agreement with the TEM image for untreated sample (Figure 4.5), whereby the sample has been surrounded by the unreacted NH_4Cl compound in a disordered manner. No crystalline phase of carbon has been detected within the untreated sample. However, the NH_4Cl compound is entirely removed from the other samples. This compound is removed after soaking and washing with hydrochloric acid, ethanol and deionised water during the purification treatment (Cheng *et al*., 2006), enabling the nanotubes being clearly observed (Figure 4.7). The XRD pattern for the treated sample shows the presence of Fe_2O_3 phase (JCPDS 73-2234), indicates that some residual reactant, i.e. Fe originated from the $Fe(C_5H_5)_2$ which still remains within the sample and has been oxidized. The Fe_2O_3 phase could be also produced during a chemical reaction between the NH_4Cl and $Fe(C_5H_5)_2$.
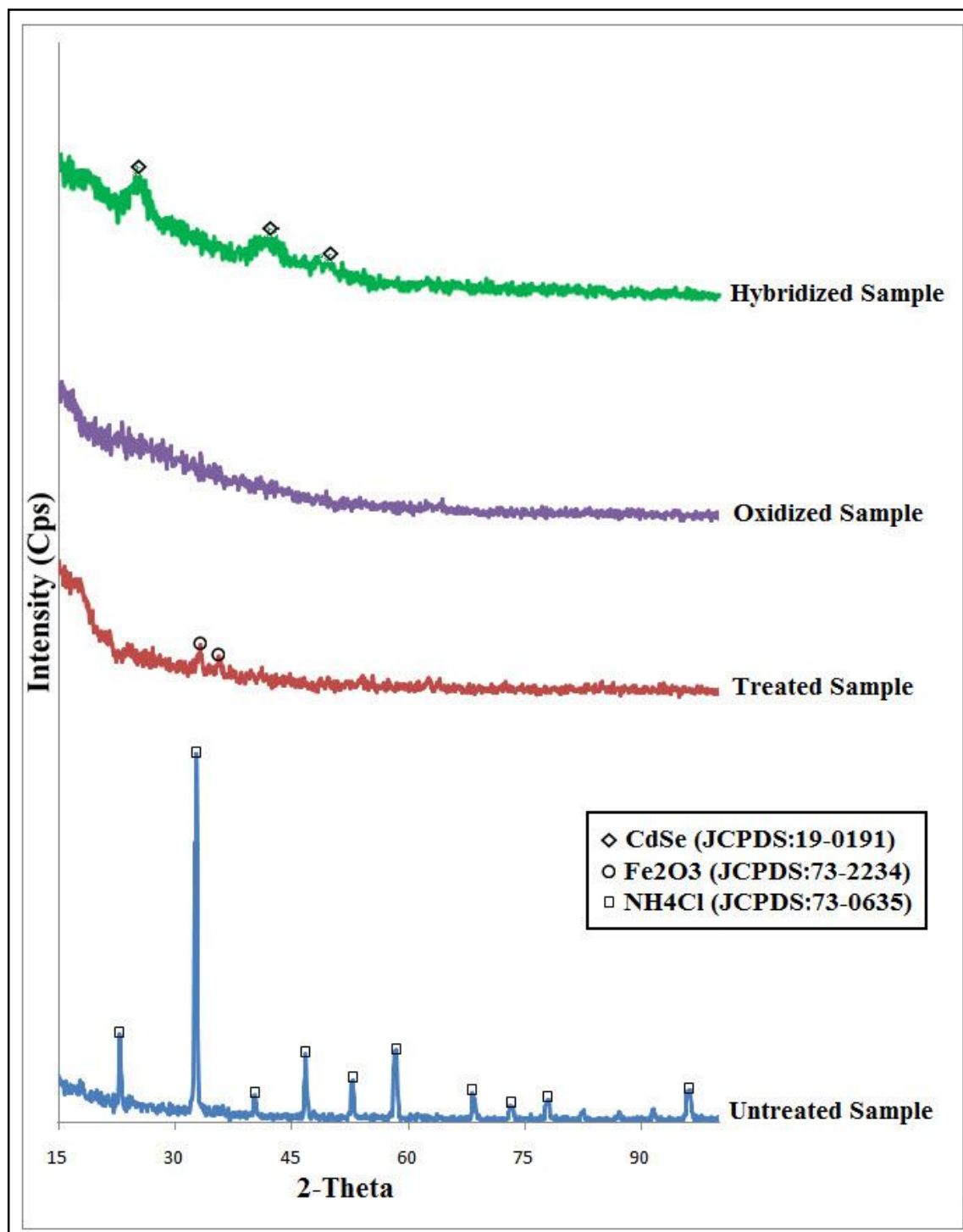
Figure 4.14 : XRD patterns for all samples at room temperature.

There is no diffraction peak due to the Fe_2O_3 phase being detected in the XRD pattern of the oxidized sample. The Fe_2O_3 has been removed completely. The intensity of the pattern is the lowest and broader than that of the treated sample. Oxidation treatment has also led to amorphization by introducing more defects towards the tubes

(Wiltshire *et al.*, 2004; Rakov, 2006). However, the CdSe phase (JCPDS 19-0191) appears in the XRD pattern after underwent hybridization. This result infers that the α-CNTs were hybridized with the CdSe QDs by attached them disorderly on the body of nanotubes, as shown in Figures 4.4, 4.11 and 4.16 and Table 4.2. The attachment of CdSe QDs on the wall of α-CNTs was confirmed in Figure 4.12 (inset) due to the presence of corresponding diffraction from (111), (220) and (311) planes of cubic CdSe. The interplanar spacing (d_{hkl}) as calculated from HRTEM, XRD and JCPDS data card, and corresponding (hkl) values of CdSe QDs are summarized in Table 4.1. Figure 4.15 shows the XRD pattern for the as-prepared CdSe QDs at room temperature. The diffraction peaks at (111), (220) and (311) planes confirm the cubic structure of CdSe QDs. These results are in good agreement with SAED image (inset in Figure 4.12).

Table 4.1: Interplanar spacing (d_{hkl}) from HRTEM, XRD and JCPDS data with corresponding (*hkl*) values of CdSe QDs.

d_{HRTEM} (Å)	d_{XRD} (Å)	d_{JCPDS} (Å)	(*hkl*)
3.501	3.563	3.510	(111)
2.140	2.148	2.149	(220)
1.830	1.844	1.833	(311)
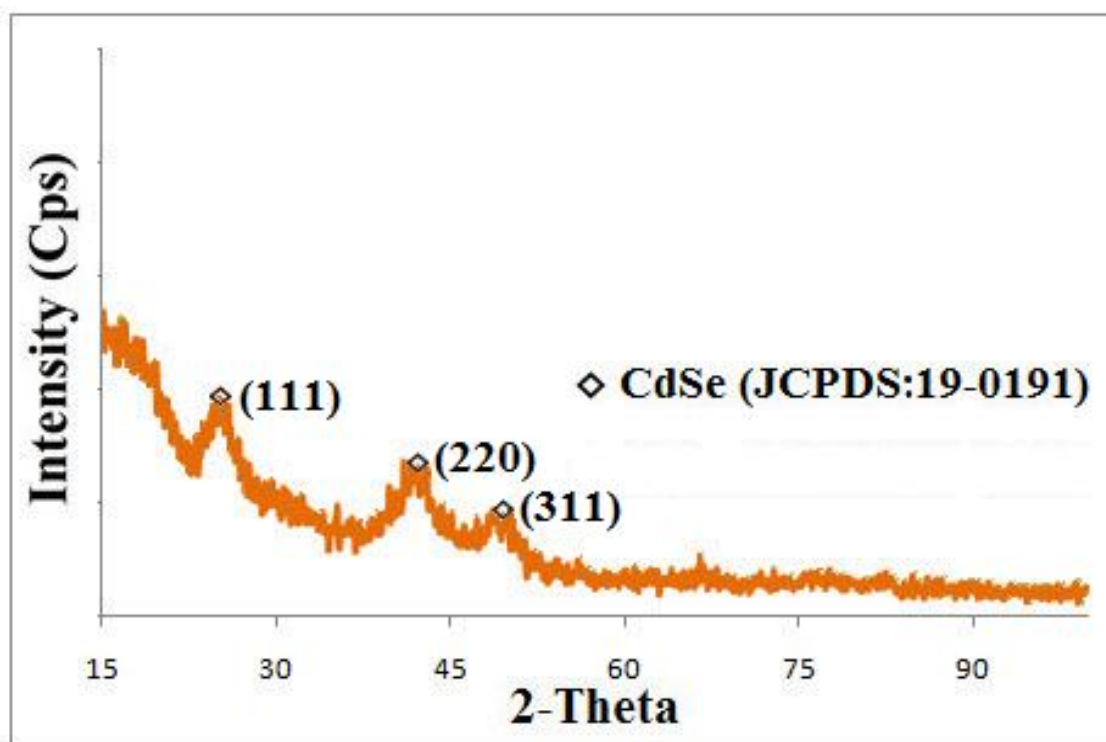
Figure 4.15 : XRD pattern for the as-prepared CdSe QDs at room temperature.

4.3 Elemental Studies

Figure 4.16 shows the EDX spectra for all samples. The respective weight and atomic percentages for the elements are presented in Table 4.2. The dominant element for all samples is carbon, which reveals the successful formation of α-CNTs via the chemical method. The presence of oxygen indicates all the samples have been oxidized to some extent. It is no doubt that elements like Fe, N and Cl were initiated from any unreacted raw materials during the reaction between $Fe(C_5H_5)_2$ and NH_4Cl compounds. These elements have been found in the untreated sample. The presence of Fe may also originate from the $Fe(C_5H_5)$ that has been used as precursor material in this work. There is a certain amount of Fe remains in the untreated sample, as evidenced by Figure 4.16(a) and Table 4.2. However, there is no Fe phase was observed in its XRD pattern (Figure 4.14).

The purification treatment for treated sample (soaking and washing the untreated sample using concentrated chloric acid) have substantially reduced the amounts of Fe, N, Cl and O quantitatively (Cheng *et al.*, 2006). Oxidation process is performed by treating the sample with a mixture of concentrated H_2SO_4 and HNO_3 acidic solutions (3:1 ratio). As a result, Fe element is further removed thoroughly in the oxidized sample. Functional group like carboxylic groups, -COOH is chemically introduced to the sample. Subsequently, the presence of Cd and Se elements in the hybridized sample provides a good evidence for the successful hybridization between α-CNTs and CdSe QDs (Figure 4.16(d) and Table 4.2). Furthermore, the molar ratio of Cd to Se is 1:1.19, (calculation is performed using the obtained data in Table 4.2), which is in conformity with the stoichiometric CdSe within experimental error. The previous HRTEM, FE-SEM and XRD analyses also confirmed the process of hybridization. During the oxidation, the α-CNTs are chemically modified and functionalized with the carboxylic groups. Therefore, the carboxylic functionalized nanotubes become more chemically reactive to an inorganic compound like the CdSe QDs (Gojny *wt al.*, 2003; Gao *et al.*, 2006; Jha *et al.*, 2011). This phenomenon facilitates the hybridization between α-CNT and CdSe QDs.

The presence of carbon peak in the EDX spectra for all samples may also originate from carbon-based contaminations from the FE-SEM chamber. Hence it is necessary to confirm further the presence of carbon using FTIR study, which will be discussed in further section.
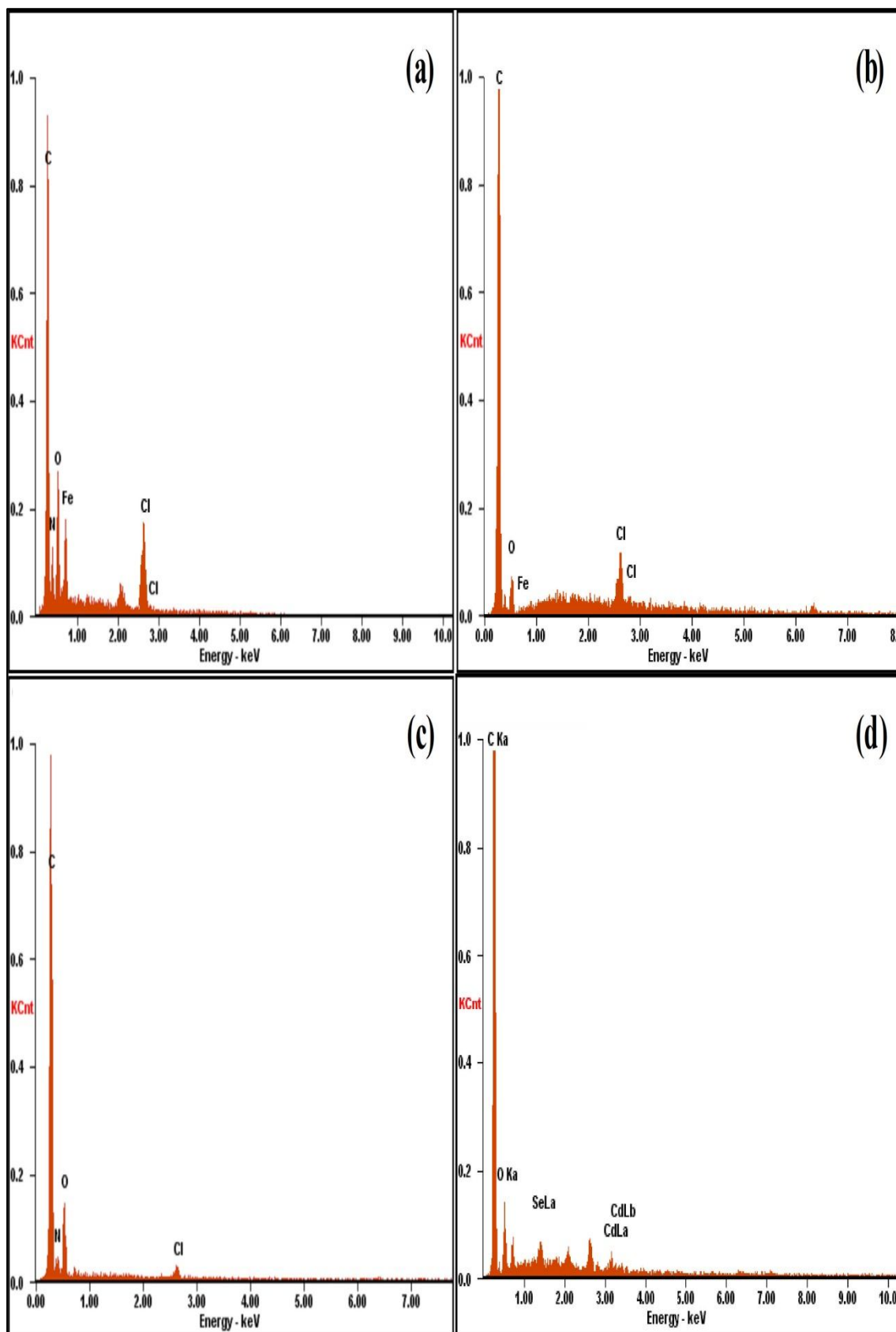
Figure 4.16 : EDX spectra of α-CNTs for (a) Untreated Sample; (b) Treated Sample; (c) Oxidized Sample; (d) Hybridized Sample.

Table 4.2 : Elemental analysis by EDX for all samples.

Sample		Elements						
		C	O	Cl	Fe	N	Cd	Se
Untreated Sample	Wt%	43.78	9.92	12.20	23.98	10.12	-	-
	At%	63.27	10.77	5.97	7.45	12.54	-	-
Treated Sample	Wt%	82.30	6.02	10.18	1.50	0	-	-
	At%	90.85	4.99	3.81	0.36	0	-	-
Oxidized Sample	Wt%	67.60	17.66	2.66	0	12.08	-	-
	At%	73.38	14.40	0.98	0	11.24	-	-
Hybridized Sample	Wt%	85.14	10.30	0	0	0	2.07	2.49
	At%	90.32	9.01	0	0	0	0.31	0.37

4.4 Optical Studies

4.4.1 FTIR Analysis

Figure 4.17 shows the FTIR spectra for the untreated, treated, oxidized and hybridized samples with their respective peaks at 1260, 1361, 1362 and 1342 cm^{-1}, which correspond to C=O vibrational bands. Besides, they exhibit characteristic peaks like C=C vibrational band at 1583, 1589, 1576 and 1579 cm^{-1}, respectively. C-C sp^{1} stretching band also appears at about 2190 cm^{-1} for all samples (Silva, 2003; Jha *et al.*, 2011). In addition, all samples display the peaks due to the presence of CO_2 (untreated sample: 2341 cm^{-1}; treated sample: 2344 cm^{-1}; oxidized sample: 2360 cm^{-1}; hybridized sample: 2346 cm^{-1}). The contamination from atmosphere leads to the introduction of CO_2 for all samples (Jana *et al.*, 2011). The detection of peaks attributable to the C=O, C=C and C-C bands is sufficient to confirm the presence of carbon in the composition

of all samples. Therefore, carbon is not sourced from any carbon-based contaminations in the FE-SEM chamber.

Another broad peak is observed in the 2800 - 3500 cm^{-1} region, which corresponds to the hydroxyl group (-OH) for both treated and oxidized samples. This band is attributable to the deformation vibration of water molecules. The use of aqueous acids and NH_4Cl in synthesizing these samples may contribute the water content. In addition, the exposure of the samples to air initiates the attachment of -OH group (absorption of moisture) towards the amorphous walls of nanotubes. The α-CNTs with a large amount of defects could easily trap the air moisture. This phenomenon is obvious especially for the oxidized sample that having a higher amount of defects during oxidation (Wiltshire *et al.*, 2004; Rakov, 2006). However, no peak attributable to this -OH group appears for the untreated sample. This implies that the moisture absorption is relatively insignificant in the untreated sample. It is suggested that the structure is not fully transformed to amorphous nanotubes during the reaction. The defective surface of this sample is less for the moisture absorption.

There are other two additional peaks attributed to sulphonate group (-SO_2O^-) and carboxylic group (-COOH) at 1121 and 1421 cm^{-1} respectively, being observed in the oxidized sample. Both the -SO_2O^- and -COOH groups could be introduced during the surface oxidation treatment using the mixture of concentrated acids (H_2SO_4 and HNO_3 acids). As being mentioned before, the oxidation process conducted using the concentrated acids could introduce any involved functional groups to enable nanotubes becoming chemically reactive (Gojny *et al.*, 2003; Gao *et al.*, 2006; Jha *et al.*, 2011). In this case, the surfaces of nanotubes have been functionalized chemically with carboxylic groups.

The hybridized sample shows no peak that is attributable to the -COOH group. This peak disappears due to the attachment of CdSe QDs to the amorphous nanotubes surfaces containing carboxyl groups. It is interestingly that two additional peaks appear at 2851 and 2920 cm⁻¹. These peaks may be attributed to the bonding between Cd and Se. These peaks are weak because the Cd-Se bond is mainly an electrovalent bond. The mid infrared (Mid IR) applied in the FTIR machine is principally concerned with the molecular vibrations typically found in organic molecules. Thus, the FTIR spectrum for the hybridized sample does not show strong bands associated with the Cd-Se stretching and deformation vibrations (Jana *et al.*, 2011).
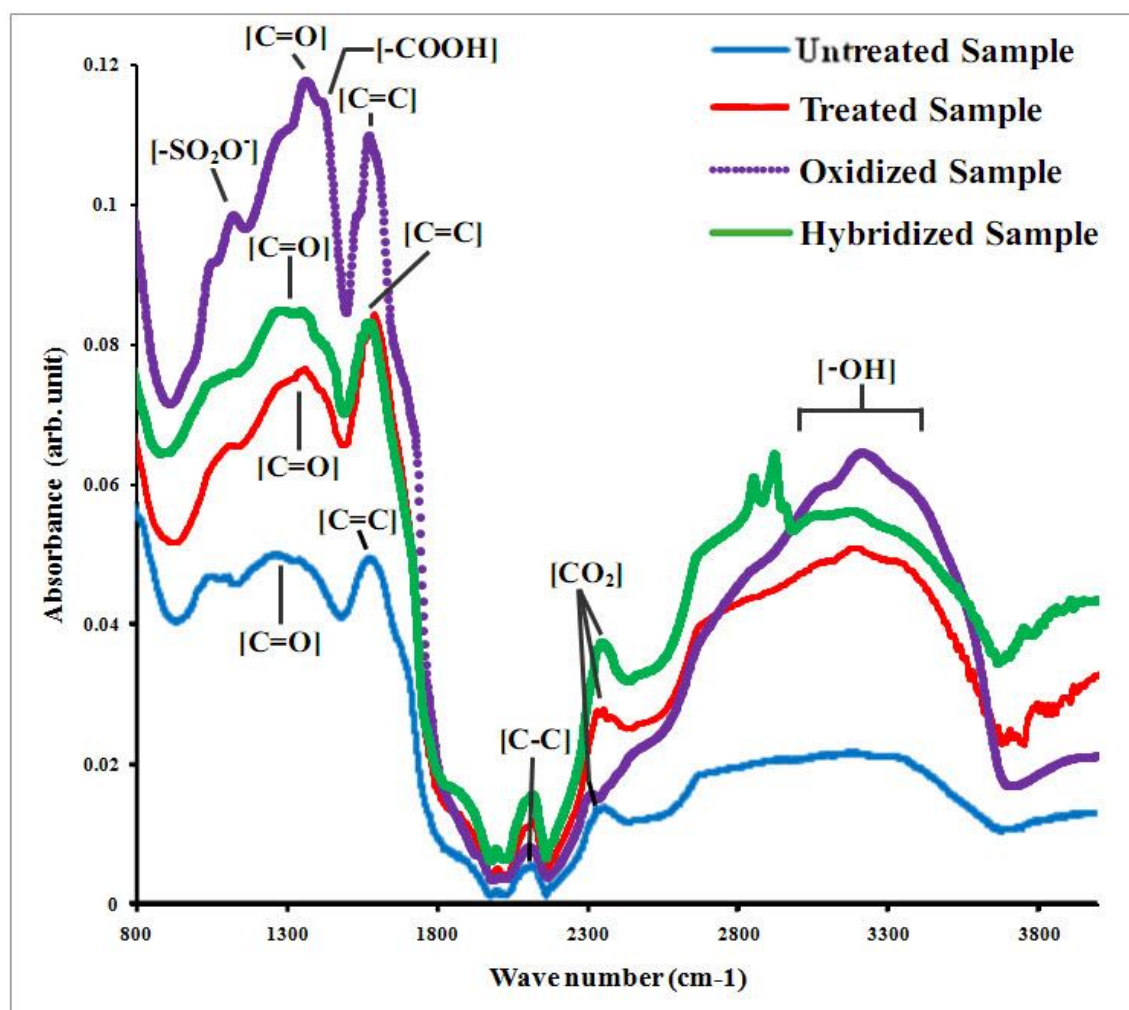

Figure 4.17 : FTIR spectra for all samples at room temperature.

4.4.2   UV-Vis Analysis

UV-Vis spectrophotometer was used to investigate the dispersion stability of nanotubes in a certain volume of alcohol (methanol) and their optical characteristics. Figure 4.18 shows the transmittance spectra for all samples. It is clear that the untreated sample has the highest intensity for its UV-Vis transmittance spectrum among others, followed by the treated, oxidized and hybridized samples. In other words, the nanotubes in the untreated sample are the least dispersed in the methanol (solvent) after receiving ultrasonication treatment. Due to the nature of CNTs, they are easily bound together by the Van der Waals force. Therefore, self-agglomeration is inevitable and thus prevents a good dispersion of nanotubes in a solvent solution (methanol) (Gojny *et al.*, 2003). The nanotubes in the untreated sample are scarcely dispersed even they have undergone ultrasonication treatment for 1 hour. Consequently, the untreated sample display a good overall UV light transmittance behavior as the excited UV light is hardly absorbed by the involved nanotubes. Most of the UV light is transmitted through the methanol instead of being absorbed by the self-agglomerated nanotubes.

The treated sample has a slightly lower intensity indicates that the dispersion of nanotubes is improved as compared to the untreated sample. The acid purification treatment (soaking and washing with concentrated chloric acids) has slightly reduced the agglomeration effect in the nanotubes. A significant decrease of the intensity of transmittance is noticed for the oxidized sample. The nanotubes in the oxidized sample have remained well dispersed in the solution with a stable dispersion characteristic as compared to both the untreated and treated samples. The surfaces of nanotubes have been chemically modified by the oxidation treatment with a concentrated mixture of acids. Thus, it results in a dramatic reduction of agglomeration effect. The nanotubes functionalized with carboxylic groups promote better dispersion stability of nanotubes

in methanol (Gao *et al.*, 2006; Jana *et al.*, 2011; Jha *et al.*, 2011). The hybridized sample shows the greatest reduction in the intensity of transmittance, hence giving the best dispersion stability.

In addition to UV-Vis transmittance analysis, visual observation has been used as an indirect approach to study the dispersion stability of the samples. Figure 4.19 presents the photographs of all samples dispersed in deionised water. Their results are in accordance with the UV-Vis transmittance results (Figure 4.18). It is obviously noticed that both the oxidized and hybridized samples remain well dispersed in methanol even after 2 weeks. However, precipitation of nanotubes has been observed in both the untreated and treated samples after 1 and 3 h from the ultrasonication process, respectively.
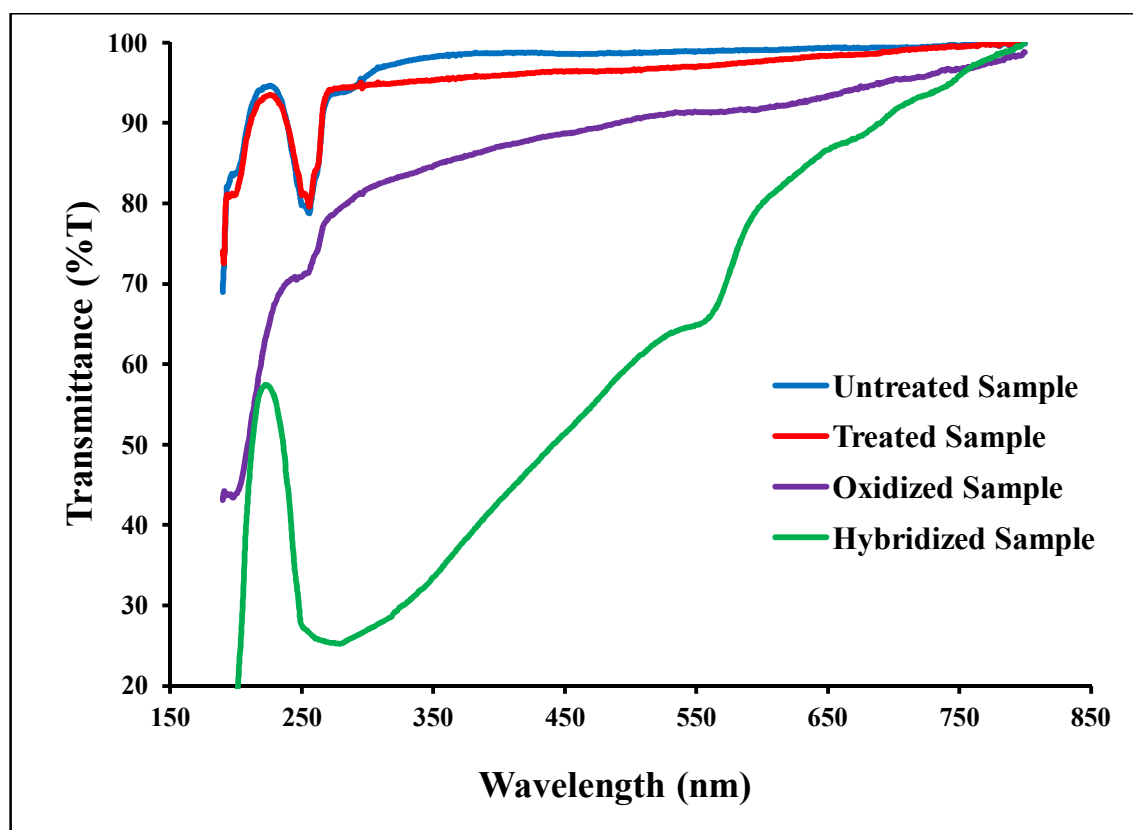
Figure 4.18 : UV-Vis transmittance spectra for all samples at room temperature after 1 h ultrasonication.
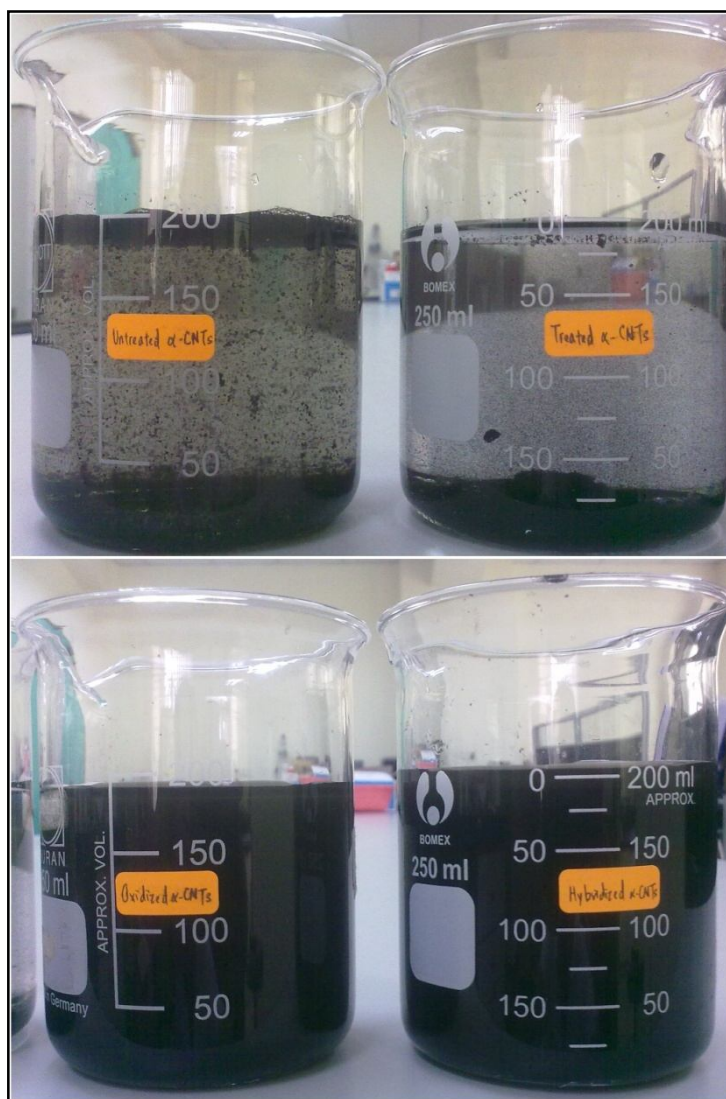
Figure 4.19 : Dispersion of all samples in methanol solvent for (a) Untreated sample, (b) Treated sample, (c) Oxidized sample and (d) Hybridized sample.

Figure 4.20 shows the UV-Vis absorption spectra of all samples at room temperature. In the range of 200 - 300 nm, all samples exhibit similar absorption characteristics; untreated sample at 252 nm (4.92 eV), treated sample at 256 nm (4.85 eV), oxidized sample at 257 nm (4.83 eV) and hybridized sample at 284 nm (4.37 eV). Table 4.3 summarized the results. α-CNTs have similar absorption behavior with crystalline CNTs since their absorption peaks fall in the same range (Kataura *et al*., 1999; Graham *et al*., 2010). The hybridized sample has the relatively largest absorption wavelength compared to others. This is probably due to the effect of the contribution of

CdSe QDs. The absorption spectra are slightly red-shifted to a longer wavelength with a decrease in the energy gap. It is suggested that the gradual increase in outer diameter of nanotubes due to the treatments (oxidation and hybridization) is responsible for the red shift phenomenon. The observed absorption peaks or bands which called the π plasmon absorbance, are associated with collective excitations of π electrons occurred for electron transition of π-π* in the nanotubes. Their absorption energy is consistent with the previous works (Pichler *et al.*, 1998; Graham *et al.*, 2010), at around 310 - 155 nm (4.0 - 8.0 eV). These absorption bands are due to transitions between spikes in the densities of states in the electronic structure of the nanotubes. This means that the observed absorption peaks are caused by the plasmon resonances in the free electron cloud of the nanotube π electrons.

In addition to that, there is another band was observed in the visible region for the hybridized sample at 589 nm (2.11 eV). This excitonic feature indicates a monodisperse of CdSe QDs in the nanotubes during hybridization. That absorption peak is red-shifted relative to the absorption peak of pristine CdSe QDs (569 nm). This is due to the attachment of CdSe QDs on the nanotubes' wall (oxidized sample) has increased the total size of the nanotubes. This electronic transition is actually shifted from higher to lower photon energies with increasing size in accordance with size quantization effect (Hamizi *et al.*, 2010; Paul *et al.*, 2010). However, if the absorption wavelength of the pristine CdSe QDs is compared to that of bulk CdSe of about 729.8 nm in size (band gap of 1.70 eV), according to literature (Zhu *et al.*, 2000), a blue shift is noticed. It is the quantum confinement effect that drives the blue shift of the absorption peak from 729.8 to 569 nm.
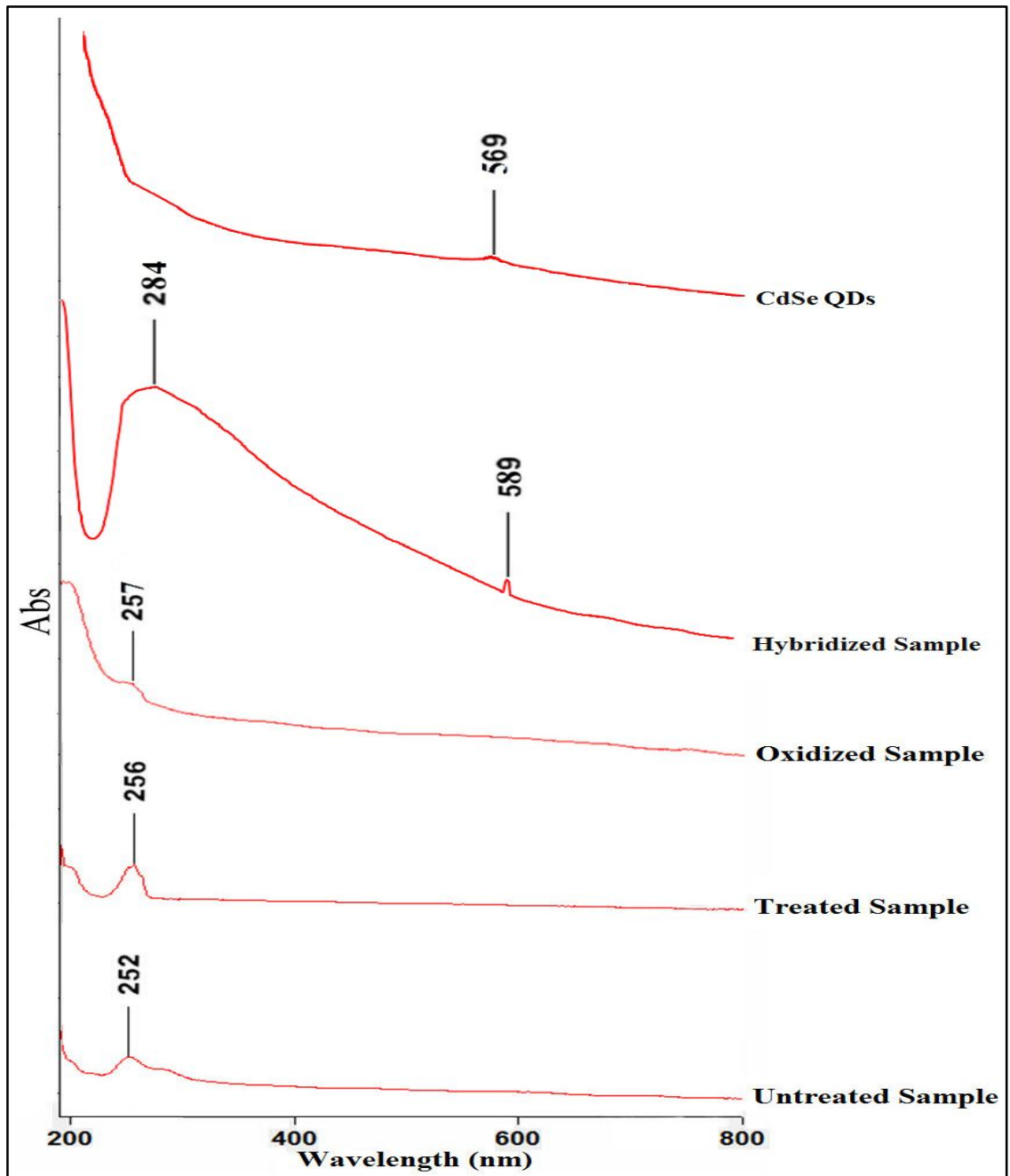
Figure 4.20 : UV-Vis absorbance spectra for all samples at room temperature.

The optical band gap (E_g) for the α-CNTs is calculated by using Tauc/Davis-Mott model (Li *et al*., 2009). According to this model, the relation between E_g and optical absorption is expressed by Equation (4.1):

$$(\alpha\ hv)^n = B\ (hv - E_g) \tag{4.1}$$

where B is a constant, *hv* is the photon energy of the incident light and *n* is the characterization index for the type of optical transition. The absorption coefficient (α) is defined by the Lambert-Beer law:

$$\alpha = - \ln A / t \qquad\qquad (4.2)$$

where A is the absorbance and *t* is the sample thickness. The E_g can be obtained from the extrapolation of the best linear parts of the curves for $(\alpha hv)^n$ versus *hv* when α is zero near the band edge region.

The presence of metallic element like the remaining Fe within the samples is believed to modify the electronic states and optical transitions of the nanotubes and causes allowed transitions rather than forbidden transitions (Li *et al*., 2009). Thus, an index value of ***n = 2*** is selected to obtain the suitable Tauc/Davis-Mott plots. E_g for all samples are thus estimated in Figure 4.21. The observed red shift phenomenon as previously discussed agrees well with the E_g obtained from the Tauc/ Davis-Mott model. Table 4.3 shows relevant data (both absorption wavelengths and E_g) obtained from both experimental data and the Tauc/Davis-Mott model. It is interesting that E_g for all samples (α-CNTs) are higher than that of the crystalline CNTs. This is in good agreement with a previous model that being conducted in the past work (Rakitin *et al*., 2000). The treated sample has the highest E_g than the untreated sample. Purification treatment has removed impurities or unreacted substances and resulted in smaller diameter of nanotubes. The size quantization effect leads to the higher value of E_g. The hybridized sample with the largest nanotubes diameter has the lowest E_g among the others.
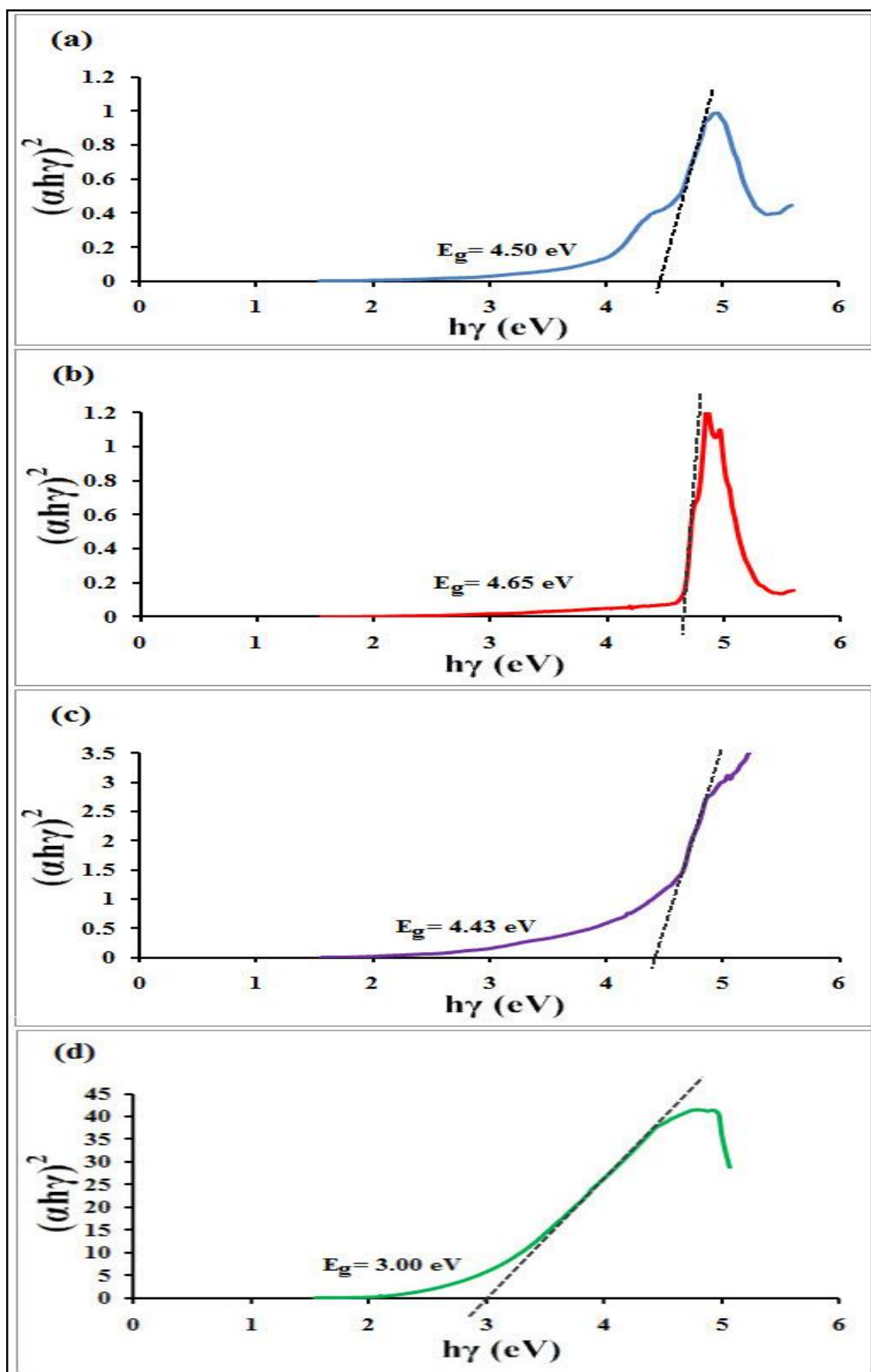
Figure 4.21 : Tauc/Davis-Mott plots for $(\alpha h\gamma)^2$ as a function of $h\gamma$ for all samples:
(a) untreated sample; (b) treated sample; (c) oxidized sample; (d) hybridized sample.

Table 4.3 : Absorption wavelength and E_g values.

Sample name	Absorption wavelength (nm)	Estimated optical band gap from Tauc/ Davis-Mott Plot (eV)
Untreated Sample	252.0	4.50
Treated Sample	256.0	4.65
Oxidized Sample	257.0	4.43
Hybridized Sample	284.0	3.00

4.4.3   Raman Analysis

Figure 4.22 displays the important Raman characteristics (D- and G-bands) for all samples at room temperature. The corresponding peaks are shown in Table 4.4. It is apparent that all α-CNT samples possess the similar Raman features of crystalline CNTs (Lou *et al*., 2003; Passacantando *et al*., 2008; Yu *et al*., 2006). The presence of the D-band for all samples infers the amorphous structure of nanotubes, which is in accordance with the morphological images (FE-SEM, TEM, HRTEM and SAED) and XRD patterns. Many structural defects are formed and dispersed within α-CNTs due to the low synthesis temperature used in this work (Liu *et al.*, 2007).

Treated sample shows more significant D-band with narrower peak as compared to that of the untreated sample. This indicates that the treated sample has a higher concentration of defects. During the purification treatment, most of the residual reagents are completely removed from the treated sample (Figures 4.2 and 4.7). It thus reveals the remaining nanotubes which are amorphous in nature. After oxidation treatment, the intensity of D-band increases and reaches the intensity of the G-band for oxidized sample. Poor structural ordering and a higher concentration of defects are attained as the oxidation treatment has led to amorphization for the structure of nanotubes. The oxidation treatment has destroyed the structure of nanotubes by introducing a large

amount of defects (Wiltshire *et al*., 2004; Rakov, 2006). The defects are not uniformly distributed along the nanotube walls. For hybridized sample, the intensity of D-band becomes higher than the G-band. The relatively strong D-band and weak G-band indicate that the nanotubes hybridized with CdSe QDs are greatly composed of amorphous carbon atoms or disordered graphite. This means that the hybridized sample is rich with unsaturated carbon atoms at degree of high disorder with dangling bonds (Yu *et al*., 2006).

The presence of G-band in all samples indicating the existence of crystallinity in the structure of α-CNTs due to the sp^2 bonded carbon atoms. However, this finding is not in conformity with the XRD pattern (Figure 4.14) that shows no crystalline peak attributable to carbon. Nevertheless, the width of G-band shows a decrease trend that deduces the reduction in the crystallinity. After underwent purification treatment, the treated sample has broader G-band than that of the untreated sample, followed by the oxidized sample which has the most insignificant G-band among other samples, revealing that the carbon in the tube walls is disordered and nanotubes are composed of amorphous carbon. Many structural defects are introduced along the nanotube walls during the oxidation treatment and contribute to more formation of amorphous nanotubes. This is assured since the relative intensity of the G-band with respect to the D-band also decreases gradually for all samples. On the contrary, the inverse of the I_D/I_G intensity ratio between G and D bands increases as shown in Table 4.4. The I_D/I_G intensity ratio is an usual measurement of the graphitic ordering (Lou *et al*., 2003). The increase of I_D/I_G implies that the number of the sp^2 bonded carbon atoms without dangling bonds have decreased and thus both of oxidation and hybridization processes substantially reduce the crystallinity of nanotubes.

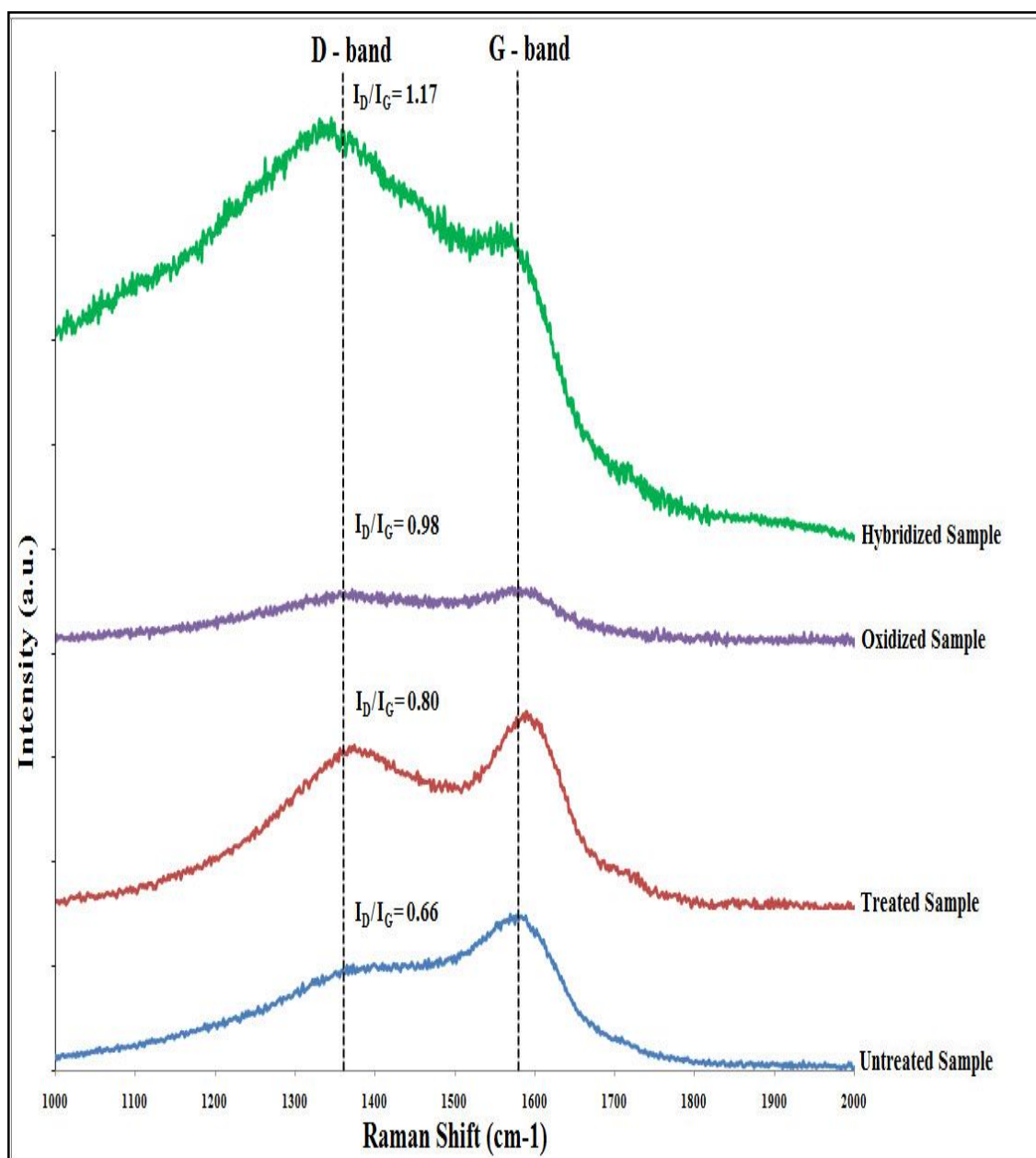**Figure 4.22 :** Raman spectra for all samples at room temperature.

Table 4.4 : The corresponding peaks' frequency (Raman shift) for all samples in Raman Spectra.

Sample Name	D-band (cm^{-1})	G-band (cm^{-1})	I_D/I_G
Untreated Sample	1365	1582	0.66
Treated Sample	1370	1590	0.80
Oxidized Sample	1365	1580	0.98
Hybridized Sample	1340	1566	1.17

4.5   Thermal Studies

The thermal stability study is conducted from weight loss measurement using TGA analysis in temperature range 40 - 1000 °C at heating rate of 10 °C/min in argon atmosphere. Figure 4.23 shows the TGA curves for all samples. The untreated sample displays a slight weight loss of 3.9 % at temperature of 100 °C due to the water vapour removal via dehydration. A sudden decrease in mass of 71.9 % occurs in temperature range of 240 - 340 °C, which is probably due to the decomposition of unreacted NH_4Cl compound. This precursor material has been detected previously in XRD pattern (Figure 4.14). Subsequently, the mass of the untreated sample almost remains stable. Finally, the mass of this sample is reduced to 4.2 % in the range of 100 - 1000 °C. Both treated and oxidized samples exhibit a similar trend in their TGA curves. They reveal greater weight losses at temperature of 100 °C due to dehydration compared to the untreated sample. Unlike the untreated sample, they show no weight loss in the range of 240 - 340 °C as the NH_4Cl compound has been removed, completely. The weight percentage of the treated and oxidized samples diminished steadily to 24.2 % and 9.4 %, respectively in the range of 100 - 1000 °C. The weight percentage of the hybridized sample only decreases from 100 % to 78.3 %, suffering the least weight loss throughout the TGA measurement. After hybridization between the oxidized nanotubes and CdSe QDs, the successfully produced hybridized sample exhibits the highest thermal stability among other samples.
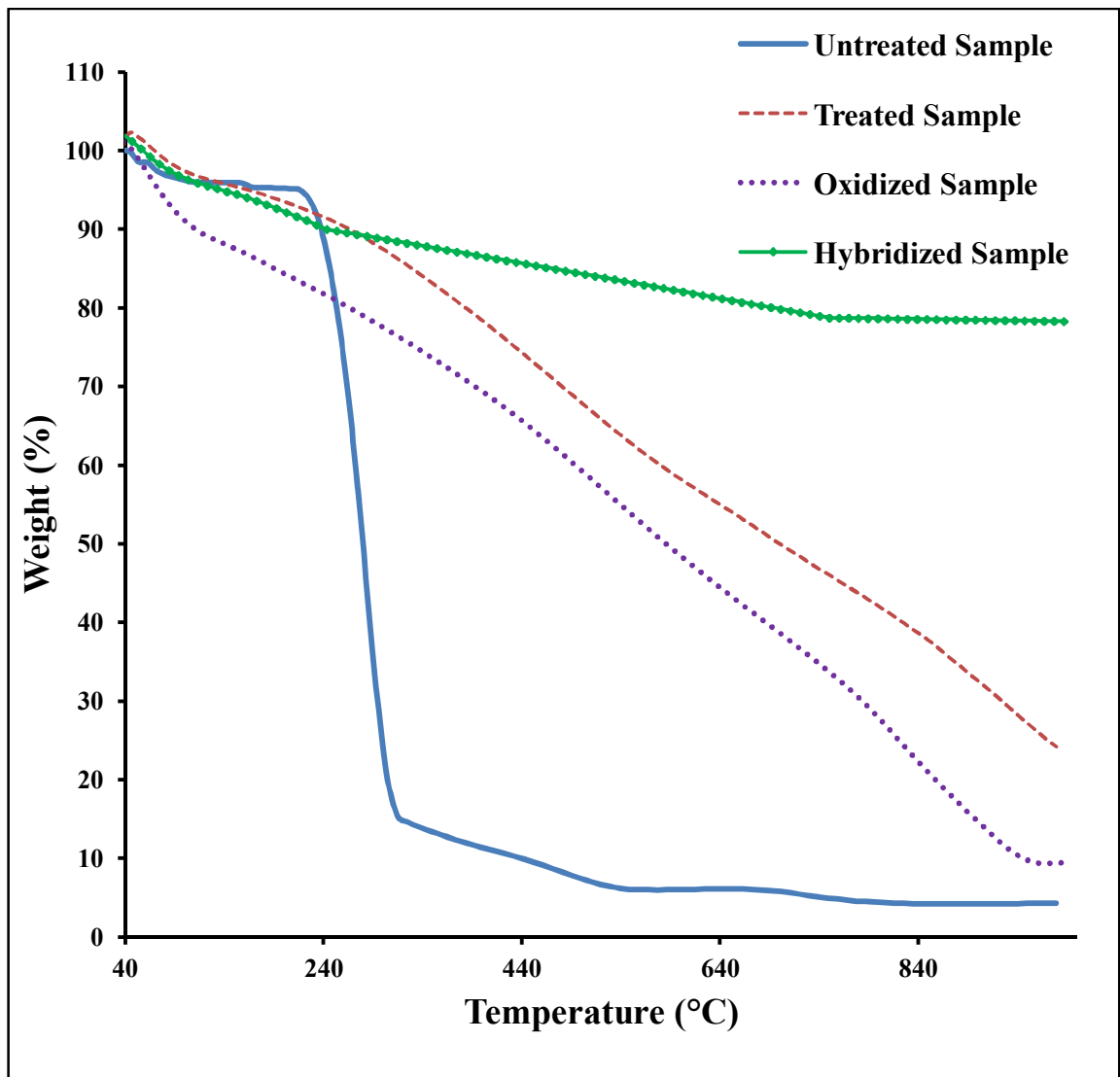
Figure 4.23 : TGA curves for all samples.

4.6   Dielectric Studies

Dielectric measurements involving both real and imaginary parts of relative complex permittivity, ε' and ε'' as the function of frequency (500 MHz to 4.5 GHz) were determined by using the VNA with a coaxial probe in slim form. All samples were fabricated into the forms of pellet. Figure 4.24 presents the permittivity response of the untreated sample, whereby its ε' and ε'' fall in the range of 2.42 - 2.67 and 0.08 - 0.26, respectively.
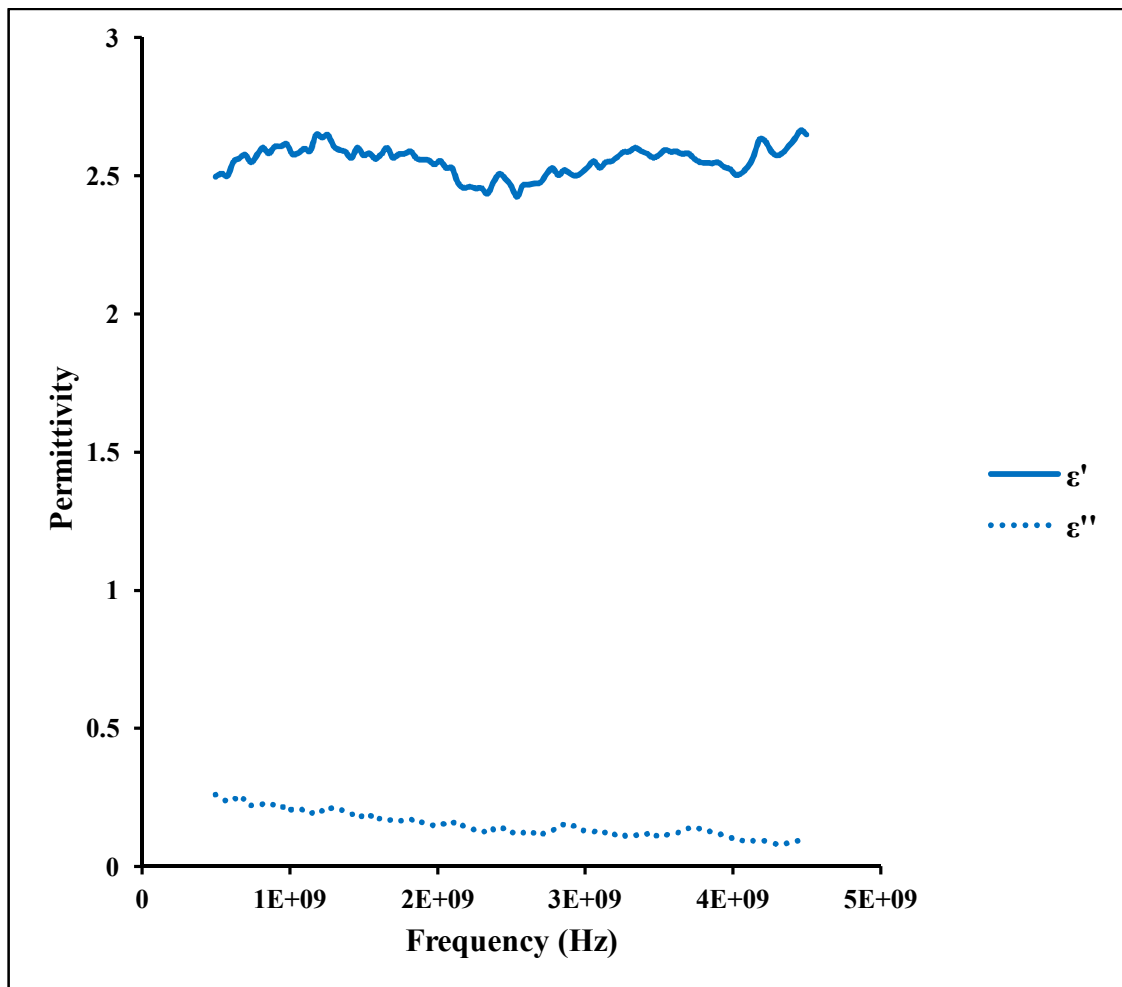
Figure 4.24 : Permittivity of the untreated sample at room temperature.

In comparison to that of the untreated sample, Figure 4.25 shows a slight decrease in permittivity response exhibited by the treated sample. Both $\varepsilon^{'}$ and $\varepsilon^{''}$ are located in the range of 1.75 - 2.03 and 0.02 - 0.12, respectively. Prior to the purification treatment, the metal Fe was found to remain as impurity within the untreated sample, as confirmed previously by the EDX results (Figure 4.16 and Table 4.2). The presence of this metallic element enhanced the dielectric property of the untreated sample (Li *et al.*, 2008; Yang *et al.*, 2009). Thus, the removal of Fe during the purification treatment reduces the permittivity response of the α-CNTs in the treated sample.

Both untreated and treated samples indicate low and nearly constant permittivity throughout the frequency range. The nanosize α-CNTs made of tubular structures with a

much defects results in lower permittivity, as compared to the carbon black, which is estimated at 2.5 - 3.0 (Internet Reference, 10/1/2012). It is suggested that the decrease in permittivity is attributed to quantum size effects. Size quantization leads to a localization of free carriers within the α-CNTs and thus reduces permittivity (Hussain *et al.*, 2007; Li et al., 2007). The lower permittivity provides a better impedance match between the material and the free space and subsequently lower front-face reflection is attainable. Such a material could be beneficial for a range of electromagnetic absorption applications which require broadband signal absorption from the radio to the microwave region. Electromagnetic compatibility (EMC) in buildings to absorb stray mobile phone signals is one of the absorption applications.
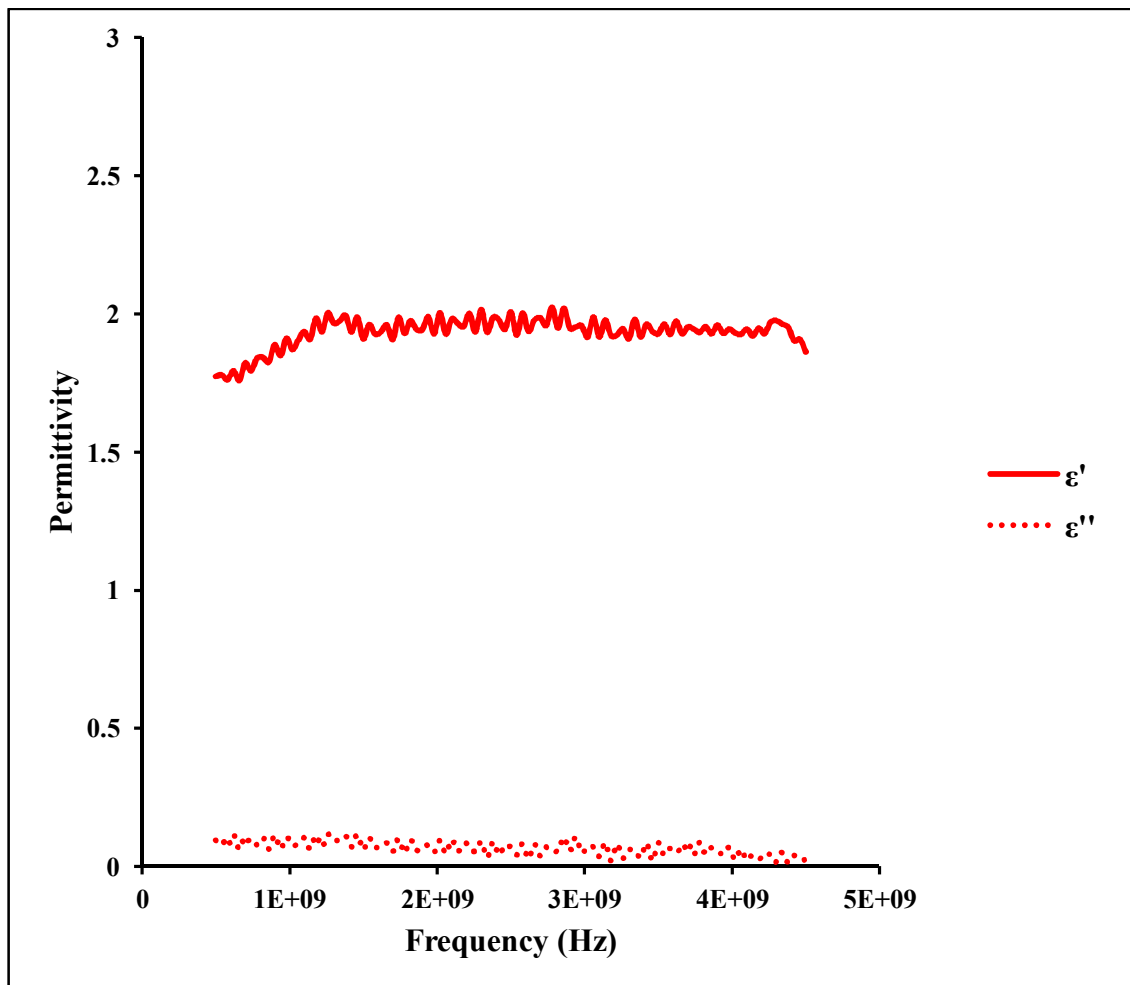
Figure 4.25 : Permittivity of the treated sample at room temperature.

Figure 4.26 shows the permittivity of the oxidized sample exhibit its permittivity response that is almost frequency independent and having a similar trend with the untreated and treated samples. In detail, the permittivity response increase significantly since both ε' and ε'' fall in the range of 3.83 - 4.56 and 0.14 - 0.52, respectively. This increment implies that chemical functionalization affects and changes the permittivity property of α-CNTs. After undergoing the oxidation process by treating the treated sample with the concentrated mixture of H_2SO_4 and HNO_3, surface modification has been performed on α-CNTs, as confirmed by the FTIR results (Figure 4.17).

Figure 4.26 : Permittivity of the oxidized sample at room temperature.

The increment in permittivity of α-CNTs via the chemical functionalization with carboxylic groups can be explained by a minicapacitor principle. The contacts with each

other in the carboxylic functionalized α-CNTs form the minicapacitors due to the presence of carboxylic groups on the surface of nanotubes. The isolation distance between the α-CNTs also diminishes with the attachment of carboxylic groups driving the increase in the capacitance of the single min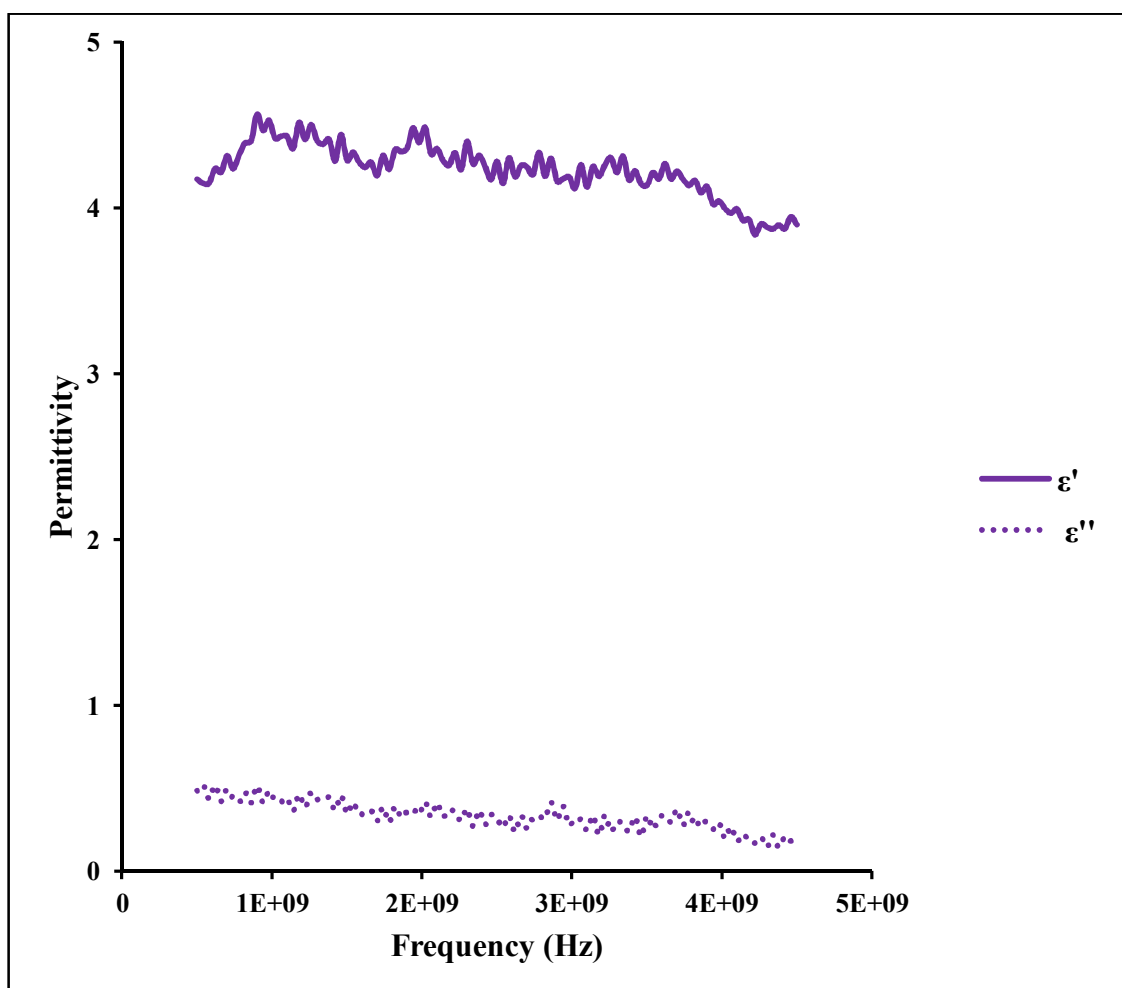icapacitor. Since the carboxylic functionalized α-CNTs (oxidized sample) possess much more minicapacitors with the relatively large capacitance, as compared to both untreated and treated sample, the higher values of ε' and ε'' are attributed to the chemical functionalization process (Ahmad $et\ al.$, 2006 ; Li $et\ al.$, 2008).

Figure 4.27 shows the frequency dependence of permittivity for the hybridized sample. The hybridized sample reveals an obvious dielectric relaxation at lower frequencies (1 GHz). Then, both ε' and ε'' decline with increasing frequency. The relaxation effect is usually associated with the orientation polarization, which indicates the alignment of electric dipoles attributed to their rotations due to the subjecting torques under an electric field. The friction accompanying the orientation of the dipoles contributes to the dielectric losses and thus the ε'' rises up and occurs in the microwave region (Nelson, $et\ al.$, 2007).

The hybridized sample exhibits the highest permittivity responses among other samples. Both ε' and ε'' rise up dramatically and reach in the range of 7.19 - 24.84 and 6.50 - 11.84, respectively. The drastic increment in permittivity is due to the successful hybridization between α-CNTs and CdSe QDs. The CdSe QDs are believed to be responsible for this drastic increase. Besides exhibiting strongly size dependent optical properties, the CdSe QDs are one of the semiconductors that have been doped to improve the dielectric constant of a CNTs-based composite (Li $et\ al.$, 2008; Yang $et\ al.$, 2009).

Based on the dispersion stability test and UV-Vis transmittance analysis conducted before, the hybridized samples display good dispersion stability in deionised water and methanol. The successful CdSe QDs coated nanotubes become less agglomerated due to smaller Van der Waals forces between nanotubes and therefore, lower agglomeration effect (fewer sedimentation) is attainable. Such environment results in higher levels of dielectric loss, which is in accordance with the highest value of $\varepsilon^{''}$. The higher value of $\varepsilon^{''}$ of a material is preferable, especially for electromagnetic absorption applications. It is because a signal is sufficiently attenuated once the radiation has entered the material, which is met for high value of $\varepsilon^{''}$ (Hussain et $al.$, 2007; Li et $al.$, 2010).
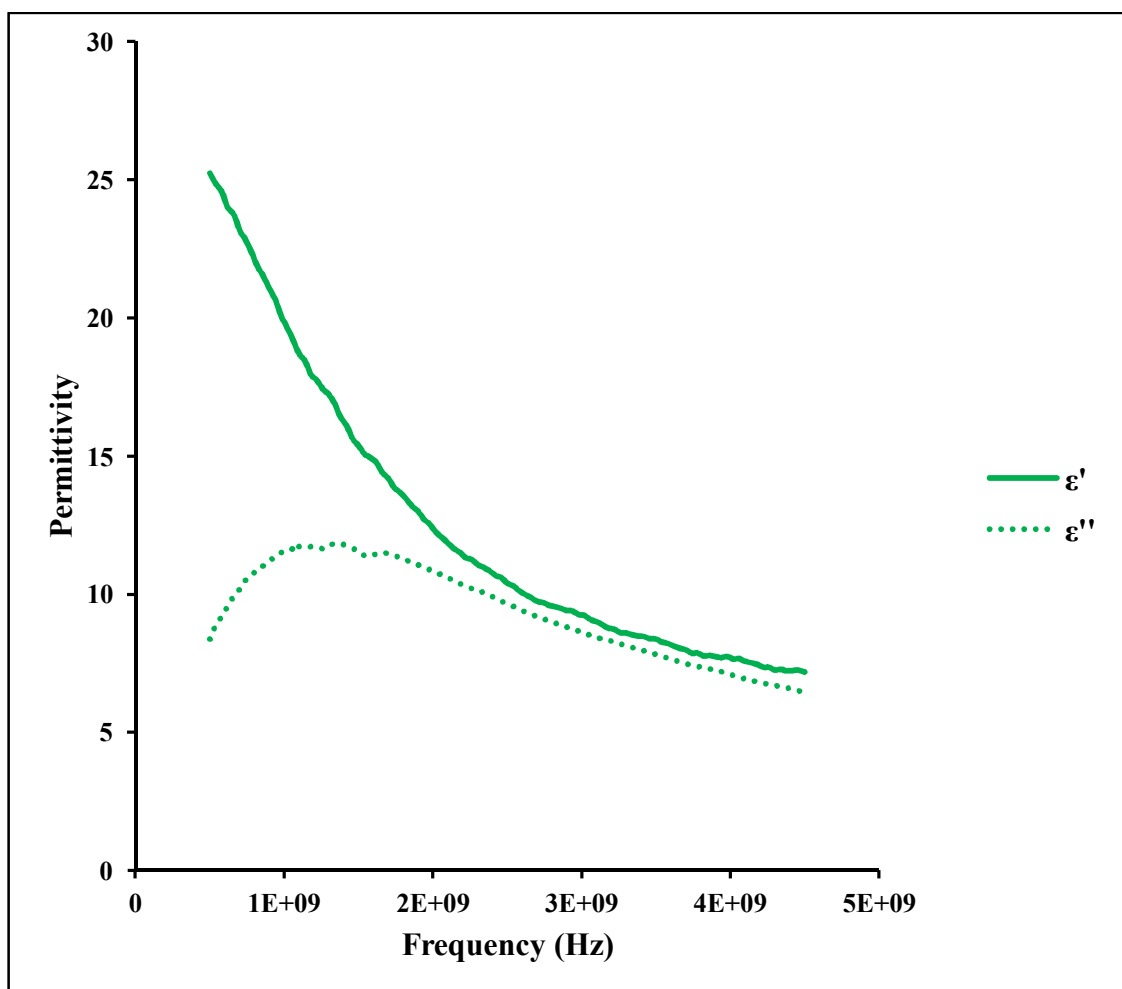

Figure 4.27 : Permittivity of the hybridized sample at room temperature.

CHAPTER FIVE: CONCLUSION AND RECOMMENDATIONS

The α-CNTs have been successfully synthesized using both $Fe(C_5H_5)_2$) and NH_4Cl powders via a simple chemical technique at a relatively low temperature of 230 °C. Various requirements for the synthesis of CNTs such as high temperature, complicated processing steps, catalyst support, longer synthesis period and expensive cost are thus eliminated. The α-CNTs made of amorphous carbon in nature are black in appearance and present in straight tubular structures with open ends. The dimensions of nanotubes: 80 - 110 nm for outer diameter; 45 - 65 nm for inner diameter; 8 - 10 μm for length. The untreated sample is observed in bundles disorderly due to the agglomeration forces between the nanotubes. Residual reactants (NH_4Cl and Fe) are then largely removed from the untreated sample after being washed with diluted HCl. The treated sample has irregular and rough surfaces implying the formation of defects within the structures due to the lower synthesis temperature. The carboxylic groups, -COOH acted as functional group have been attached on the surfaces of the α-CNTs (treated sample) infers the successful oxidation process. The oxidized sample displays the reduction of the agglomeration effect due to the oxidation treatment (surface modification treatment). More defects have also been introduced towards the nanotubes. The hybridized sample shows an increase in the thickness and roughness of its nanotubes, the best dispersion stability and the size quantization effect due to the attachment of CdSe QDs on the nanotubes surfaces. The outer diameters of nanotubes (120 - 150 nm) are the highest among other samples.

All the samples (α-CNTs) exhibit the phenomena of π plasmon absorbance ($E_π$) in the UV regions. The E_g for the untreated sample, treated sample, oxidized sample and hybrid sample are predicted as 4.50 eV, 4.65 eV, 4.43 and 3.00 eV, respectively. Two identical bands which correspond to the D and G bands of graphite for characterizing

CNTs are present in Raman spectra for all samples. The oxidation and hybridization processes introduce more defects and thus reduce crystallinity of the α-CNTs. The α-CNTs exhibited lower permittivity in frequency range of 500MHz - 4.5 GHz but their permittivity property can be increased via oxidation and hybridization processes. The hybridized sample can act as a potential dielectric material and displays the best thermally stable characteristic among other samples.

In order to understand the involved interactions between the α-CNTs and the CdSe QDs, two additional samples would be prepared and studied for the future works. They are the mixture of as-prepared sample with CdSe QDs and the mixture of treated (purified) sample with CdSe QDs.

Owing to the fact that the luminescence properties of CdSe QDs have been well established according to literature survey, photoluminescence characterization study should be conducted in future work. This investigation is to fully comprehend the optical absorption and excitation of the CdSe QDs attached on the α-CNTs. Besides that, the resistivity and magnetic properties of the α-CNTs have not been explored. These are necessary in order to unveil their optical and electromagnetic potentials, especially for the hybrid, α-CNTs/CdSe QDs. In addition of the CdSe QDs, there is also strong interest to develop hybrid materials between other semiconductor nanoparticles and the α-CNTs with the hope of discovering new properties due to their unique and structurally defined optical and electronic properties, which may suit them for applications in opto-electronic devices, laser diodes, liquid-crystal display (LCD) devices and so on.

REFERENCES

Ahmad, K., Pan, W., & Shi, S. L. (2006). Electrical conductivity and dielectric properties of multiwalled carbon nanotube and alumina composites. *Applied Physics Letter, 89*(13) 133122-133124

Ahmed, Sk. F., Mitra, M. K., & Chattopadhya, K. K. (2007a). Low-macroscopic field emission from silicon-incorporated diamond-like carbon film synthesized by dc PECV. *Applied Surface Science, 253*(12) 5480-5484.

Ahmed, Sk. F., Mitra, M. K., & Chattopadhya, K. K. (2007b). The effect of fluorine doping and temperature on the field emission from diamond-like carbon films. *Journal of Physic: Condensed Matter, 19*(34), 346233-346247.

Banerjee, D., Jha, A., & Chattopadhyay, K. K. (2009). Low-temperature synthesis of amorphous carbon nanoneedle and study on its field emission property. *Physica E, 41*(7), 1174-1178.

Berber, S., Kwon,Y. K., & Tománek, D. (2000). Unusually high thermal conductivity of carbon nanotubes. *Physical Review Letters, 84*(20), 4613-4616.

Bethune, D. S., Kiang, C. H., de Vries, M. S., Gorman, G., Savoy, R., Vazquez, J., & Bayers, R. (1993). Cobalt-Catalysed Growth of Carbon Nanotubes with Single-Atomic-Layer Walls. *Nature, 363*, 605-607.

Byrappa, K., & Adschiri, T. (2007). Hydrothermal technology for nanotechnology. *Progress in Crystal Growth and Characterization of Materials, 53*(2), 117-166.

Chan, W. C., & Nie, S. M. (1998). Quantum dot bioconjugates for ultrasensitive nonisotopic detection. *Science 281*(5385), 2016-2018.

Chen, J., Perebeinos, V., Freitag, M., Tsang, J., Fu, Q., Liu, J., & Avouris, Ph. (2005). Bright infrared emission from electrically induced excitons in carbon nanotubes. *Science 310*(5751), 1171-1174.

Cheng, Tao, Fang, ZhiYong, Zou, GuiFu, Hu, QiXiu, Hu, Biao, Yang, XiaoZhi, & Zhang, YouJin. (2006). A one-step single source route to carbon nanotubes. *Bulletin of Materials Science, 29*(7), 701-704.

Chik, H., & Xu, J. M. (2004). Nanometric superlattices: non-lithographic fabrication, materials, and prospects. *Materials Science and Engineering: R: Reports, 43*(4), 103-138.

Ci, Lijie, Wei, Bingqing, Xu, Cailu, Liang, Ji, Wu, Dehai, Xie, Sishen, Zhou, Weiya, Li, Yubao, Liu, Zuqin, & Tang, Dongsheng. (2001). Crystallization behavior of the amorphous carbon nanotubes prepared by the CVD method. *Journal of Crystal Growth, 233*(4), 823-828.

Ci, Lijie, Zhu, Hongwei, Wei, Bingqing, Xu, Cailu, & Wu, Dehai. (2003). Annealing amorphous carbon nanotubes for their application in hydrogen storage. *Applied Surface Science, 205*(1-4), 39-43.

Collins, P. G., Bradley, K., Ishigami, M., & Zettl, A. (2000). Extreme oxygen sensitivity of electronic properties of carbon nanotubes. *Science*, *287*(5459), 1801-1804.

Dinesh, J., Eswaramoorthy, M., & Rao, C. N. R. (2007). Use of amorphous carbon nanotube brushes as templates to fabricate GaN nanotube brushes and related materials. *Journal of Physical Chemistry C*, *111*(2), 510-513.

Dresselhaus, M. S., Dresselhaus, G., Jorio, A., Souza Filho, A. G., & Saito, R. (2002). Raman spectroscopy on isolated single wall carbon nanotubes. *Carbon*, *40*(12), 2043-2061.

Ebbesen, T. W., & Ajayan, P. M. (1992). Large-scale synthesis of carbon nanotubes. *Nature*, *358*, 220-222.

Endo, M. (1988). Grow carbon fibres in the vapour phase, *Chemtech*, *18*(9), 568-576.

Freitag, M., Martin, Y., Misewich, J. A., Martel, R., & Avouri, Ph. (2003). Photoconductivity of single carbon nanotubes. *Nano Letters 3*(8), 1067-1071.

Gao, Chao, Li, Wenwen, Jin, Yi Zheng, & Kong, Hao. (2006). Facile and large-scale synthesis and characterization of carbon nanotube/silver nanocrystal nanohybrids. *Nanotechnology*, *17*(12), 2882-2890.

Gao, Mei, Dai, Liming, & Wallace, Gordon G. (2003). Biosensors Based on Aligned Carbon Nanotubes Coated with Inherently Conducting Polymers. *Electroanalysis*, *15*(13), 1089-1094.

Gojny, FH., Nastalczyk, J., Roslaniec, Z., & Schulte, K (2003). Surface modified multi-walled carbon nanotubes in CNT/epoxy-composites. *Chemical Physics Letters*, *370*(5-6), 820-824.

Graham, A. R., Dan, H. M., Robin, J. N., & Andrei, N. K. (2010). UV-vis absorption spectroscopy of carbon nanotubes: Relationship between the π-electron plasmon and nanotube diameter. *Chemical Physics Letters*, *493*(1-3), 19-23.

Guo, T., Nikolaev, P., Rinzler, A. G., Tománek, D., Colbert, D. T., & Smalley, R. E. (1995). Self-assembly of tubular fullerenes. *Journal of Physical Chemistry*, *99*(27), 10694-10697.

Hamizi, N. A., & Johan, M. R. (2010). Synthesis and size dependent optical studies in CdSe quantum dots via inverse micelle technique. *Materials Chemistry and Physics*, *124*(1), 395-398.

Hussain, S., Youngs, I. J., & Ford, I. J. (2007). Electromagnetic properties of nanoparticle colloids at radio and microwave frequencies. *Journal of Physics D: Applied Physcis*, *40*(17), 5331-5337.

Hitoshi Nishino, Chiharu Yamaguchi, Haruyuki Nakaoka, Ryoichi Nishida. (2003). Carbon nanotube with amorphous carbon wall: α-CNT. *Carbon*, *41*(11), 2165-2167.

Hu, G., Cheng, M. J., Ma, D., & Bao, X. H. (2003). Synthesis of carbon nanotube bundles with mesoporous structure by a self-assembly solvothermal route. *Chemistry of Materials, 15*(7), 1470-1473.

Hungria, A. B., Juárez, B. H., Klinke, C., Weller, H., & Midgley, P. A. (2008). 3-D characterization of CdSe nanoparticles attached to carbon nanotubes. *Nano Research*, 1(1), 89-97.

Hutchison, J. L., Kiselev, N. A., Krinichnaya, E. P., Krestinin, A. V., Loutfy, R. O., Morawsky, A. P., Muradyan, V. E., Obraztsova, E. D., Sloan, J., Terekhov, S.V., & Zakharov, D.N. (2001). Double-walled carbon nanotubes fabricated by a hydrogen arc discharge method. Carbon, *39*(5), 761-770.

Iijima, S. (1991). Helical microtubules of graphitic carbon. *Nature, 354* , 56-58.

Jason, K. V., Jonathan, J. B., Jeffery, E. R., Allan, E. B., Geoffrey, L. W., & Bradly, D. F. (2004). Low-temperature growth of carbon nanotubes from the catalytic decomposition of carbon tetrachloride. *Journal of The American Chemical Society, 126*(32), 9936-9937.

Jana, S., Banerjee, D., Jha, A., & Chattopadhyay, K. K. (2011). Fabrication of PbS nanoparticles coated amorphous carbon nanotubes: Structural, thermal and field emission properties. *Materials Research Bulletin*, *46*(10), 1659-1664.

Jha, A., Banerjee, D., & Chattopadhyay, K. K. (2011). Improved field emission from amorphous carbon nanotubes by surface functionalization with stearic acid. *Carbon*, *49*(4),1272-1278.

Jorio, A., Dresselhaus, G., & Dresselhaus, M. S. (Eds.). (2008). *Carbon nanotubes - advanced topics in the synthesis, structure, properties and applications*. New York: Springer-Verlag Berlin Heidelberg.

José-Yacamán, M., Miki-Yoshida, Rendón, M. L., & Santiesteban, J. G. (1993). Catalytic growth of carbon microtubules with fullerene structure. *Applied Physics Letters*, *62*(2), 202-204.

Juárez, Beatriz H., Klinke, Christian, Kornowski, Andreas, & Weller, Horst. (2007). Quantum dot attachment and morphology control by carbon nanotubes. *NanoLetters*, *7*(12), 3564-3568.

Kataura, H., Kumazawa, Y., Maniwa, Y., Umezu, I., Suzuki, S., Ohtsuka, Y. & Achiba, Y. (1999). Optical properties of single-wall carbon nanotubes. *Synthetic Metals*, *103*, 2555-2558.

Kolosnjaj, J., Szwarc, H., & Moussa, F. (2007). Toxicity studies of carbon nanotubes. *Advances in Experimental Medicine and Biology 620*, 181-204.

Krupka, J. (2006). Frequency domain complex permittivity measurements at microwave frequencies. *Measurement Science and Technology, 17*(6), R55-R70.

Kueseng, K., & Jacob, K. I. (2006). Natural rubber nanocomposites with SiC nanoparticles and carbon nanotubes. *European Polymer Journal*, *42*(1), 220-227.

Li, Q., Xue, Qingzhong, Hao, Lanzhong, Gao, Xili, & Zheng, Qingbin. (2008). Large dielectric constant of functionalized carbon nanotubes/polymer composites. *Composites Science and Technology*, *68*(10-11), 2290-2296.

Li, Qiao-ling, Zhang, Cun-rui, & Li, Jian-qiang. (2010). Synthesis and microwave absorption of BaTiO$_3$-polypyrrole composite. *Chinese Journal of Chemical Physics*, *23*(5), 603-607.

Li, W. Z., Xie, S. S., Qian, L. X., Chang, B. H., Zou, B. S., Zhou, W.Y., Zhao, R. A., & Wang, G. (1996). Large-scale synthesis of aligned carbon nanotubes. *Science*, *274*(5293), 1701-1703.

Li, Xinming, Zhu, Hongwei, Wei, Jinquan, Wang, Kunlin, Xu, Eryang, Li, Zhen, & Wu, Dehai. (2009). Determination of band gaps of self-assembled carbon nanotube films using Tauc/Davis–Mott model. *Applied Physics A: Materials Science & Processing*, *97*(2), 341-344.

Li, Yan-Huei, & Lue, Juh-Tzeng. (2007). Dielectric constants of single-wall carbon nanotubes at various frequencies. *Journal of Nanoscience and Nanotechnology*, *7*(9), 3185-3188.

Liu, Boyang, Jia, Dechang Jia, Zhou, Yu, Feng, Haibo, & Meng, Qingchang. (2007). Low temperature synthesis of amorphous carbon nanotubes in air. *Carbon*, *45*(8), 1710-1713.

Liu, YN, Song, XL, Zhao, TK, Zhu, JW, Hirscher, M, & Philipp, F. (2004). Amorphous carbon nanotubes produced by a temperature controlled DC arc discharge. *Carbon*, *42*(8-9), 1852-1855.

Lou, Zhensong, Chen, Qianweng, Wang, W., & Zhang, Yufeng. (2003). Synthesis of carbon nanotubes by reduction of carbon dioxide with metallic lithium. *Carbon*, *41*(15), 3063-3074.

Lu, Chenguang, Akey, Austin, Wang, Wei, & Herman, Irving. (2009). Versatile formation of CdSe nanoparticle-single walled carbon nanotube hybrid structures. *Journal of The American Chemical Society*, *131*(10), 3446-3447.

Luo, Tao, Chen, Luyang, Bao, Keyan, Yu, Weichao, & Qian, Yitai. (2006). Solvothermal preparation of amorphous carbon nanotubes and Fe/C coaxial nanocables from sulfur, ferrocene, and benzene. *Carbon*, *44*(13), 2844-2848.

Matthews, M. J., Pienta, M. A., Dresselhaus, G., Dresselhaus, M. S., & Endo, M. (1999). Origin of dispersive effects of the Raman D band in carbon materials. *Physical Review B*, *59*(10), R6585-R6588.

Melissa Paradise & Tarun Goswami. (2007). Carbon nanotubes - Production and industrial applications. *Materials & Design*, *28*(5), 1477-1489.

Meyyappan, M. (2005). *Carbon nanotubes science and applications*. Boca Raton: CRC Press LLC.

Neelakanta, P. S. (1995). *Handbook of Electromagnetic Materials*. London: CRC Press LLC.

Nelson, S. O., Guo, Wen-chuan, Trabelsi, S., & Kays, S. J. (2007). Dielectric spectroscopy of watermelons for quality sensing. *Measurement Science and Technology*, *18*(7), 1887-1892.

O'Connell, M. J. (2006). *Carbon nanotubes properties and applications*. Boca Raton: CRC Press.

Passacantando, M., Bussolotti, F., Grossi, V., Santucci, S., Ambrosio, A., Ambrosio, M., Ambrosone, G., Carillo, V., Coscia, U., Maddalena, P., Perillo, E., & Raulo, A. (2008). Applied Physics Letters, 93(5), 051911.

Paul, R., Kumbhakar, P., & Mitra, A. K. (2010). Synthesis and study of photoluminescence of carbon nanotube/ZnS hybrid nanostructures. *Journal of Experimental Nanoscience, 5*(4), 363-373.

Peter, J. F. H. (2009). *Carbon nanotube science: Synthesis, properties and applications*. New York: Cambridge University Press.

Pichler, T., Knupfer, M., Golden, M. S., Fink, J., Rinzler, A. & Smalley, R. E. (1998). Localized and delocalized electronic states in single-wall carbon nanotubes. *Physical Review Letters*, *80*(21), 4729-4732.

Rakitin, A., Papadopoulos, C., & Xu, JM. (2000). Electronic properties of amorphous carbon nanotubes. *Physical Review B*, *61*(8), 5793-5796.

Rakov, E. G. (2006). Chemistry of carbon nanotubes. In Yury Gogotsi, *Nanomaterials Handbook*. Boca Raton: CRC Press.

Reference from ASI Instruments, *Dielectric constants chart*. Retrieved 6 January 2012, from http://www.asiinstr.com/technical/DielectricConstants.htm#SectionC.

Ren, Z. F., Huang, Z. P., Xu, J. W., Wang, J. H., Bush, P., Siegal, M. P., & Provencio, P. N. (1998). Synthesis of large arrays of well-aligned carbon nanotubes on glass. *Science*, *282*(5391), 1105-1107.

Robel, I., Bunker, B. A., & Kamat, P. V. (2005). Single-walled carbon nanotube-CdS nanocomposites as light-harvesting assemblies: Photoinduced charge-transfer interactions. *Advanced Materials*, *17*(20), 2458-2463.

Saito, R., Dresselhaus, G., & Dresselhaus, M. S. (Eds.). (1988). *Physical properties of carbon nanotubes*. London: Imperial College Press.

Saito, Y., & Uemura, S. (2000). Field emission from carbon nanotubes and its application to electron sources. *Carbon, 38*(2), 169-182.

Scott, C. D., Arepalli, S., Nikolaev, P., & Smalley, R. E. (2001). Growth mechanism for single wall carbon nanotubes in a laser ablation process. *Applied Physics A*, *72*(5), 573-580.
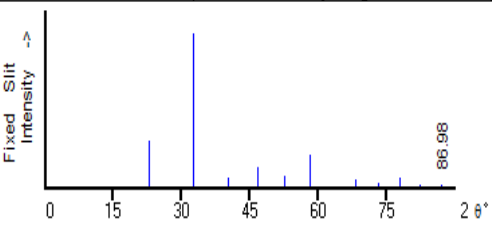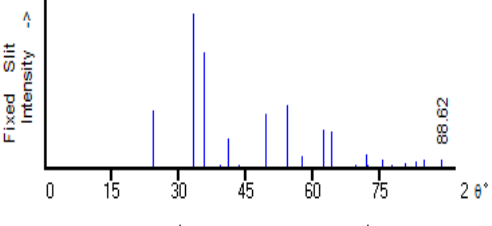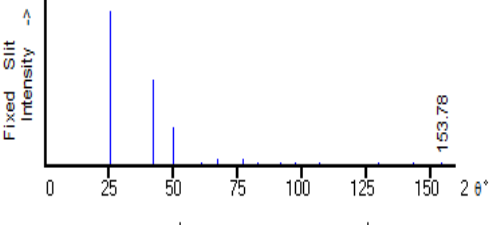
Silva, S. R. P. (2003). *Properties of amorphous carbon*. London: INSPEC, The Institution of Electrical Engineers.

Speck, S., Endo, M., & Dresselhaus, M. S. (1989). Structure and intercalation of thin benzene derived carbon fibers. *Journal of Crystal Growth*, *94*(4), 834-848.

Sui, Y. C., Acosta, D. R., González-León, J. A., Bermúdez, A., Feuchtwanger, J., Cui, B. Z., Flores, J. O., & Saniger, J. M. (2001). Structure, thermal stability, and deformation of multibranched carbon nanotubes synthesized by CVD in the AAO template. *Journal of Physical Chemistry B*, *105*(8), 1523-1527.

Tibbetts, G. G., Gorkiewicz, D. W., & Alig, R. L. (1993). A new reactor for growing carbon-fibers from liquid-phase and vapor-phase hydrocarbons. *Carbon*, *31*(5),809-814.

Wang, W. Z., Huang, J. Y., Wang, D. Z., & Ren, Z. F. (2005b). Low-temperature hydrothermal synthesis of multiwall carbon nanotubes. *Carbon*, *43*(6), 1328-1331.

Wang, W. Z., Poudel, B., Wang, D. Z., & Ren, Z. F. (2005a). *Synthesis of multiwalled carbon nanotubes through a modified Wolff-Kishner reduction process*. *Journal of The American Chemical Society*, *127*(51), 18018-18019.

Wang, X., Li, Q., Xie, J., Jin, Z., Wang, J., Li, Y., Jiang, K., & Fan, S. (2009). Fabrication of ultralong and electrically uniform single-walled carbon nanotubes on clean substrates. *Nano Letters*, *9*(9), 3137-3141.

Wang, Xizhang, Hu, Zheng, Wu, Qiang, & Chen, Yi. (2002). Low-temperature catalytic growth of carbon nanotubes under microwave plasma assistance. *Catalysis Today*, *72*(3-4), 205-211.

Wang, Y. C., Lue, J. T., & Pauw, K. F. (2009). Dielectric constants of multiwall carbon nanotubes from direct current to microwave frequencies. *Journal of Nanoscience and Nanotechnology*, *9*(3), 1734-1740.

Wiltshire, J. G., Khlobystov, A. N., Li, L. J., Lyapin, S. G., Briggs, G. A. D., & Nicholas, R. J. (2004). Comparative studies on acid and thermal based selective purification of HiPCO produced single-walled carbon nanotubes. *Chemical Physics Letters*, 3*86*(4-6), 239-243.

Wu, W. Z., Zhu, Z. P., & Liu, Z. Y. (2002). Amorphous carbon nano-particles prepared by explosion of nitrated pitch. *Carbon*, *40*(11), 2034-2037.

Xiong, Yujie, Xie, Yi, Li, Xiaoxu, & Li, Zhengquan. (2004). Production of novel amorphous carbon nanostructures from ferrocene in low-temperature solution. *Carbon*, *42*(8-9), 1447-1453.

Yang, C., Lin, Yuanhua, & Nan, C.W. (2009). Modified carbon nanotubes composite with high dielectric constant, low dielectric loss and large energy density. *Carbon*, *47*(4), 1096-1101.

Yang, Y., Hu, Z., Wu, Q., Lü, Y. N., Wang, X. Z., & Chen, Y. (2003). Template-confined growth and structural characterization of amorphous carbon nanotubes. *Chemical Physics Letters*, *373*(5-6), 580-585.

Yu, Guojun, Gong, Jinlong, Wang, Sen, Zhu, Dezhang, He, Suixia, & Zhu, Zhiyuan. (2006). Etching effects of ethanol on multi-walled carbon nanotubes. *Carbon*, 44(7), 1218-1224.

Zhang, Zhijing, Dewan, Christina, Kothari, Saumya, Mitra, Saibal, & Teeters, Dale. (2005). Carbon nanotube synthesis, characteristics, and microbattery applications. *Materials Science and Engineering B*, *116*(3), 363-368.

Zhao, N. H., Wang, G. J., Huang, Y., Wang, B., Yao, B. D., & Wu, Y. P. (2008). Preparation of nanowire arrays of amorphous carbon nanotube-coated single crystal SnO_2. *Chemistry of Materials*, *20*(8), 2612-2614.

Zhao, N. H., Yang, L. C., Zhang, P., Wang, G. J., Wang, B., Yao, B. D., & Wu, Y. P. (2010). Polycrystalline SnO2 nanowires coated with amorphous carbon nanotube as anode material for lithium ion batteries. *Materials Letters*, *64*(8), 972-975.

Zhao, N. Q., He, C. N., Du, X. W., Shi, C. S., Li, J. J., & Cui, L. (2006). Amorphous carbon nanotubes fabricated by low-temperature chemical vapor deposition. *Carbon*, *44*(9), 1859-1862.

Zhao, N.H., Zhang, P., Yang, L.C., Fu, L. J., Wang, B., & Wu, Y. P. (2009). Tunable amorphous carbon nanotubes prepared by a simple template. *Materials Letters*, *63*(22), 1955-1957.

Zhao, Tingkai, Liu, Yongning, & Zhu, Jiewu. (2005). Temperature and catalyst effects on the production of amorphous carbon nanotubes by a modified arc discharge. *Carbon*, *43*(14), 2907-2912.

Zhu, Junjie, Palchik, O., Chen, Siguang, & Gedanken, A. (2000). Microwave assisted preparation of CdSe, PbSe, and $Cu_{2-x}Se$ Nanoparticles. *Journal of Physicals Chemistry B*, *104*(31), 7344-7347.

Internet References

(URL_ http://www.asiinstr.com/technical/Dielectric Constants.htm), 10/1/2012

Card 73-0365

73-0365	Quality: C

CAS Number:

Molecular Weight: 53.49
Volume[CD]: 58.28
Dx: 1.524   Dm:

Sys: Cubic
Lattice: Primitive
S.G.: Pm3m (221)
Cell Parameters:
a 3.877   b   c
α   β   γ

I/Icor: 4.92
Rad: CuKa1
Lambda: 1.54060
Filter:
d-sp: calculated

ICSD # : 022141

N H4 Cl
Ammonium Chloride
Ref: Calculated from ICSD using POWD-12++, (1997)
Ref: Sirdeshmukh, D.B., Deshpande, V.T., Acta Crystallogr., Sec. B, 26, 295 (1970)

2θ	Int-f	h	k	l	2θ	Int-f	h	k	l	2θ	Int-f	h	k	l
22.919	301	1	0	0	52.751	77	2	1	0	77.844	65	3	1	0
32.636	999 *	1	1	0	58.241	208	2	1	1	82.436	17	3	1	1
40.256	67	1	1	1	68.380	54	2	2	0	86.980	15	2	2	2
46.825	128	2	0	0	73.171	31	2	2	1					

Card 73-2234

73-2234	Quality: C

CAS Number:

Molecular Weight: 159.69
Volume[CD]: 100.46
Dx: 5.279   Dm:

Sys: Rhombohedral
Lattice: Rhomb-centered
S.G.: R3c (167)
Cell Parameters:
a 5.424   b   c
α 55.280   β   γ

I/Icor: 3.01
Rad: CuKa1
Lambda: 1.54060
Filter:
d-sp: calculated

ICSD # : 024791

Fe2 O3
Iron Oxide
Ref: Calculated from ICSD using POWD-12++, (1997)
Ref: Shirane, G et al., J. Phys. Chem. Solids, 10, 35 (1959)

2θ	Int-f	h	k	l	2θ	Int-f	h	k	l	2θ	Int-f	h	k	l
24.163	366	1	1	0	57.638	76	3	3	2	78.828	4	1̄	3	1
33.179	999 *	1	2	1	62.476	249	1	3	0	79.539	1	2̄	2	1
35.651	739	1̄	1	0	64.040	233	2̄	1	1	80.636	14	1̄	3	0
39.310	20	2	2	2	66.074	3	2	3	0	80.768	28	3	4	1
40.886	190	1	2	0	69.644	20	2	4	2	83.017	36	4	4	2
43.534	16	0	2	0	72.001	81	3	4	3	84.554	2	4	4	4
49.493	342	2	2	0	72.334	19	3	4	2	84.993	52	3̄	2̄	1
54.104	400	2	3	1	75.244	3	2	4	1	88.622	49	2	4	0
56.192	7	1̄	2	0	75.503	49	2̄	2	0					
57.483	13	1̄	1	2	77.791	19	1	4	1					

Card 19-0191

19-0191	Quality: I

CAS Number: 1306-24-7

Molecular Weight: 191.37
Volume[CD]: 224.42
Dx: 5.664   Dm:

Sys: Cubic
Lattice: Face-centered
S.G.: F4̄3m (216)
Cell Parameters:
a 6.077   b   c
α   β   γ

SS/FOM: F13=11(0.054, 21)
I/Icor:
Rad: CuKa
Lambda: 1.5418
Filter: Ni
d-sp:

Cd Se
Cadmium Selenide
Ref: Takahashi, Govermental Industrial Research Institute, Osaka, Japan, Private Communication, (1967)

2θ	Int-f	h	k	l	2θ	Int-f	h	k	l	2θ	Int-f	h	k	l
25.354	100	1	1	1	76.777	4	4	2	2	129.60	2	5	5	1
42.008	55	2	2	0	82.401	2	5	1	1	143.32	2	6	4	2
49.698	25	3	1	1	91.550	2	4	4	0	153.77	2	7	3	1
60.941	2	4	0	0	97.161	2	5	3	1					
67.081	4	3	3	1	106.63	2	6	2	0					

APPENDIX B

Curve Name: **Untreated Sample**					
Values:					
Index	Time [s]	Sample Temp [°C]	Ref. Temp [°C]	Mass [mg]	Mass [%]
0	0	36.0537	30.0000	5.4997	99.9945
59	59	44.2772	39.8333	5.4940	99.8900
118	118	53.1441	49.6667	5.4214	98.5700
177	177	62.1958	59.5000	5.4181	98.5100
236	236	71.4105	69.3333	5.3609	97.4700
295	295	80.7469	79.1667	5.3290	96.8900
354	354	90.1584	89.0000	5.3108	96.5600
413	413	99.6118	98.8333	5.2916	96.2100
472	472	109.1785	108.6667	5.2790	95.9811
531	531	118.7313	118.5000	5.2785	95.9722
590	590	128.3789	128.3333	5.2780	95.9633
649	649	138.0352	138.1667	5.2775	95.9544
708	708	147.7633	148.0000	5.2770	95.9455
767	767	157.4835	157.8333	5.2740	95.8915
826	826	167.2297	167.6667	5.2446	95.3570
885	885	177.0234	177.5000	5.2430	95.3271
944	944	186.824	187.3333	5.2408	95.2877
1003	1003	196.5452	197.1667	5.2352	95.1849
1062	1062	206.2151	207.0000	5.2349	95.1795
1121	1121	216.0906	216.8333	5.2247	94.9952
1180	1180	225.8452	226.6667	5.1569	93.7618
1239	1239	235.4841	236.5000	5.0089	91.0709
1298	1298	245.029	246.3333	4.7265	85.9364
1357	1357	254.5447	256.1667	4.3447	78.9945
1416	1416	264.0135	266.0000	3.8458	69.9236
1475	1475	273.4886	275.8333	3.2211	58.5655
1534	1534	283.1319	285.6667	2.4960	45.3818
1593	1593	293.1567	295.5000	1.7488	31.7964
1652	1652	303.7061	305.3333	1.1417	20.7582
1711	1711	314.6307	315.1667	0.8461	15.3836
1770	1770	324.893	325.0000	0.8020	14.5818
1829	1829	334.8344	334.8333	0.7727	14.0491
1888	1888	344.669	344.6667	0.7466	13.5745
1947	1947	354.4355	354.5000	0.7242	13.1673
2006	2006	364.1932	364.3333	0.6991	12.7109
2065	2065	373.9626	374.1667	0.6772	12.3127
2124	2124	383.7328	384.0000	0.6563	11.9327
2183	2183	393.4893	393.8333	0.6367	11.5764
2242	2242	403.2401	403.6667	0.6162	11.2036
2301	2301	412.988	413.5000	0.6000	10.9091
2360	2360	422.7384	423.3333	0.5833	10.6055

2419	2419	432.4885	433.1667	0.5634	10.2436
2478	2478	442.1945	443.0000	0.5430	9.8727
2537	2537	451.9139	452.8333	0.5226	9.5018
2596	2596	461.6087	462.6667	0.5010	9.1091
2655	2655	471.2982	472.5000	0.4763	8.6600
2714	2714	480.9666	482.3333	0.4530	8.2364
2773	2773	490.649	492.1667	0.4288	7.7964
2832	2832	500.2885	502.0000	0.4066	7.3927
2891	2891	509.9331	511.8333	0.3835	6.9727
2950	2950	519.5326	521.6667	0.3646	6.6291
3009	3009	529.1082	531.5000	0.3506	6.3745
3068	3068	538.6867	541.3333	0.3406	6.1927
3127	3127	548.2714	551.1667	0.3317	6.0309
3186	3186	557.8359	561.0000	0.3280	5.9636
3245	3245	567.4231	570.8333	0.3280	5.9636
3304	3304	577.0182	580.6667	0.3270	5.9455
3363	3363	586.5979	590.5000	0.3280	5.9636
3422	3422	596.1722	600.3333	0.3293	5.9873
3481	3481	605.7482	610.1667	0.3312	6.0218
3540	3540	615.3405	620.0000	0.3312	6.0218
3599	3599	624.927	629.8333	0.3330	6.0545
3658	3658	634.4645	639.6667	0.3350	6.0909
3717	3717	644.0132	649.5000	0.3350	6.0909
3776	3776	653.596	659.3333	0.3350	6.0909
3835	3835	663.15	669.1667	0.3340	6.0727
3894	3894	672.6891	679.0000	0.3310	6.0182
3953	3953	682.2659	688.8333	0.3269	5.9436
4012	4012	691.8015	698.6667	0.3215	5.8455
4071	4071	701.3317	708.5000	0.3156	5.7382
4130	4130	710.864	718.3333	0.3070	5.5818
4189	4189	720.4152	728.1667	0.2972	5.4036
4248	4248	729.9346	738.0000	0.2874	5.2255
4307	4307	739.476	747.8333	0.2779	5.0527
4366	4366	749.0508	757.6667	0.2701	4.9109
4425	4425	758.6075	767.5000	0.2640	4.8000
4484	4484	768.1577	777.3333	0.2573	4.6782
4543	4543	777.7297	787.1667	0.2491	4.5291
4602	4602	787.3042	797.0000	0.2456	4.4655
4661	4661	796.8354	806.8333	0.2420	4.4000
4720	4720	806.3936	816.6667	0.2370	4.3091
4779	4779	815.9499	826.5000	0.2350	4.2727
4838	4838	825.4742	836.3333	0.2340	4.2545
4897	4897	835.0187	846.1667	0.2320	4.2182
4956	4956	844.5552	856.0000	0.2320	4.2182
5015	5015	854.085	865.8333	0.2320	4.2182
5074	5074	863.6221	875.6667	0.2314	4.2073
5133	5133	873.1606	885.5000	0.2320	4.2182

5192	5192	882.7449	895.3333	0.2321	4.2200
5251	5251	892.3483	905.1667	0.2310	4.2000
5310	5310	901.9723	915.0000	0.2310	4.2000
5369	5369	911.5647	924.8333	0.2310	4.2000
5428	5428	921.1747	934.6667	0.2300	4.1818
5487	5487	930.7945	944.5000	0.2306	4.1927
5546	5546	940.4197	954.3333	0.2310	4.2000
5605	5605	950.1049	964.1667	0.2325	4.2273
5664	5664	959.7895	974.0000	0.2350	4.2727
5723	5723	969.4996	983.8333	0.2340	4.2545
5782	5782	979.2361	993.6667	0.2350	4.2727

Curve Name: **Treated Sample**					
Values:					
Index	Time [s]	Sample Temp [°C]	Ref. Temp [°C]	Mass [mg]	Mass [%]
0	0	35.9697	30.0000	4.1995	99.9881
59	59	44.4440	39.8333	4.2946	102.2524
118	118	53.2515	49.6667	4.2728	101.7333
177	177	62.2908	59.5000	4.2351	100.8357
236	236	71.4672	69.3333	4.1921	99.8119
295	295	80.8010	79.1667	4.1513	98.8405
354	354	90.1989	89.0000	4.1175	98.0357
413	413	99.7318	98.8333	4.0924	97.4381
472	472	109.3062	108.6667	4.0710	96.9286
531	531	118.8973	118.5000	4.0534	96.5095
590	590	128.5882	128.3333	4.0393	96.1738
649	649	138.2649	138.1667	4.0267	95.8738
708	708	148.0072	148.0000	4.0125	95.5357
767	767	157.7955	157.8333	3.9987	95.2071
826	826	167.6321	167.6667	3.9847	94.8738
885	885	177.4274	177.5000	3.9693	94.5071
944	944	187.3158	187.3333	3.9513	94.0786
1003	1003	197.1649	197.1667	3.9335	93.6548
1062	1062	207.0877	207.0000	3.9157	93.2310
1121	1121	216.9819	216.8333	3.8959	92.7595
1180	1180	226.9076	226.6667	3.8747	92.2548
1239	1239	236.8239	236.5000	3.8534	91.7476
1298	1298	246.7307	246.3333	3.8314	91.2238
1357	1357	256.6474	256.1667	3.8075	90.6548
1416	1416	266.5441	266.0000	3.7796	89.9905
1475	1475	276.3930	275.8333	3.7504	89.2952
1534	1534	286.2715	285.6667	3.7201	88.5738
1593	1593	296.1093	295.5000	3.6877	87.8024
1652	1652	305.9435	305.3333	3.6535	86.9881
1711	1711	315.7635	315.1667	3.6191	86.1690

1770	1770	325.5948	325.0000	3.5852	85.3619
1829	1829	335.3922	334.8333	3.5480	84.4762
1888	1888	345.1660	344.6667	3.5100	83.5714
1947	1947	354.9788	354.5000	3.4723	82.6738
2006	2006	364.7356	364.3333	3.4343	81.7690
2065	2065	374.5066	374.1667	3.3963	80.8643
2124	2124	384.2386	384.0000	3.3576	79.9429
2183	2183	393.9878	393.8333	3.3186	79.0143
2242	2242	403.7205	403.6667	3.2797	78.0881
2301	2301	413.4177	413.5000	3.2369	77.0690
2360	2360	423.1445	423.3333	3.1961	76.0976
2419	2419	432.8181	433.1667	3.1540	75.0952
2478	2478	442.4819	443.0000	3.1118	74.0905
2537	2537	452.1820	452.8333	3.0679	73.0452
2596	2596	461.8568	462.6667	3.0253	72.0310
2655	2655	471.5336	472.5000	2.9823	71.0071
2714	2714	481.1922	482.3333	2.9387	69.9690
2773	2773	490.8430	492.1667	2.8957	68.9452
2832	2832	500.4981	502.0000	2.8525	67.9167
2891	2891	510.1367	511.8333	2.8111	66.9310
2950	2950	519.7886	521.6667	2.7673	65.8881
3009	3009	529.3936	531.5000	2.7256	64.8952
3068	3068	538.9991	541.3333	2.6849	63.9262
3127	3127	548.6061	551.1667	2.6445	62.9643
3186	3186	558.2130	561.0000	2.6044	62.0095
3245	3245	567.7904	570.8333	2.5676	61.1333
3304	3304	577.3740	580.6667	2.5315	60.2738
3363	3363	586.9357	590.5000	2.4947	59.3976
3422	3422	596.4938	600.3333	2.4595	58.5595
3481	3481	606.0654	610.1667	2.4260	57.7619
3540	3540	615.6143	620.0000	2.3940	57.0000
3599	3599	625.1860	629.8333	2.3601	56.1929
3658	3658	634.7583	639.6667	2.3276	55.4190
3717	3717	644.3026	649.5000	2.2962	54.6714
3776	3776	653.8911	659.3333	2.2638	53.9000
3835	3835	663.4880	669.1667	2.2296	53.0857
3894	3894	673.0568	679.0000	2.1970	52.3095
3953	3953	682.6634	688.8333	2.1627	51.4929
4012	4012	692.2515	698.6667	2.1283	50.6738
4071	4071	701.8375	708.5000	2.0944	49.8667
4130	4130	711.4285	718.3333	2.0630	49.1190
4189	4189	721.0099	728.1667	2.0314	48.3667
4248	4248	730.5674	738.0000	1.9979	47.5690
4307	4307	740.0896	747.8333	1.9661	46.8119
4366	4366	749.6374	757.6667	1.9357	46.0881
4425	4425	759.1701	767.5000	1.9046	45.3476
4484	4484	768.7007	777.3333	1.8726	44.5857

4543	4543	778.2338	787.1667	1.8411	43.8357
4602	4602	787.7615	797.0000	1.8101	43.0976
4661	4661	797.2842	806.8333	1.7766	42.3000
4720	4720	806.8224	816.6667	1.7439	41.5214
4779	4779	816.3446	826.5000	1.7098	40.7095
4838	4838	825.8647	836.3333	1.6754	39.8905
4897	4897	835.3926	846.1667	1.6403	39.0548
4956	4956	844.9270	856.0000	1.6052	38.2190
5015	5015	854.4647	865.8333	1.5687	37.3500
5074	5074	863.9943	875.6667	1.5267	36.3500
5133	5133	873.5310	885.5000	1.4837	35.3262
5192	5192	883.0951	895.3333	1.4440	34.3810
5251	5251	892.7056	905.1667	1.4013	33.3643
5310	5310	902.3394	915.0000	1.3596	32.3714
5369	5369	911.9802	924.8333	1.3182	31.3857
5428	5428	921.6088	934.6667	1.2745	30.3452
5487	5487	931.2371	944.5000	1.2293	29.2690
5546	5546	940.7985	954.3333	1.1839	28.1881
5605	5605	950.3954	964.1667	1.1405	27.1548
5664	5664	959.9749	974.0000	1.0965	26.1071
5723	5723	969.6010	983.8333	1.0549	25.1167
5782	5782	979.2626	993.6667	1.0172	24.2190

Curve Name: **Oxidized Sample**

Values:

Index	Time [s]	Sample Temp [°C]	Ref. Temp [°C]	Mass [mg]	Mass [%]
0	0	22.2475	30.0000	4.0997	99.9927
59	59	29.6718	39.8333	4.1573	101.3976
118	118	37.9233	49.6667	4.1479	101.1683
177	177	46.5897	59.5000	4.1050	100.1220
236	236	55.5578	69.3333	4.0389	98.5098
295	295	64.7363	79.1667	3.9642	96.6878
354	354	74.1158	89.0000	3.8921	94.9293
413	413	83.5919	98.8333	3.8243	93.2756
472	472	93.2552	108.6667	3.7660	91.8537
531	531	103.0152	118.5000	3.7202	90.7366
590	590	112.7687	128.3333	3.6823	89.8122
649	649	122.6326	138.1667	3.6529	89.0951
708	708	132.5038	148.0000	3.6284	88.4976
767	767	142.4351	157.8333	3.6066	87.9659
826	826	152.3461	167.6667	3.5831	87.3927
885	885	162.3409	177.5000	3.5590	86.8049
944	944	172.3447	187.3333	3.5326	86.1610
1003	1003	182.3785	197.1667	3.5066	85.5268
1062	1062	192.3995	207.0000	3.4777	84.8220

1121	1121	202.4833	216.8333	3.4502	84.1512
1180	1180	212.5665	226.6667	3.4249	83.5341
1239	1239	222.6798	236.5000	3.3979	82.8756
1298	1298	232.7995	246.3333	3.3720	82.2439
1357	1357	242.8931	256.1667	3.3454	81.5951
1416	1416	252.9873	266.0000	3.3171	80.9049
1475	1475	263.1257	275.8333	3.2881	80.1976
1534	1534	273.2086	285.6667	3.2591	79.4902
1593	1593	283.3090	295.5000	3.2275	78.7195
1652	1652	293.3911	305.3333	3.1978	77.9951
1711	1711	303.5103	315.1667	3.1667	77.2366
1770	1770	313.6003	325.0000	3.1342	76.4439
1829	1829	323.7022	334.8333	3.1034	75.6927
1888	1888	333.8020	344.6667	3.0706	74.8927
1947	1947	343.8774	354.5000	3.0367	74.0659
2006	2006	353.9645	364.3333	3.0037	73.2610
2065	2065	364.0446	374.1667	2.9699	72.4366
2124	2124	374.0959	384.0000	2.9351	71.5878
2183	2183	384.1564	393.8333	2.9000	70.7317
2242	2242	394.1635	403.6667	2.8639	69.8512
2301	2301	404.1866	413.5000	2.8283	68.9829
2360	2360	414.1878	423.3333	2.7913	68.0805
2419	2419	424.1934	433.1667	2.7530	67.1463
2478	2478	434.1802	443.0000	2.7137	66.1878
2537	2537	444.1448	452.8333	2.6744	65.2293
2596	2596	454.1142	462.6667	2.6317	64.1878
2655	2655	464.0697	472.5000	2.5901	63.1732
2714	2714	473.9900	482.3333	2.5473	62.1293
2773	2773	483.9506	492.1667	2.5033	61.0561
2832	2832	493.8796	502.0000	2.4589	59.9732
2891	2891	503.8202	511.8333	2.4144	58.8878
2950	2950	513.6934	521.6667	2.3693	57.7878
3009	3009	523.5913	531.5000	2.3246	56.6976
3068	3068	533.4852	541.3333	2.2798	55.6049
3127	3127	543.3635	551.1667	2.2351	54.5146
3186	3186	553.2512	561.0000	2.1911	53.4415
3245	3245	563.1206	570.8333	2.1463	52.3488
3304	3304	572.9825	580.6667	2.1027	51.2854
3363	3363	582.8460	590.5000	2.0593	50.2268
3422	3422	592.6974	600.3333	2.0174	49.2049
3481	3481	602.5443	610.1667	1.9754	48.1805
3540	3540	612.4171	620.0000	1.9333	47.1537
3599	3599	622.2657	629.8333	1.8935	46.1829
3658	3658	632.0855	639.6667	1.8527	45.1878
3717	3717	641.9095	649.5000	1.8134	44.2293
3776	3776	651.7347	659.3333	1.7739	43.2659
3835	3835	661.5867	669.1667	1.7337	42.2854

3894	3894	671.4631	679.0000	1.6960	41.3659
3953	3953	681.2789	688.8333	1.6573	40.4220
4012	4012	691.1237	698.6667	1.6184	39.4732
4071	4071	700.9656	708.5000	1.5803	38.5439
4130	4130	710.8040	718.3333	1.5406	37.5756
4189	4189	720.6199	728.1667	1.5017	36.6268
4248	4248	730.4470	738.0000	1.4617	35.6512
4307	4307	740.2866	747.8333	1.4217	34.6756
4366	4366	750.1517	757.6667	1.3810	33.6829
4425	4425	759.9637	767.5000	1.3372	32.6146
4484	4484	769.8066	777.3333	1.2941	31.5634
4543	4543	779.6451	787.1667	1.2469	30.4122
4602	4602	789.4791	797.0000	1.1981	29.2220
4661	4661	799.3018	806.8333	1.1454	27.9366
4720	4720	809.1313	816.6667	1.0900	26.5854
4779	4779	818.9481	826.5000	1.0330	25.1951
4838	4838	828.7571	836.3333	0.9750	23.7805
4897	4897	838.5574	846.1667	0.9211	22.4659
4956	4956	848.3747	856.0000	0.8653	21.1049
5015	5015	858.1923	865.8333	0.8133	19.8366
5074	5074	868.0083	875.6667	0.7611	18.5634
5133	5133	877.8392	885.5000	0.7109	17.3390
5192	5192	887.6926	895.3333	0.6604	16.1073
5251	5251	897.5670	905.1667	0.6124	14.9366
5310	5310	907.5029	915.0000	0.5638	13.7512
5369	5369	917.3912	924.8333	0.5160	12.5854
5428	5428	927.2548	934.6667	0.4717	11.5049
5487	5487	937.1040	944.5000	0.4336	10.5756
5546	5546	946.9983	954.3333	0.4063	9.9098
5605	5605	956.8828	964.1667	0.3865	9.4268
5664	5664	966.6957	974.0000	0.3824	9.3268
5723	5723	976.5840	983.8333	0.3830	9.3415
5782	5782	986.5359	993.6667	0.3840	9.3659

Curve Name: **Hybridized Sample**					
Values:					
Index	Time [s]	Sample Temp [°C]	Ref. Temp [°C]	Mass [mg]	Mass [%]
0	0	21.1516	30.0000	4.1000	100.0000
59	59	28.9544	39.8333	4.2158	102.8244
118	118	37.3880	49.6667	4.1846	102.0634
177	177	46.1227	59.5000	4.1500	101.2195
236	236	55.1700	69.3333	4.1110	100.2683
295	295	64.4101	79.1667	4.0700	99.2683
354	354	73.8290	89.0000	4.0312	98.3220
413	413	83.3523	98.8333	3.9980	97.5122

472	472	92.9645	108.6667	3.9721	96.8805
531	531	102.6645	118.5000	3.9503	96.3488
590	590	112.4555	128.3333	3.9327	95.9195
649	649	122.2921	138.1667	3.9170	95.5366
708	708	132.1373	148.0000	3.9020	95.1707
767	767	142.0271	157.8333	3.8872	94.8098
826	826	151.9792	167.6667	3.8728	94.4585
885	885	161.9457	177.5000	3.8562	94.0537
944	944	171.9258	187.3333	3.8381	93.6122
1003	1003	181.9350	197.1667	3.8193	93.1537
1062	1062	192.0238	207.0000	3.7991	92.6610
1121	1121	202.1116	216.8333	3.7780	92.1463
1180	1180	212.2044	226.6667	3.7577	91.6512
1239	1239	222.3526	236.5000	3.7367	91.1390
1298	1298	232.4748	246.3333	3.7132	90.5659
1357	1357	242.6166	256.1667	3.6908	90.0195
1416	1416	252.7641	266.0000	3.6817	89.7986
1475	1475	262.8826	275.8333	3.6727	89.5777
1534	1534	273.0195	285.6667	3.6636	89.3568
1593	1593	283.1392	295.5000	3.6546	89.1359
1652	1652	293.2142	305.3333	3.6455	88.9150
1711	1711	303.2852	315.1667	3.6365	88.6941
1770	1770	313.3984	325.0000	3.6274	88.4731
1829	1829	323.4863	334.8333	3.6183	88.2522
1888	1888	333.6121	344.6667	3.6093	88.0313
1947	1947	343.6646	354.5000	3.6002	87.8104
2006	2006	353.7427	364.3333	3.5912	87.5895
2065	2065	363.8004	374.1667	3.5821	87.3686
2124	2124	373.8531	384.0000	3.5731	87.1477
2183	2183	383.8806	393.8333	3.5640	86.9268
2242	2242	393.8947	403.6667	3.5549	86.7059
2301	2301	403.9179	413.5000	3.5459	86.4850
2360	2360	413.8999	423.3333	3.5368	86.2640
2419	2419	423.8691	433.1667	3.5278	86.0431
2478	2478	433.8377	443.0000	3.5187	85.8222
2537	2537	443.8053	452.8333	3.5097	85.6013
2596	2596	453.7378	462.6667	3.5006	85.3804
2655	2655	463.6873	472.5000	3.4915	85.1595
2714	2714	473.6098	482.3333	3.4825	84.9386
2773	2773	483.5686	492.1667	3.4734	84.7177
2832	2832	493.4536	502.0000	3.4644	84.4968
2891	2891	503.3712	511.8333	3.4553	84.2759
2950	2950	513.2856	521.6667	3.4463	84.0549
3009	3009	523.1694	531.5000	3.4372	83.8340
3068	3068	533.0628	541.3333	3.4281	83.6131
3127	3127	542.9659	551.1667	3.4191	83.3922

3186	3186	552.8455	561.0000	3.4100	83.1713
3245	3245	562.7170	570.8333	3.4010	82.9504
3304	3304	572.6490	580.6667	3.3919	82.7295
3363	3363	582.5148	590.5000	3.3829	82.5086
3422	3422	592.3616	600.3333	3.3738	82.2877
3481	3481	602.2200	610.1667	3.3647	82.0668
3540	3540	612.0810	620.0000	3.3557	81.8458
3599	3599	621.9268	629.8333	3.3466	81.6249
3658	3658	631.7367	639.6667	3.3376	81.4040
3717	3717	641.5715	649.5000	3.3285	81.1831
3776	3776	651.4103	659.3333	3.3195	80.9622
3835	3835	661.2346	669.1667	3.3104	80.7413
3894	3894	671.0947	679.0000	3.3013	80.5204
3953	3953	680.9319	688.8333	3.2923	80.2995
4012	4012	690.7712	698.6667	3.2832	80.0786
4071	4071	700.6187	708.5000	3.2742	79.8577
4130	4130	710.4665	718.3333	3.2651	79.6367
4189	4189	720.2946	728.1667	3.2560	79.4158
4248	4248	730.1280	738.0000	3.2470	79.1949
4307	4307	739.9587	747.8333	3.2379	78.9740
4366	4366	749.7776	757.6667	3.2289	78.7531
4425	4425	759.5711	767.5000	3.2281	78.7342
4484	4484	769.3406	777.3333	3.2273	78.7153
4543	4543	779.0923	787.1667	3.2266	78.6965
4602	4602	788.8856	797.0000	3.2258	78.6776
4661	4661	798.7529	806.8333	3.2250	78.6587
4720	4720	808.5356	816.6667	3.2242	78.6398
4779	4779	818.5868	826.5000	3.2235	78.6209
4838	4838	828.4368	836.3333	3.2227	78.6021
4897	4897	838.3143	846.1667	3.2219	78.5832
4956	4956	848.1554	856.0000	3.2211	78.5643
5015	5015	857.8406	865.8333	3.2204	78.5454
5074	5074	867.6396	875.6667	3.2196	78.5265
5133	5133	877.4903	885.5000	3.2188	78.5077
5192	5192	887.3632	895.3333	3.2180	78.4888
5251	5251	897.2828	905.1667	3.2173	78.4699
5310	5310	907.1954	915.0000	3.2165	78.4510
5369	5369	917.0996	924.8333	3.2157	78.4321
5428	5428	926.9714	934.6667	3.2149	78.4133
5487	5487	936.8629	944.5000	3.2142	78.3944
5546	5546	946.7526	954.3333	3.2134	78.3755
5605	5605	956.6420	964.1667	3.2126	78.3566
5664	5664	966.5663	974.0000	3.2118	78.3377
5723	5723	976.4856	983.8333	3.2111	78.3189
5782	5782	986.4309	993.6667	3.2103	78.3000